NUREG/CR-4189
SAND85-0576
R4
Printed November 1985

# TRAC-PF1/MOD 1 Independent Assessment: Semiscale MOD-2A Feedwater-Line Break (S-SF-3) and Steam-Line Break (S-SF-5) Tests

Dean Dobranich

Prepared by
Sandia National Laboratories
Albuquerque, New Mexico 87185 and Livermore, California 94550
for the United States Department of Energy
under Contract DE-AC04-76DP00789



Prepared for
U. S. NUCLEAR REGULATORY COMMISSION

Available from

Superintendent of Documents
U.S. Government Printing Office
Post Office Box 37082
Washington, D.C. 20013-7982

and

National Technical Information Service
Springfield, VA 22161

NUREG/CR-4189
SAND85-0576
R4

# TRAC-PF1/MOD1 INDEPENDENT ASSESSMENT: SEMISCALE MOD-2A FEEDWATER-LINE BREAK (S-SF-3) AND STEAM-LINE BREAK (S-SF-5) TESTS

Dean Dobranich

Date Published: November 1985

Sandia National Laboratories
Albuquerque, NM 87185
Operated By
Sandia Corporation
for the
U. S. Department of Energy

Prepared for
Reactor Systems Research Branch
Division of Accident Evaluation
Office of Nuclear Regulatory Research
U. S. Nuclear Regulatory Commission
Washington, DC 20555
Under Memorandum of Understanding DOE 40-550-75
NRC FIN No. A-1374

## ABSTRACT

The TRAC-PF1/MOD1 independent assessment project at Sandia is part of an overall effort funded by the NRC to determine the ability of various systems codes to predict the detailed thermal/hydraulic response of LWRs during accident and off-normal conditions. As part of this effort, calculations for Semiscale Mod-2A test S-SF-3, a feedwater-line break test, and S-SF-5, a steam-line break test, were performed with TRAC-PF1/MOD1.

Most aspects of both the S-SF-3 and S-SF-5 steady-state calculations were found to be in good agreement with data. However, the need for a better steam separator model was identified from the S-SF-3 calculation. Overall, the qualitative behavior of both transients was calculated reasonably well; however, there were some discrepancies in the prediction of the quantitative behavior. The results for the S-SF-3 transient calculation indicate that the primary-to-secondary heat transfer degradation began too early. This was possibly due to overprediction of entrainment in the steam generator boiler, leading to an incorrect calculation of the secondary-side fluid distribution during the steady state. However, there was insufficient data to verify this. Results for the S-SF-5 transient calculation indicate that the primary-side fluid temperature response to a steam-line break was in reasonable agreement with data but the pressure response did not coincide with the data. Uncertainties in the data are sufficient to prevent us from determining the exact cause of this discrepancy, but there is indirect evidence that the calculated rate of phase change in the pressurizer was incorrect.

CONTENTS

LIST OF FIGURES

LIST OF TABLES

## ACKNOWLEDGEMENTS

The author wishes to thank Lubomyra N. Kmetyk, who prepared most of the Semiscale Mod-2A input deck for the TRAC-PF1/MOD1 assessment calculations and who helped to review this report. Also, thanks go to Jan Frey for final preparation of the report, and to Mildred Elrick for graphics and code maintenance support.

# 1.0 INTRODUCTION

The TRAC-PF1/MOD1 independent assessment project at Sandia National Laboratories in Albuquerque (SNLA) is part of an overall effort funded by the Nuclear Regulatory Commission (NRC) to determine the ability of various systems codes to predict the detailed thermal/hydraulic response of light water reactors during accident and off-normal conditions. As part of this effort, calculations for Semiscale Mod-2A test S-SF-3, a feedwater-line break test, and S-SF-5, a steam-line break test, were performed with TRAC-PF1/MOD1.

TRAC-PF1/MOD1 [1] is the latest version of a systems code developed at the Los Alamos National Laboratory to provide advanced best-estimate predictions of postulated accidents in pressurized water reactors (PWRs). TRAC (Transient Reactor Analysis Code) features a two-fluid, nonequilibrium, hydrodynamics model with a flow-regime-dependent constitutive equation treatment. Early versions of TRAC were designed primarily to simulate large-break loss-of-coolant accidents. Additional models have been incorporated in TRAC-PF1/MOD1 to allow simulation of a broad range of accidents relevant to current licensing issues. (Version 11.6 of TRAC-PF1/MOD1 was used for all the calculations reported herein.)

TRAC-PF1/MOD1 is being assessed at SNLA by comparing calculated results with data from various integral and separate effects tests. Among these is the Semiscale Mod-2A SF series of tests conducted at the Idaho National Engineering Laboratory (INEL). This series consisted of three feedwater-line break tests and two steam-line break tests. The primary objectives of this test series were to investigate the primary-to-secondary heat transfer response during the tests and to provide a data base for reactor safety computer code assessment.

The S-SF-3 transient is a feedwater-line break test initiated from full-power steady-state conditions. The break size was originally chosen to simulate a 14% break in a full-scale Combustion Engineering plant. The scaling criterion for the break area was based on the secondary-side liquid mass to break area ratio in order to preserve the "time-to-empty" of the broken loop (BL) secondary side. Because the actual Semiscale secondary-side inventory was greatly different from what the experimenters had planned, the Semiscale break size instead simulated a 4.6% break in a full scale plant. Further information regarding the facility and this test is given in the Experimental Operating Specification [2], the Quick Look Report [3], and the Experimental Data Report [4].

The S-SF-5 transient is a steam-line break test initiated from hot-standby conditions. Hot-standby conditions were chosen because they were expected to result in the most severe transient with respect to overcooling. The break size was chosen to simulate a 50% break of a steam line at the flow restrictor of a full-scale four-loop Westinghouse PWR. To simulate communication between the BL and intact loop (IL) steam generators, both steam generators were allowed to blow down until the IL steam-line valve was closed upon receipt of a low BL secondary-side pressure signal. (The IL steam-line break orifice is three times the area of the BL steam-line break orifice.) Further information regarding this test is given in the Quick Look Report [5], the Experimental Data Report [6], and the Experimental Operating Specification [2].

Some of the experimental data plots presented in this report were taken from data tapes and some were reproduced from plots in the S-SF-3 and S-SF-5 post-test analysis reports [7,8]. The plots taken from references 7 and 8 do not contain data before the initiation of the transient (i.e., steady state) as do the plots from the data tapes. Also, the plots from references 7 and 8 terminate sooner. The experimental data are always presented as dashed lines; the curves from the TRAC calculations are presented as solid lines.

## 2.0 SEMISCALE MOD-2A FACILITY

The Semiscale test facility is located at INEL and supported by the NRC. The designation "Mod-2A" represents the configuration of the facility used for several different test series including the SF series. Semiscale is a scaled integral test facility, shown in Figure 2.0.1, and is used to investigate thermal and hydraulic phenomena which occur during hypothesized loss-of-coolant accidents and operational transients in a PWR. The system was scaled to have a core power and system fluid volume 1/1705th of a four-loop PWR, and consists of two primary coolant loops connected to an electrically-heated core in a pressure vessel which has an external downcomer. Each coolant loop contains an active pump and steam generator. The intact loop has three times the fluid volume and loop mass flow of the broken loop and represents three operational loops in a typical four-loop PWR. The pressurizer is connected to this loop. A more detailed description of the facility is provided in Appendix I and additional information pertaining to the Semiscale Mod-2A system is contained in references 9 and 10.

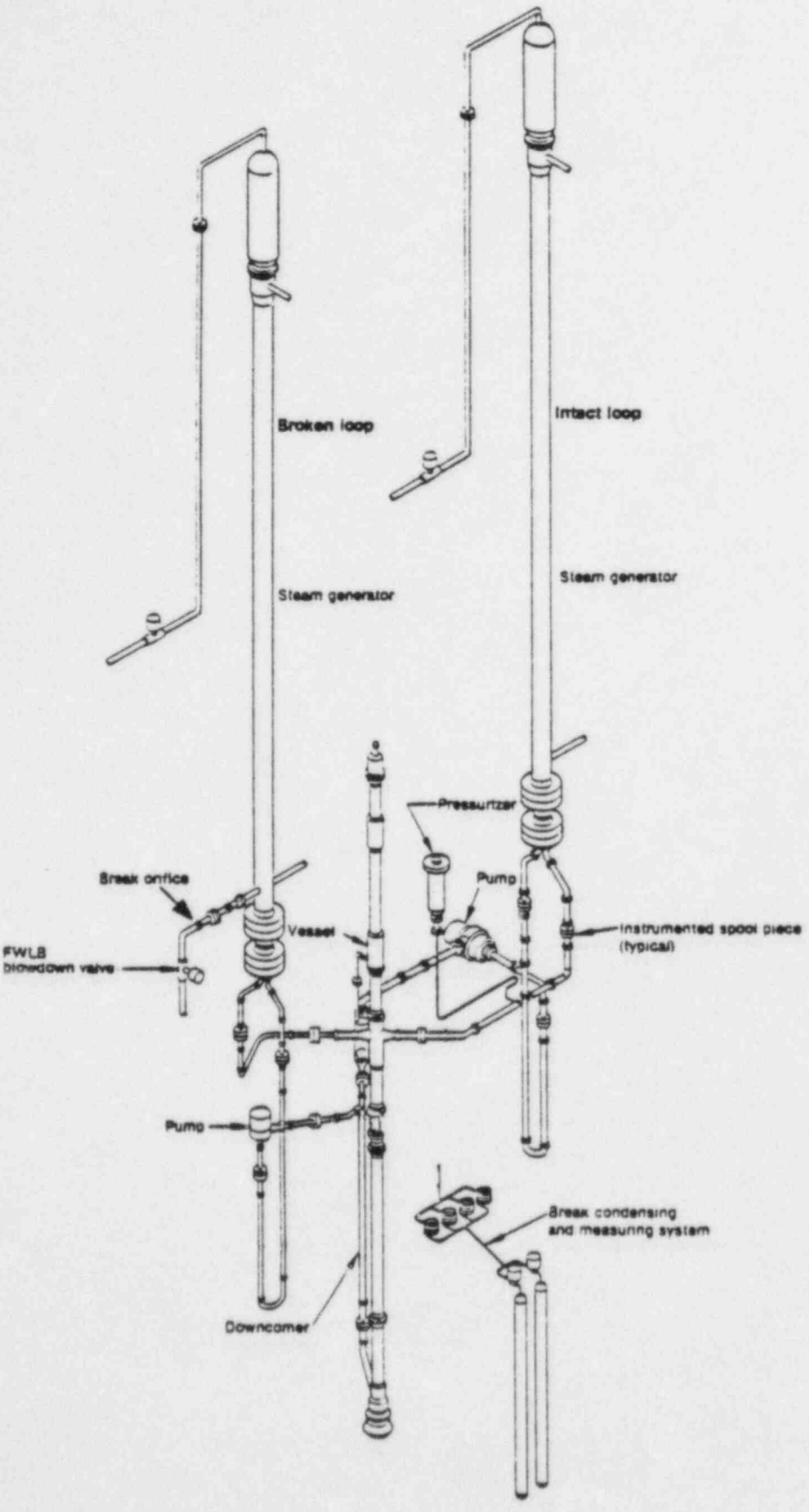


Figure 2.0.1 The Semiscale Mod-2A Test Facility

## 3.0 TRAC-PF1/MOD1 INPUT MODEL

Geometric information for the TRAC input deck was taken primarily from RELAP5 input decks developed at SNLA for the Mod-2A system. These decks were used for various RELAP5 assessment calculations. [11,12] The RELAP5 Mod-2A input deck was converted to a TRAC-PF1/MOD1 deck as part of our assessment work for the Semiscale Mod-2A S-IB-3 transient [13]. Information particular to the SF series configuration was obtained from references 2 through 8 and the S-IB-3 deck was modified to reflect this slightly different system.

The input changes necessary for modifying the S-IB-3 deck included changes to the steam generator secondary sides, addition of control and trip logic peculiar to feedwater-line and steam-line breaks, and removal of the accumulator, accumulator check valve, and primary-side break components which were not required for the SF series. A major change made to both the IL and BL secondary sides was the addition of a TEE to allow injection of feedwater to the bottom of the downcomer, instead of at the top (with the old injection location at the top of the downcomer still used for auxiliary feedwater (AFW) injection). With the feedwater injection at the bottom of the downcomer, there was no downcomer gravitational head to help drive recirculation flow. The piping necessary to initiate the feedwater-line break and to allow isolation of the secondary sides was also added. In the SF experiments, the breaks were modeled as orifices in the feedwater line (for S-SF-3) and the steam lines (for S-SF-5). The reported orifice areas were used in the TRAC model at the break junctions together with the implementation of the choked flow model at those junctions. There was no hydraulic communication between the secondary sides in either test.

Form-loss coefficients (K factors) were added to model the tube support plates on the secondary side, as opposed to using the automatic form-loss calculation provided in TRAC. The annular flow friction-factor option was used in the downcomer and the homogeneous flow friction-factor option was used in the boiler region. The use of K factors and the choice of friction-factor options was based on our experience with modeling the B&W once-through steam generator tests [14] using TRAC-PF1/MOD1.

Another modification of interest was the addition of a leakage path from the primary side. This path was modeled using two TEE components located at the bottom of the intact loop pump suction. A BREAK component was attached to the side tube of one TEE and a FILL component was attached to the other. A K factor (determined by trial and error) was added to the junction adjacent to the BREAK to achieve the reported steady-state leakage rate; the FILL component was used to provide the necessary makeup flow. During the transient the makeup supply was terminated, as was done in the experiment. We felt that this modification might be important because the reported steady-state leakage rate is of the same order of magnitude as the HPI flow rate during the transients [3,5].

A component schematic for the TRAC-PF1/MOD1 input model of the Semiscale Mod-2A system is shown in Figure 3.0.1. (The same input model, except for different trip logic, was used for both transients.) Both loops are modeled, with the intact loop shown on the left, the broken loop on the right, and the vessel in the middle. This model contains 35 components, with a total of 184 1-D mesh cells and 48 3-D

mesh cells in the VESSEL. The noding diagram in Figure 3.0.2 shows the 24 axial levels and 2 azimuthal sectors of the vessel. (The radial dimensions have been expanded to improve the appearance of this figure.) The vessel external downcomer and the downcomer bypass line were modeled with TEE components. The support columns and guide tube were modeled with PIPE components connected internally to the vessel. Ninety-three of the 1-D mesh cells of this model are in the two steam generators. Also, a total of 260 heat slabs was used to model the heat structures; 119 of these were in the steam generators.

We assumed that the environmental heat losses from the primary system were accurately compensated for by guard heaters in the experiment and therefore adiabatic boundary conditions were used for external surfaces in the input model. The steam generator secondary side external surfaces were also modeled adiabatically even though they did not have guard heaters attached in the tests; we felt that the losses were small enough (6 kW [3]) to warrant this approximation. The single-phase and two-phase homologous head and torque curves for the coolant pumps were based on data supplied by INEL [9]. The accumulators were not required for these tests and therefore were not modeled. The tube-to-tube spacing was used as the heated equivalent diameter on the secondary sides of the steam generators. We have found from experience with both TRAC and RELAP5 that this is a more representative value than the standard heat transfer diameter (4.0 times the flow area divided by the heated perimeter) for flow through a tube bank. Two input listings for this model are provided in Appendix II; one listing is for the input model with the S-SF-3 initial conditions and trips, and the other listing is for the input model with the S-SF-5 initial conditions and trips.

An input model consisting entirely of 1-D components was also constructed; i.e., the 3-D VESSEL was replaced with a 1-D CORE along with additional PIPEs and TEEs. This model was used to perform fast-running parametric cases for the S-SF-3 test and will be discussed in Section 6.0. The input listing for this 1-D model is also included in Appendix II.

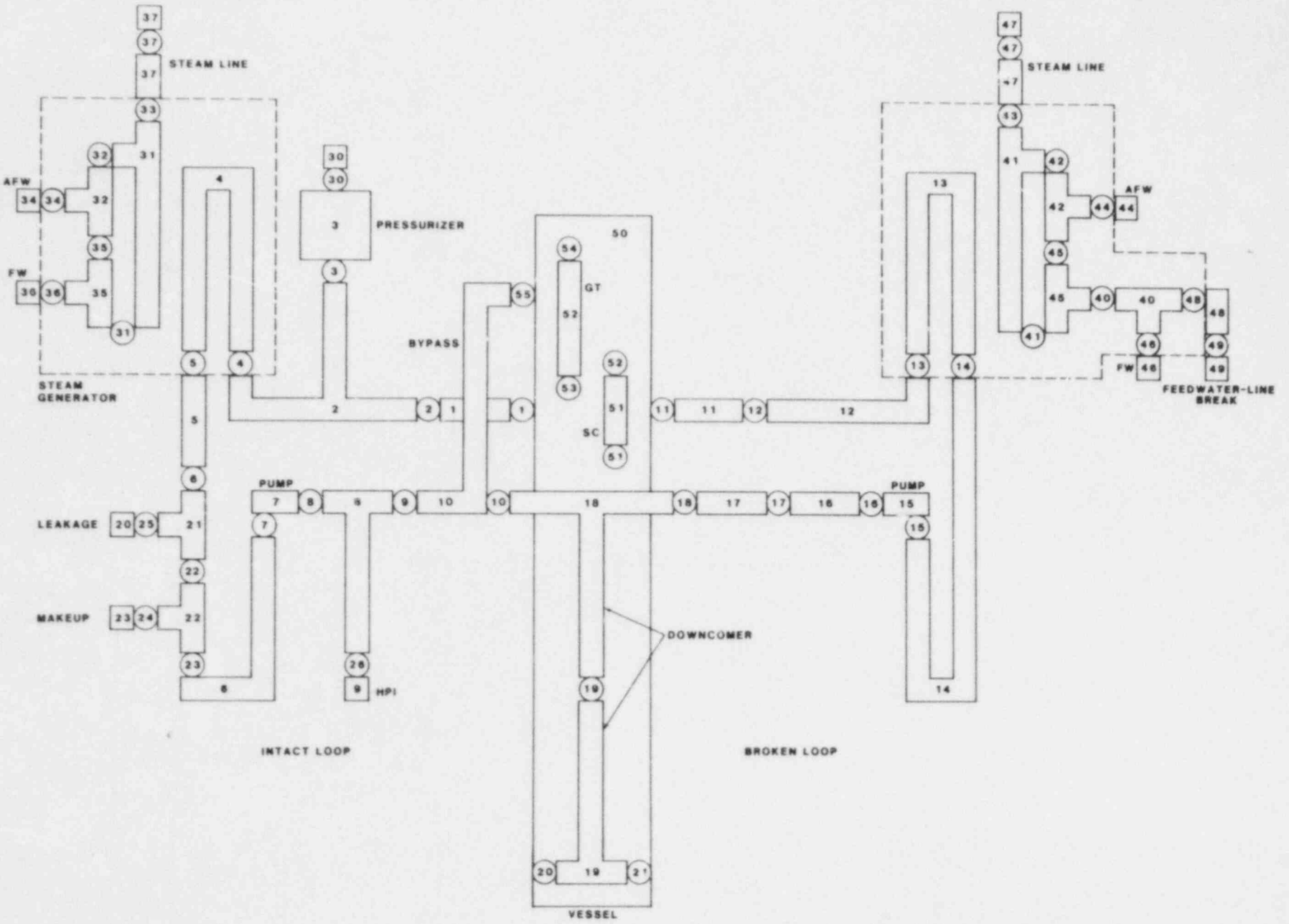


Figure 3.0.1 TRAC-PF1/MOD1 Component Schematic of the Semiscale Test Facility

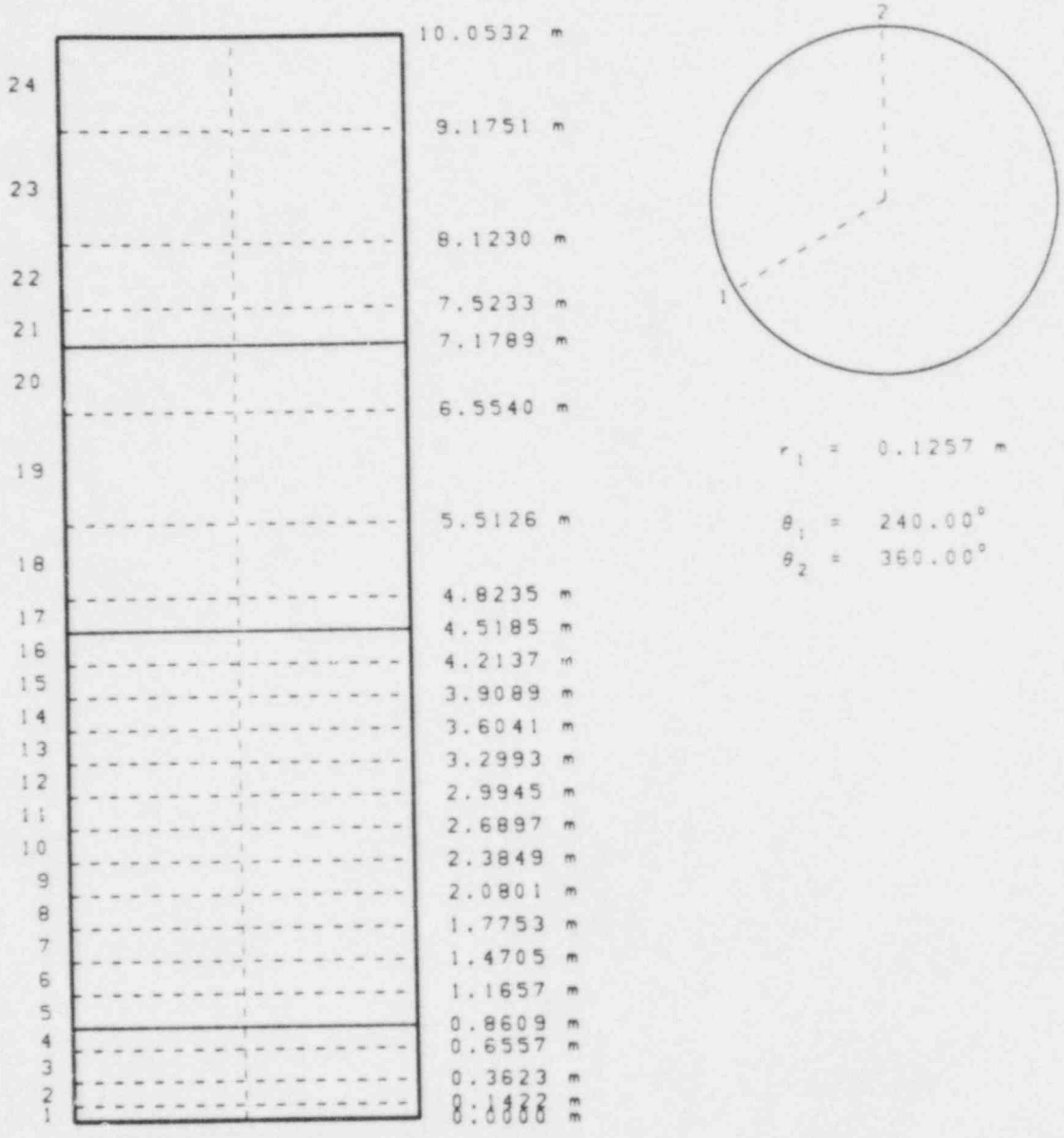


Figure 3.0.2 TRAC-PF1/MOD1 Noding Diagram of the Semiscale Mod-2A Vessel

## 4.0 S-SF-3 STEADY-STATE CALCULATION

The S-SF-3 boundary conditions as specified in the TRAC input model are given in Table 4.0.1. Steady-state conditions were achieved in the calculation with the help of control block logic built into the input deck. One such control block was included to adjust the pump speeds to achieve the reported loop flow rates. Also included was a control block to adjust the feedwater flow to achieve the reported secondary-side inventory. The control logic for both the pump speeds and the feedwater flows is of the form

$$PNEW = POLD\,[\,c \times R + (1 - c)\,]$$

where PNEW is the new value of the parameter being adjusted, POLD is the value of the parameter at the previous time step, c is an arbitrary constant (0.2 for the pump speed controller and 0.5 for the feedwater controller), and R is the ratio of the desired-to-actual control block input (pump speed for pump controller and steam generator secondary-side inventory or water level for the feedwater controller). The value of c and the control block minimum and maximum limits are adjusted on a trial and error basis to prevent over- or under-control, which could lead in turn to undesired oscillations.

We encountered considerable difficulties attempting to model the steam separators located in the steam domes. (These are mechanical separation devices that employ swirl vanes to remove liquid drops from the exiting vapor.) As an alternative to modeling the steam separator, a steady-state calculation was performed without a separator model. This preliminary steady-state calculation was performed to help us gain insight into the flow behavior on the secondary side and to determine if the primary-side conditions could be accurately predicted. We found that, if the separator is not modeled, the feedwater must be increased by over a factor of three to compensate for the considerable amount of liquid being entrained by the exiting vapor in the calculation; this was done by the feedwater control block which was set up to maintain the reported secondary-side inventory. Although the feedwater flow rate was too high, the remaining steady-state conditions on both the secondary and primary sides were in fairly good agreement with experimental data.

The secondary-side exit vapor, liquid, and total mass flow rates for this case (no separator model) are shown in Figure 4.0.1. About 70% of the intact loop power load was removed by generation of vapor which exited the steam dome at a rate of about 0.7 kg/s. The remaining 30% of the power load was removed by the heating of the liquid to saturation temperature. However, while a steady state can be achieved if the separator is not modeled, we felt it would be preferable to implicitly model the separator and thereby allow injection of feedwater at the correct rate. The distribution of the secondary-side fluid should also be more representative of the experiment if the separator is modeled.

A separate TRAC input model was then prepared which contained only the intact loop steam generator with appropriate boundary conditions. (This was done to allow easier and quicker investigation of the steam separator and feedwater flows.) A number of calculations were performed using this model. Figures 4.0.2 through 4.0.4 are plots from these calculations.

The normal method available in TRAC to model the separator involves the input of a K factor greater than 1.0E24 at the desired cell edge. This triggers logic in TRAC that sets the liquid friction factor equal to the input K factor (essentially infinite liquid friction) and also sets the interfacial friction to zero. Use of this option was not successful at first. The cell immediately below the separator filled as the entrained liquid was separated from the exiting vapor. The exit vapor flow rate, therefore, decreased to zero while vapor generation in the boiler continued. As a result, the cell pressure increased to the limit of TRAC's thermodynamic properties routines. To prevent this unwanted pressure increase, the accumulated liquid must be removed from the cell via the downcomer. Unfortunately, the liquid would not flow into the downcomer fast enough.

Several attempts to correct this difficulty were made, including moving the location of the separator, making the downcomer connection pipe vertical, and adjusting the initial conditions and control block parameters in an attempt to "creep up" on the desired conditions. Moving the separator location to the top of the cell adjacent to the downcomer connection and making the downcomer connection pipe vertical improved downcomer flow but were not sufficient to solve the problem. After much effort, the desired steady-state conditions on the secondary side were achieved by carefully adjusting the control block parameters and initial conditions. We found that, when using the controller as described above, it was necessary to set the upper limit for feedwater flow only 7% higher than the desired flow to prevent overshooting the desired inventory. It was also necessary to use an initial inventory less than the desired inventory and to allow the feedwater controller to increase the feedwater flow. The response was very sensitive to any changes made by the controller and it took a great deal of trial and error to find the appropriate control block parameters and initial conditions. Perhaps a more sophisticated controller could have been developed to reduce the controller sensitivity, but this was not attempted because the effort did not seem warranted.

The feedwater flow rate and steam-line flow rate are plotted in Figure 4.0.2 for the "steam generator stand-alone" case using the separator model. The small fluctuations of the feedwater flow rate are a result of the controller action to adjust the inventory. The steam-line flow rate exhibits sharp periodic fluctuations. The use of a separator K appears to introduce this oscillatory behavior; however, the average exit flow rate is correct. The inventory, shown in Figure 4.0.3, slowly converges to the desired value of 114.7 kg. The flow into the downcomer is shown in Figure 4.0.4. This quantity was not measured during the experiment, but represents the amount of fluid recirculating through the steam generator including the liquid separated from the exiting vapor. The calculated recirculation ratio (downcomer flow rate divided by the feedwater flow rate) is about 2.6.

A stand-alone input model for the BL steam generator was also constructed and the above procedure of adjusting the initial conditions and control block parameters was repeated. However, additional difficulties were encountered with the broken loop steam generator. Although the desired inventory was achieved, the secondary-side pressure increased to about 7.1 MPa, instead of the desired 6.46 MPa, as shown in Figure 4.0.5. Lowering the desired inventory from 126 kg to 112 kg did not alleviate the problem. However, moving the separator to the exit of the boiler and decreasing the exit pressure boundary condition to 5.7 MPa resulted in the calculation of the correct secondary-side pressure. It is not understood why such a

large pressure drop across the separator for the BL steam generator occurs. Unfortunately, when this stand-alone steam generator model was included in the full system, it did not behave in the same way and a steady state could not be achieved. Addition of a controller to adjust the exit pressure to achieve the desired steam dome pressure was also unsuccessful.

An alternate method of modeling the separator was then tried. This method does not include use of the large separator K but instead involves the use of an artificially-large flow area at the steam dome exit. The large area has the effect of reducing the exit vapor flow such that the amount of entrained liquid is decreased to essentially zero. If the area was made too large, difficulties in the numerics caused the code to fail. If the area was too small, insufficient separation occurred. However, an area 50 times larger than the physical area was found to work well. In fact, this separator model worked much more smoothly than the normal separator-K model in conjunction with the feedwater controller. The stand-alone steam generator model ran about 30% faster when using the increased area than when using the separator K. The steady-state calculation was repeated using this increased flow area separator model on the broken loop and the separator K model on the intact loop.

The measured steady-state results for S-SF-3 are given in Table 4.0.2 along with the calculated results with and without a separator model on the secondary sides. (Uncertainties are included with the measured values when available.) This table shows that relatively good agreement with data is being achieved. The secondary-side inventories are included in this table (even though they really are specified boundary conditions) because it was not always possible to achieve the exact reported value due to the sensitivity of the control blocks used. The calculated BL pump speed does not agree well with the reported value for two reasons. First, only the single phase pump curves for the broken loop were known (we used the two-phase curves of the intact loop pump), and second, the geometry of the BL pump for the test was different from when the pump was characterized.

Multiplying the reported loop mass flow rate by the enthalpy difference from cold leg to hot leg at the reported temperatures yields a power level of about 2.1 MW; this is inconsistent with the reported power level of 2.0 MW. This inconsistency reflects the 2 K uncertainty in the temperature measurements along with the approximately 5% uncertainty in the mass flow rate measurements. In the TRAC calculation, the mass flow rates are being set by a controller to exactly equal the reported flow rates and the core power is set to equal the reported power. Therefore, the uncertainty associated with the mass flow rate will be reflected in the calculated loop temperatures.

Table 4.0.1. S-SF-3 Boundary Conditions

| | |
|---|---|
| Core Power (MW): | 2.0 |
| Pressurizer Pressure (MPa): | 15.13 |
| Pressurizer Liquid Mass (kg): | 12.4 |
| Loop Flow Rates (kg/s): | |
| IL | 8.45 |
| BL | 2.16 |
| Secondary-Side Pressure (MPa): | |
| IL | 6.31 |
| BL | 6.46 |
| Feedwater Temperature (K): | |
| IL | 528.0 |
| BL | 525.0 |
| Auxiliary Feedwater Temperature (K): | |
| IL | 298.0 |
| BL | 298.0 |
| HPI Liquid Temperature (K): | 300.0 |

Table 4.0.2. S-SF-3 Steady-State Results

| Parameter | Measured | Calculated | |
|---|---|---|---|
| | | No Separator | Separator |
| Fluid Temperatures (K): | | | |
| IL Hot Leg | 598.1±2.2 | 600.5 | 600.9 |
| IL Cold Leg | 563.0±2.2 | 569.2 | 569.6 |
| Fluid Temperatures (K): | | | |
| BL Hot Leg | 598.7±2.2 | 599.6 | 600.1 |
| BL Cold Leg | 561.5±2.2 | 565.9 | 566.5 |
| Secondary-Side Inventories (kg): | | | |
| IL | 114.7 | 114.6 | 115.0 |
| BL | 126.4 | 125.6 | 126.9 |
| Pump Speeds (rad/s) | | | |
| IL | 244±5 | 244.7 | 244.7 |
| BL | 1010±21 | 1314.0 | 1316.0 |
| Feedwater Flow Rates (kg/s): | | | |
| IL | 1.0 | 3.9 | 0.96 |
| BL | 0.25 | 1.3 | 0.25 |
| Leakage (kg/s): | 0.005 | 0.005 | 0.005 |

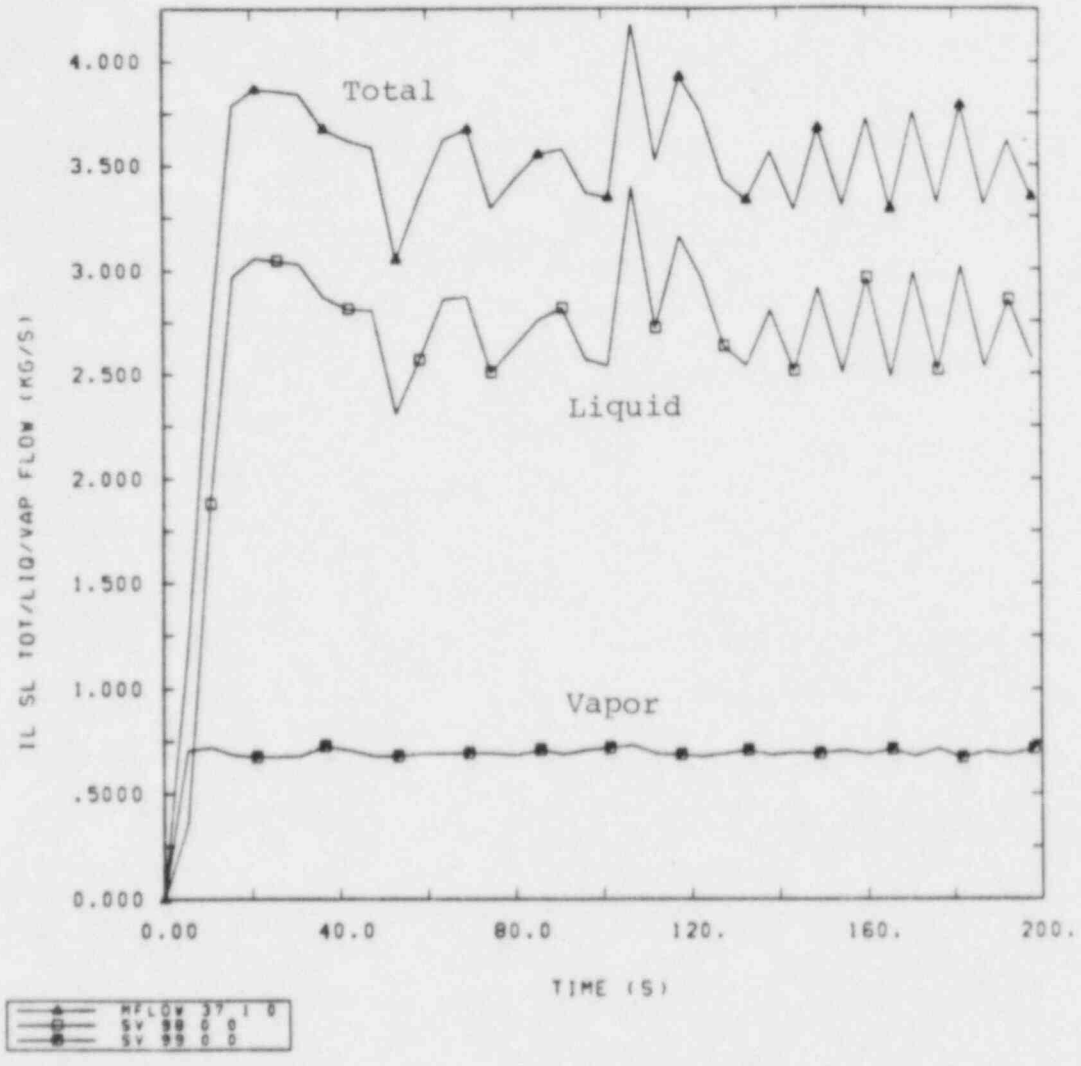


Figure 4.0.1 Total, Liquid, and Vapor Flow Rates for IL Secondary-Side Steam Generator Exit, S-SF-3 Steady State, No Separators

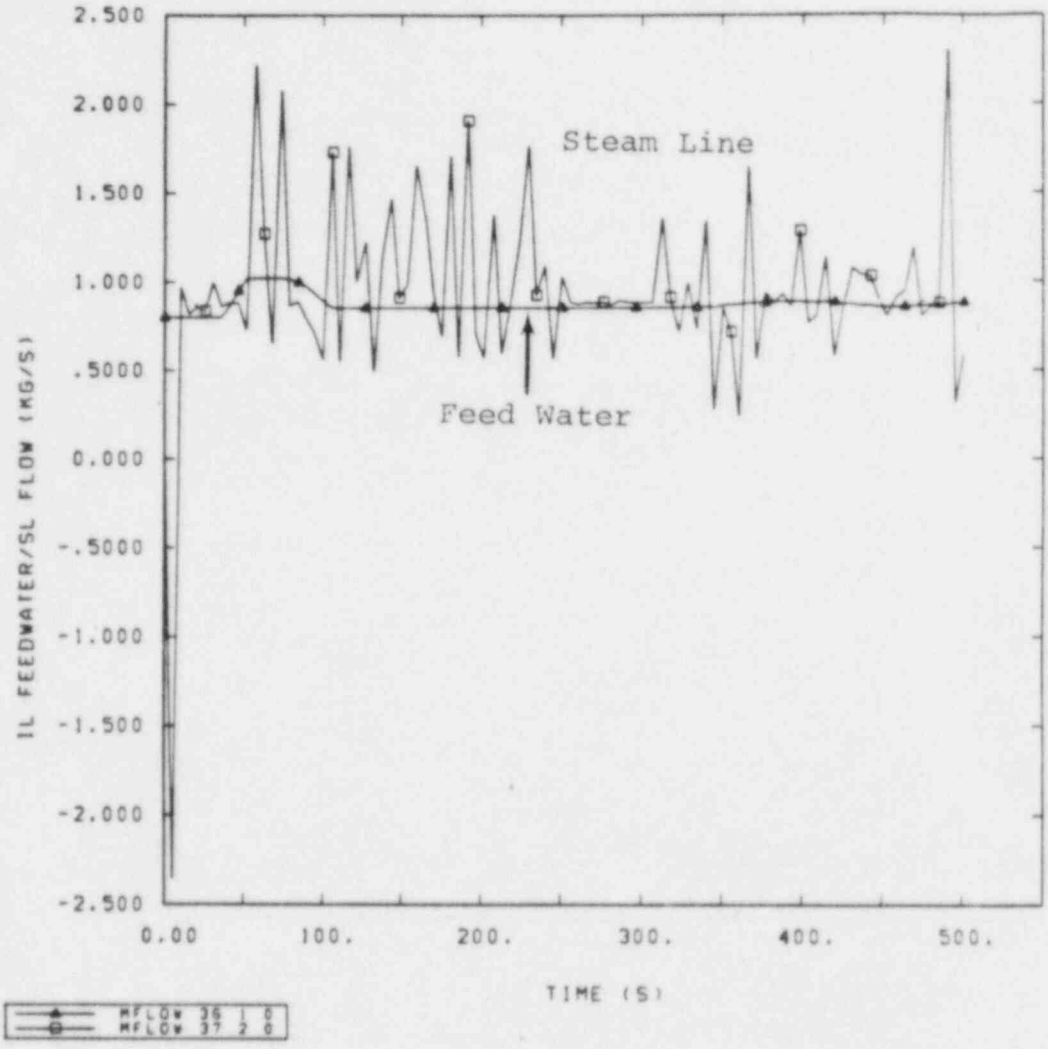


Figure 4.0.2 IL Feedwater and Steam-Line Flow Rates, S-SF-3 Steady State, Stand-Alone IL Steam Generator Model

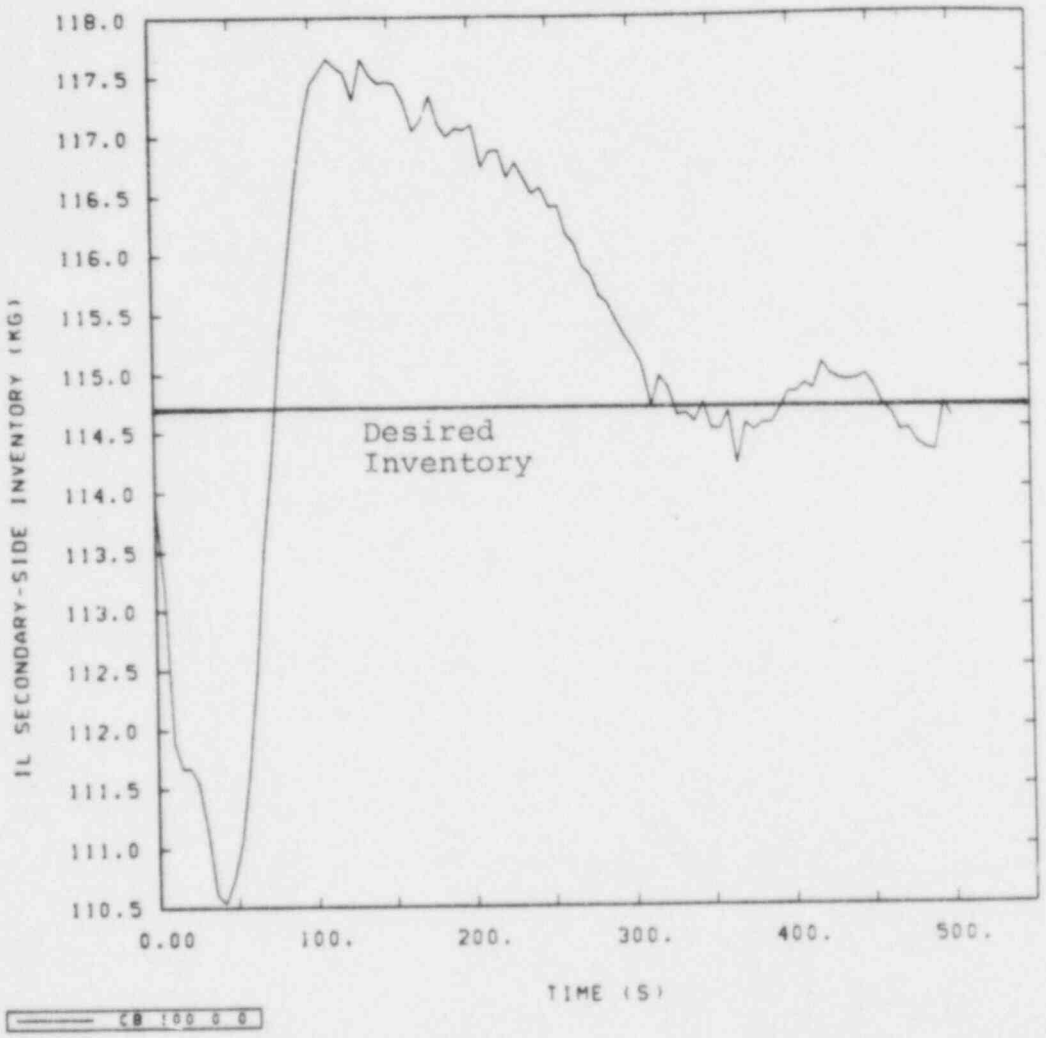


Figure 4.0.3 IL Secondary-Side Inventory, S-SF-3 Steady State, Stand-Alone IL Steam Generator Model

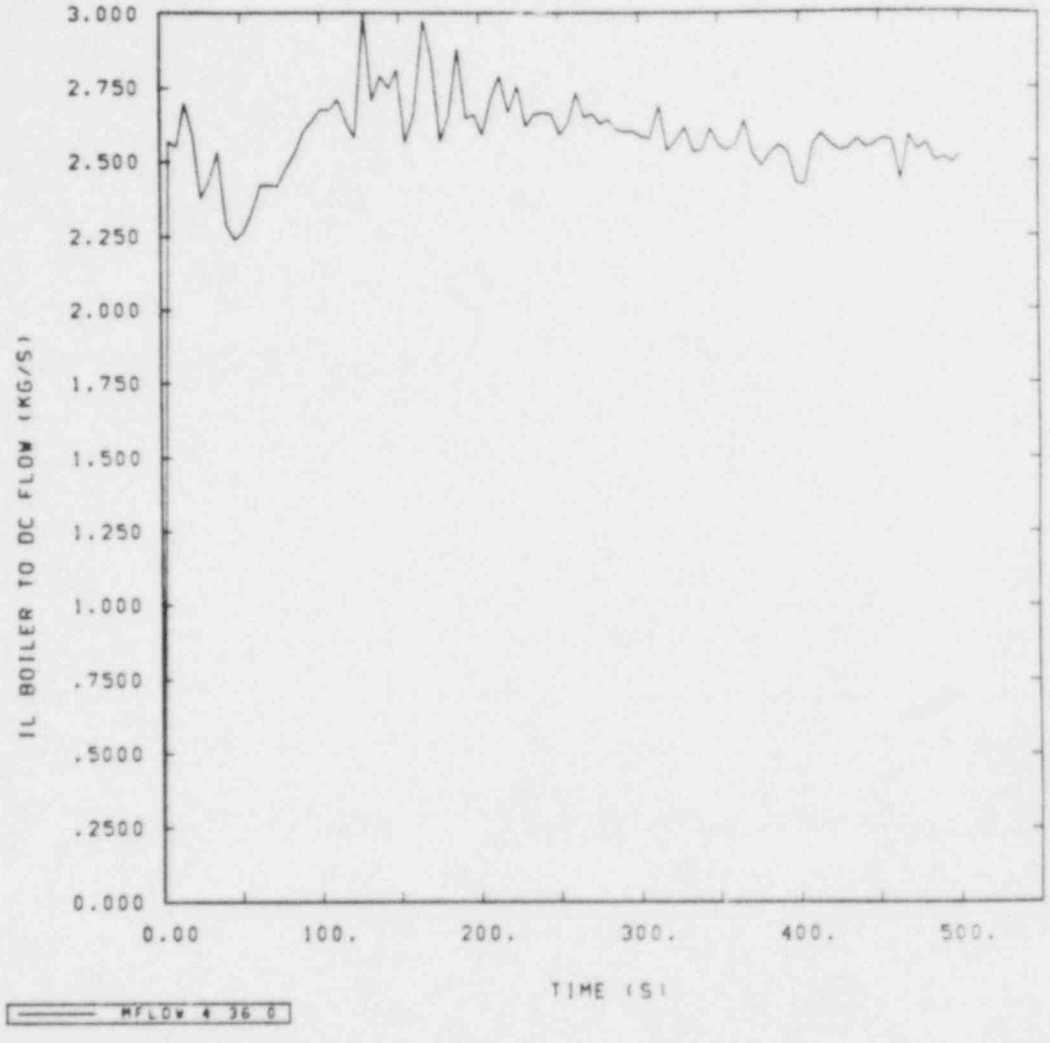


Figure 4.0.4 Boiler to Downcomer Flow Rate in IL Steam Generator, S-SF-3 Steady State, Stand-Alone IL Steam Generator Model

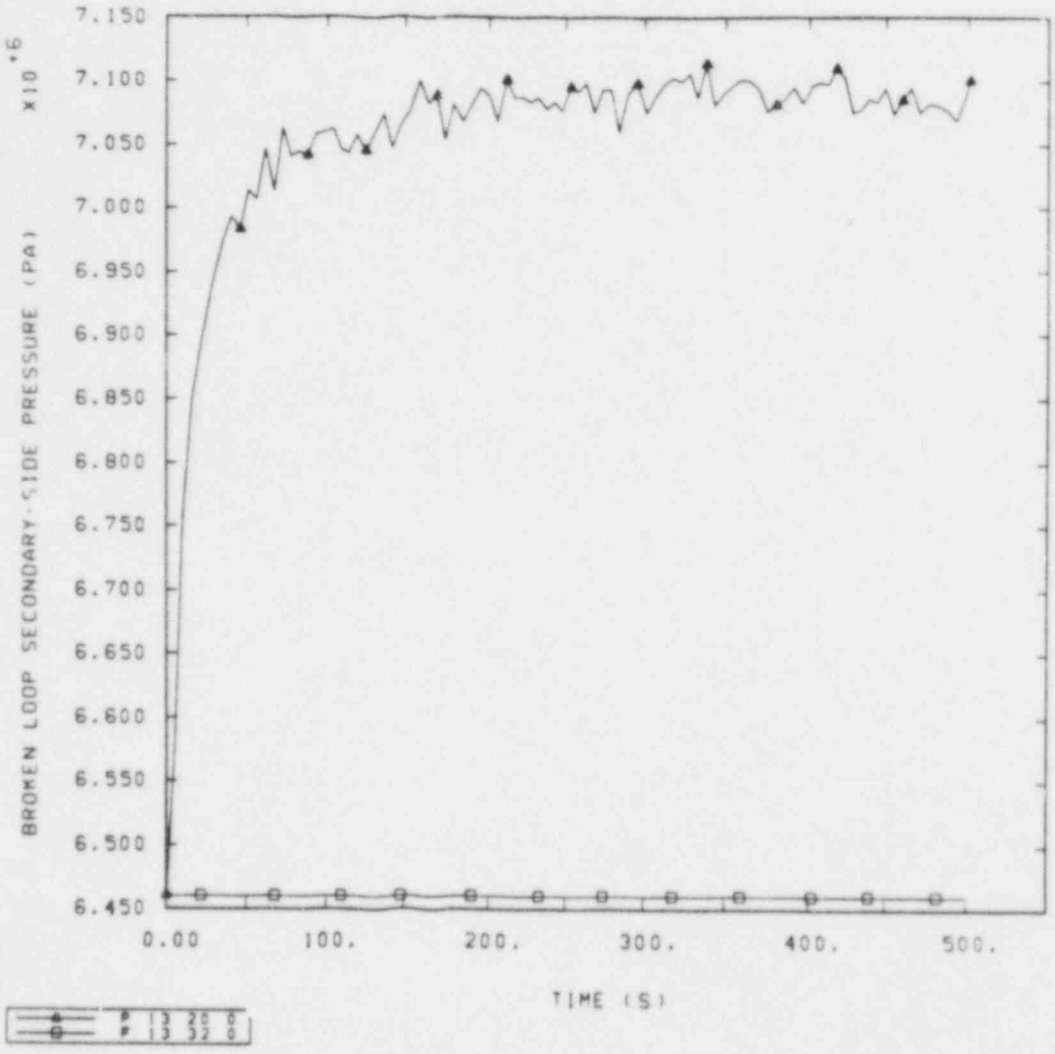


Figure 4.0.5 BL Secondary-Side Pressure, S-SF-3 Steady State, Stand-Alone BL Steam Generator Model

## 5.0 S-SF-3 BASE CASE TRANSIENT CALCULATION

The feedwater-line break transient calculation was run beginning from the steady-state calculation that used different separator models on the two steam generators as described in Section 4.0. Decay power following the simulated reactor scram was preprogrammed for the experiment; therefore, this power versus time-after-trip curve was input as a boundary condition in the TRAC model. The main feedwater was stopped for both steam generators at the initiation of the transient. (The termination of feedwater is significant in that it greatly affects the transient response, as will be discussed.) Also, the auxiliary feedwater flow was input as a flow versus time-after-trip table as specified in the experiment. The pump coastdown curves were taken from the operating specifications [2] and were specified as pump speed-versus-time tables. High pressure injection flow was modeled as a pressure-dependent boundary condition.

The S-SF-3 transient event sequences for both the calculation and the experiment are given in Table 5.0.1. Except for the overpressure signal, all the events were programmed to occur at the specified time. The overpressure signal was programmed to occur when the pressurizer pressure exceeded 15.86 MPa. Receipt of the overpressure signal activated reactor scram, primary-side coolant pump coastdown, and steam isolation valve closure. The overpressure signal was calculated to occur too early because the IL primary-to-secondary heat transfer degradation began too early in the TRAC calculation. Another discrepancy between the TRAC calculation and the experiment is that the feedwater-line break flow rate was greatly underpredicted by TRAC.

Figure 5.0.1 shows the feedwater-line break mass flow rates for the TRAC calculation and for the experiment. The large mass flow spike at the beginning of the experiment was probably due to a slug of cold liquid upstream of the break valve that had not been heated during the steady state. As can be seen, the experimental data curve between 15 s and 100 s is about a factor of two greater than the TRAC-calculated curve. This was also observed in the RELAP5 post-test calculation of this experiment [7]. INEL determined in that calculation that a subcooled discharge coefficient of about 1.6 was required to match this part of the experimental data. Also, a two-phase discharge coefficient of 0.84 was used in the RELAP5 calculation to match the break flow data after 100 s. Discharge coefficients of 1.0 were used in the TRAC calculations for the entire transient. We used values of 1.0 because we felt the INEL value of 1.6 for the subcooled discharge coefficient was not physically justifiable. The two-phase discharge coefficient was not very important because the break flow was subcooled fluid for most of the transient. Also, as will be discussed, the break flow was not a dominant factor in the transient.

After 100 s, the mass flow rate in the experiment dropped to around 0.1 kg/s while the TRAC-calculated mass flow rate was about 0.3 kg/s. The reason for the drop at 100 s in the experiment can be seen in Figure 5.0.2, which shows the densities upstream of the break for the experiment and for the TRAC calculation. In the experiment, the density dropped substantially when two-phase fluid (predominately vapor) began to exit the break. This also occurred in the calculation but not until 300 s. In both the experiment and the calculation, the drop in density occurred when the BL secondary-side inventory dropped to around 15% of the initial

steady-state value as shown in Figure 5.0.3. The inventory in the experiment dropped much faster than in the calculation because of the greater initial break flow. The change in slope for the calculated inventory at 62 s is due to steam-line valve closure. Loss of BL inventory after this time was due only to the break flow.

The reason for the break flow underprediction may be a problem with the choked flow models or it may be related to an inadequate representation of the break geometry or the downcomer/boiler geometry in the TRAC input model. Based on INEL's similar difficulties with predicting the break flow using RELAP5 [7], we feel that it is unlikely that the choked-flow model is as far off as this calculation indicates, and that this particular test is not suitable for assessing TRAC's choked-flow model.

Before the simulated reactor scram, the BL steam dome pressure, as shown in Figure 5.0.4, remained relatively constant, as if no break had occurred. This is because only liquid (low specific volume) was exiting the break at this time. The underprediction of break flow therefore did not significantly affect the primary-side transient response with respect to the time of reactor scram. After reactor scram, the measured pressure decreased because the volumetric flow rate out the break was greater than the rate of vapor generation. Because the break flow rate was underpredicted, vapor generation in the calculation was sufficient to cause a pressure increase when the steam-line valve was closed at the time of reactor scram.

The phenomenon found to control the initial transient response was the heat transfer degradation that occurred as a result of feedwater termination. During the steady state, the BL steam generator secondary side had a larger inventory than the intact loop but was carrying only 20% of the heat load. Also, as already mentioned, the small feedwater-line break was not large enough to influence the transient response before the time of reactor scram. Therefore, the primary-to-secondary heat transfer was dominated by the intact loop. After the feedwater was terminated at the initiation of the transient, the IL heat transfer decreased while the BL heat transfer initially increased. However, the combined IL and BL heat transfer represented a net decrease of the heat transfer rate.

Figure 5.0.5 shows the secondary-side inventory for the intact loop. The inventory in the IL secondary side decreased at the same rate as in the experiment before reactor scram. The closure of the steam-line valve at the time of reactor scram ended the inventory decrease. Because reactor scram in the calculation occurred 26 s earlier than in the experiment, much less IL secondary-side inventory was boiled away in the calculation compared to in the experiment. Auxiliary feedwater was initiated at 150 s and caused the inventory to increase at that time.

The IL steam dome pressure after reactor scram for the calculation was greater than that in the experiment as shown in Figure 5.0.6. This is due to the greater inventory remaining in the IL secondary side in the calculation after reactor scram, as discussed previously. Vapor generation in the boiler continued, but, with the steam-line valve closed, there was about 15% less available volume for the vapor to expand into in the calculation.

The primary-to-secondary heat transfer rates for the intact loop and the broken loop are shown in Figures 5.0.7 and 5.0.8, respectively, for the TRAC calculation

and for the experiment. The combined BL and IL initial heat transfer rate in the TRAC calculation is 2.0 MW, which equals the steady-state core power as desired. The differences between the calculated and measured steady-state heat transfer rates are due to measurement uncertainty as stated in reference 7. The experimental curves should therefore be used for trend information only.

The heat transfer rate calculated automatically by TRAC was determined according to Newton's law of cooling, while the experimental rate was determined by multiplying the experimental primary-side loop mass flow rate by the specific heat and the temperature difference across the steam generator entrance and exit plena. We recalculated the TRAC heat transfer rates for several times with the same method used in the experiment and found the results to be nearly identical to the results using Newton's law of cooling. We could have included control blocks in the input to calculate the heat transfer rate the same way as in the experiment but neglected to do so (although the control blocks were added for the S-SF-5 calculation). Because the results were nearly the same for both methods, we did not bother to rerun the S-SF-3 calculations with these control blocks.

As seen in Figure 5.0.7, the IL heat transfer degradation in the TRAC calculation began almost immediately after the feedwater was terminated at the initiation of the transient. However, in the experiment, there was a delay of about 20 s before degradation began and therefore a delay in the time of reactor scram. Before reactor scram occurred, the steam line was open and core power remained at the steady-state level. Therefore, the wall-to-liquid area available for heat transfer decreased as the steam generator inventory was boiled away in the calculation. As the area decreased, the heat transfer degraded and the primary-side fluid temperature and pressure increased. The most plausible way for the heat transfer degradation to be delayed in the calculation is if the wall-to-liquid area is temporarily maintained by a fluid redistribution within the steam generator secondary side. There apparently was no such redistribution of fluid at the initiation of the transient. This indicates that the fluid distribution during steady state may not be correct in the TRAC calculation. This could be a result of inadequate geometric modeling of the steam generator or a problem with one of TRAC's hydrodynamics models such as the interfacial drag model.

As already mentioned, the BL steam generator contained a larger secondary-side inventory than the IL steam generator but was carrying only 20% of the heat load. Therefore, the BL primary-to-secondary heat transfer was not as sensitive to the loss of feedwater as was the IL steam generator heat transfer. The BL hot-leg liquid temperature, shown in Figure 5.0.9, was increasing as a result of the IL heat transfer degradation immediately upon termination of feedwater and before reactor scram. Because the wall-to-liquid heat transfer area was not decreasing as rapidly as the hot-leg temperature was increasing, the BL heat transfer rate (Figure 5.0.8) actually slightly increased before reactor scram in the TRAC calculation. To a lesser extent, a small increase in the BL heat transfer rate also occurred in the experiment.

Although there was a small increase in the heat transfer rate on the broken loop prior to scram, the large decrease on the intact loop resulted in a net decrease in the primary-to-secondary heat transfer rate. This caused the primary-side pressure to increase as demonstrated by the pressurizer pressures shown in Figure 5.0.10. The

TRAC-calculated pressure was seen to slowly increase at the initiation of the transient whereas the measured pressure slightly decreased before abruptly increasing at around 75 s. In the experiment, the pressurizer heaters were used to maintain the desired steady-state pressure. At the initiation of the transient the heaters were turned off and the pressure slowly dropped. Turning the heaters off in the experiment suppressed the pressure increase that probably would have occurred due to the initial small amount of primary-to-secondary heat transfer degradation. A small pressure decrease did not occur in the TRAC calculation because it was not necessary to use heaters to maintain the primary-side pressure. (Environmental heat losses and guard heaters were not modeled in the TRAC calculation.) The early calculated primary-side pressurization is attributed to this effect in addition to the early primary-to-secondary heat transfer degradation.

The increase in primary-side pressure resulted in a reactor scram signal being generated. Reactor scram occurred at 88 s in the experiment compared to 62 s in the TRAC calculation. (This 26 s time difference is apparent in all of the plots which demonstrate the transient response.) After reactor scram, the measured and calculated pressures decreased at about the same rate until around 150 s. At that time the calculated pressure leveled as the rate of heat transfer to the secondary sides equilibrated with the decay power. However, the experimental plots indicate at that time that the primary-to-secondary heat transfer rate was greater than the decay power and the measured pressure continued to decrease.

As mentioned earlier, the total reported primary-to-secondary steady-state heat transfer rate in the experiment did not equal the reported steady-state power; measurement uncertainty was listed as the reason for this discrepancy. This discrepancy is large enough to preclude making any comparison between heat transfer rates and decay power during the test. The pressure decrease could only have occurred if the primary-side fluid was cooling (contraction) or if fluid was escaping from the system (leakage). An approximate calculation indicates that heat losses of about 75 kW would be required to account for the measured pressure decrease rate, corresponding to a temperature decrease rate of about 0.1 K/s. All of the temperature measurements taken throughout the primary system show a temperature decrease rate that is an order of magnitude less than this after around 100 s. Because the measured temperature throughout the primary side remained relatively constant, part of the pressure decrease may be due to an increase in the primary-side leakage. The leakage would have to increase by a factor of about 3 over the reported steady-state value to account for the entire pressure decrease.

With respect to the secondary side, the early reactor scram and the underprediction of the break flow account for the differences between the calculated and measured secondary-side parameters.

Table 5.0.1. S-SF-3 Transient Sequence of Events

| Event | Time (s) Experiment | Calculation |
|---|---|---|
| Close Feedwater Valves (3 s to close) | -2 | -2 |
| Open Feedwater Break Valve, Terminate Makeup Flow, Turn Pressurizer Heaters Off | 0 | 0 |
| Primary-Side Overpressure Signal: | 88 | 62 |
| Reactor Scram<br>Begin Coolant Pump Coastdown<br>Close Steam Isolation Valves | | |
| Initiate IL and BL AFW | 150 | 150 |
| Terminate BL AFW | 300 | 300 |

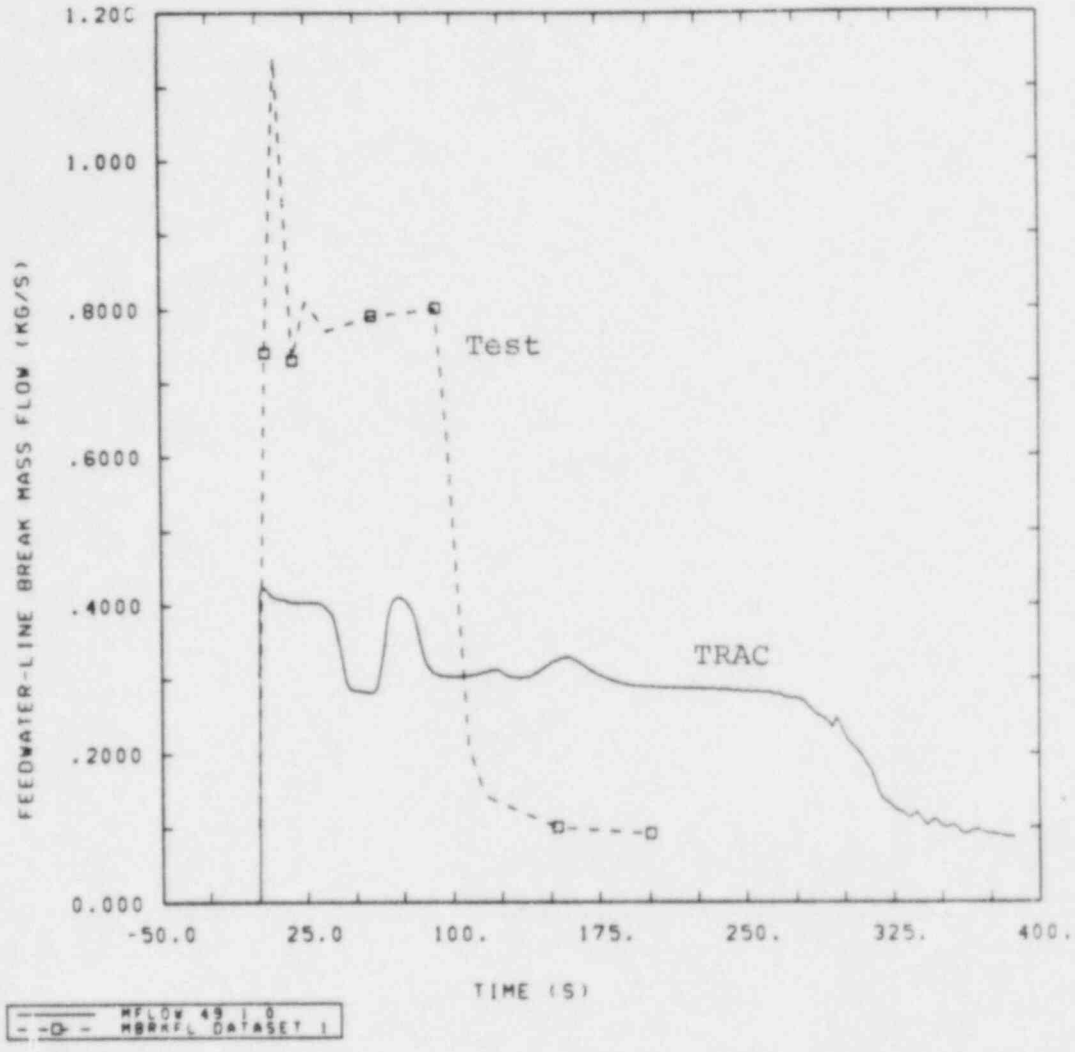


Figure 5.0.1 Feedwater-Line Break Mass Flow Rate, S-SF-3 Base Case Transient

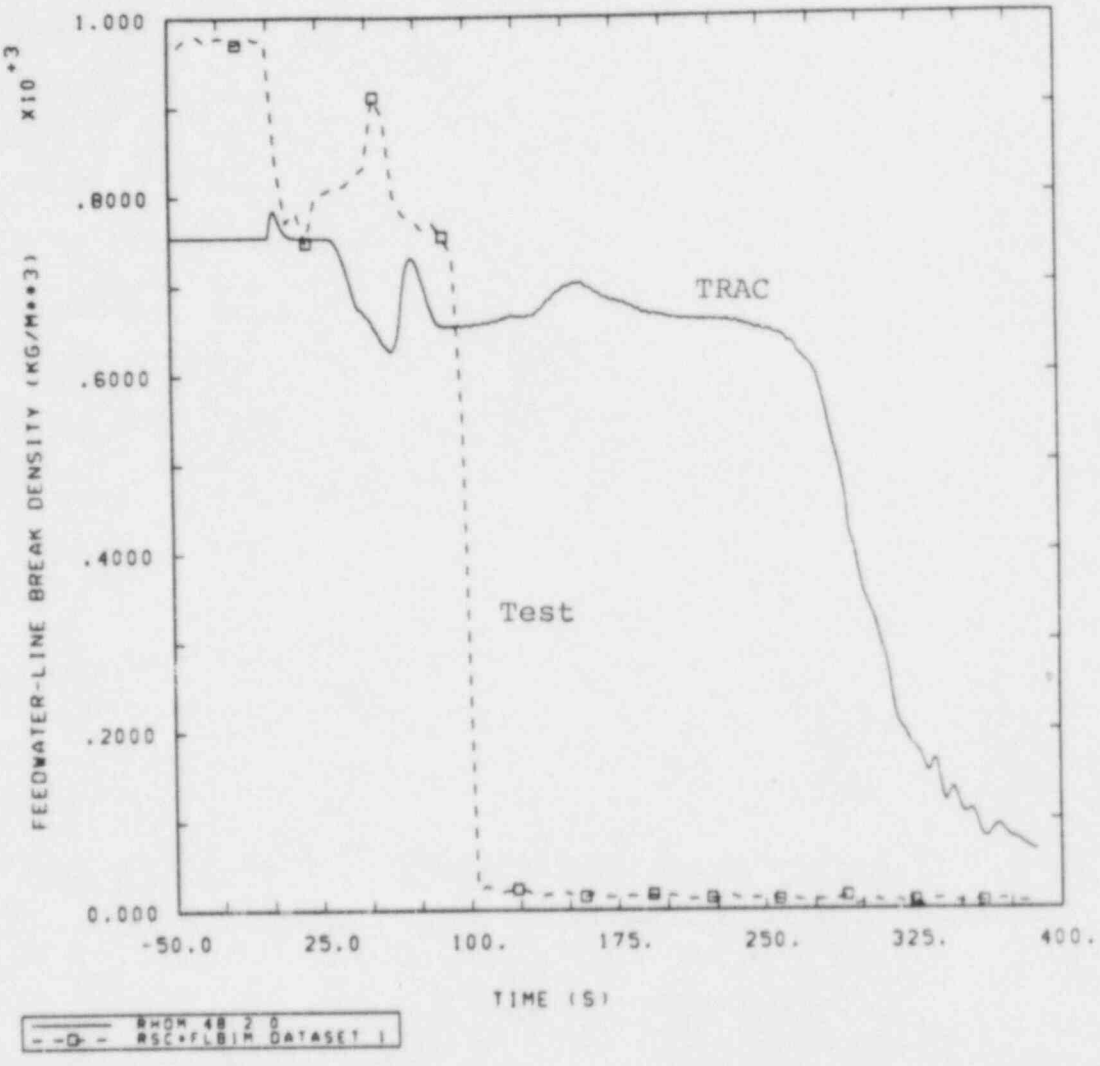


Figure 5.0.2 Fluid Density Upstream of Break, S-SF-3 Base Case Transient

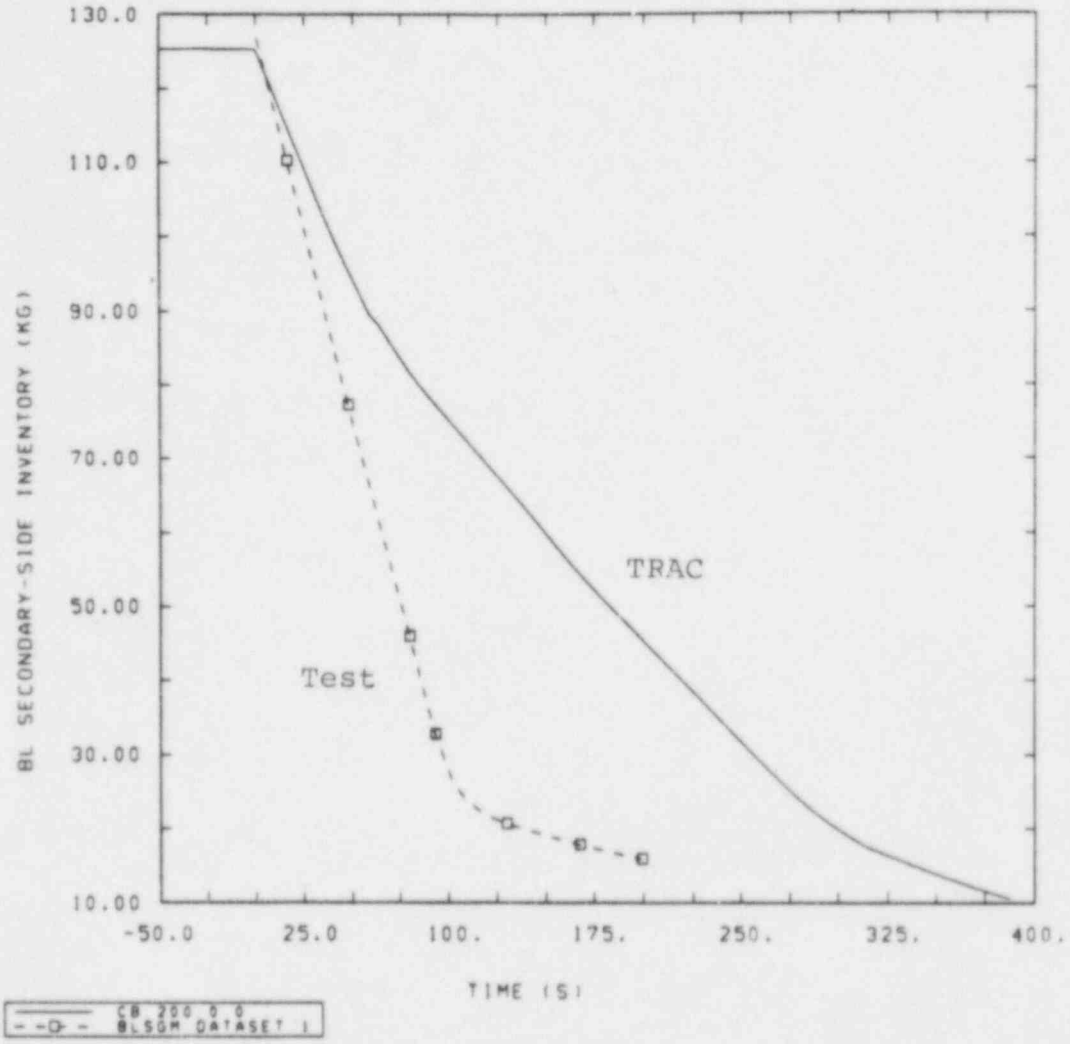


Figure 5.0.3 BL Secondary-Side Inventory, S-SF-3 Base Case Transient

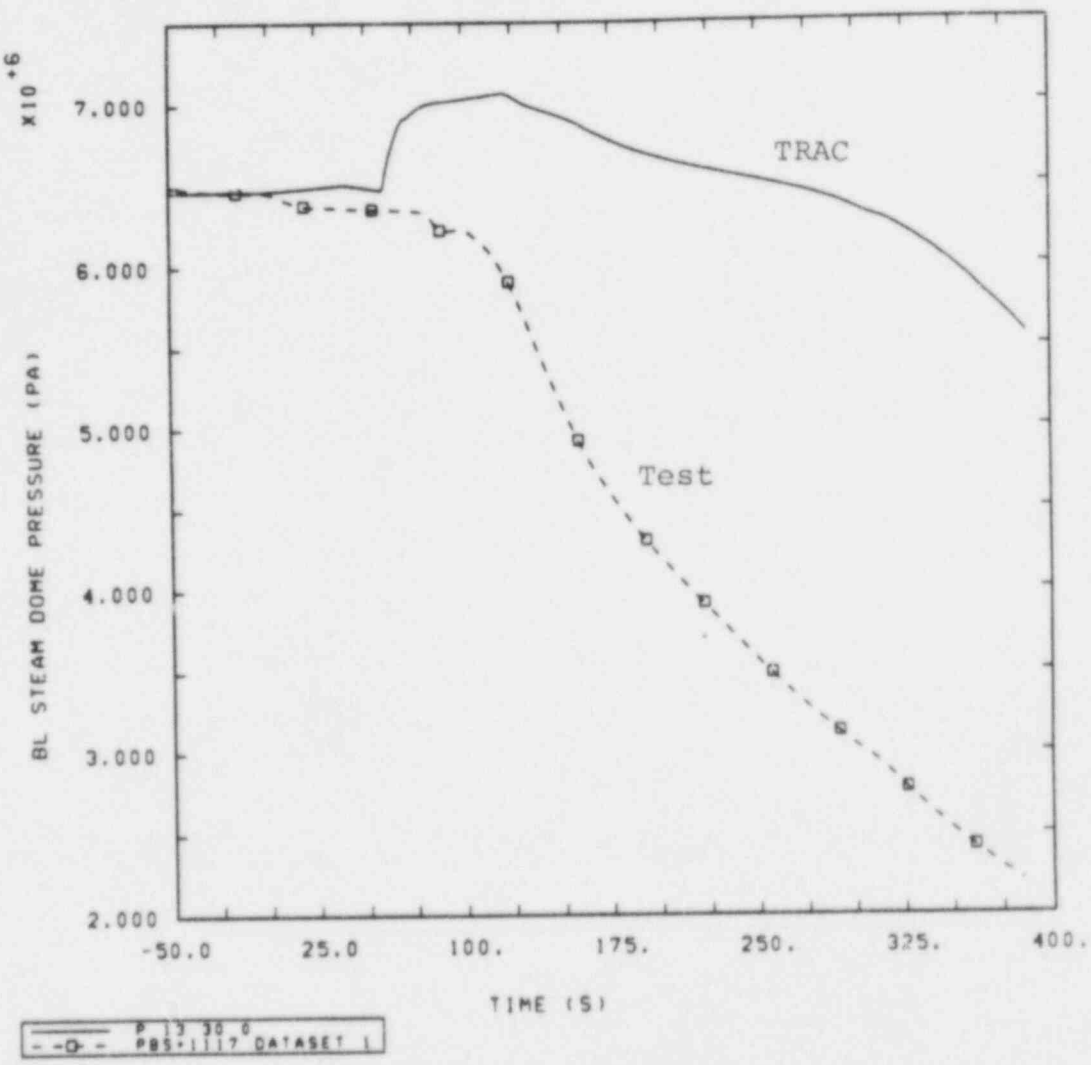


Figure 5.0.4 BL Steam Dome Pressure, S-SF-3 Base Case Transient

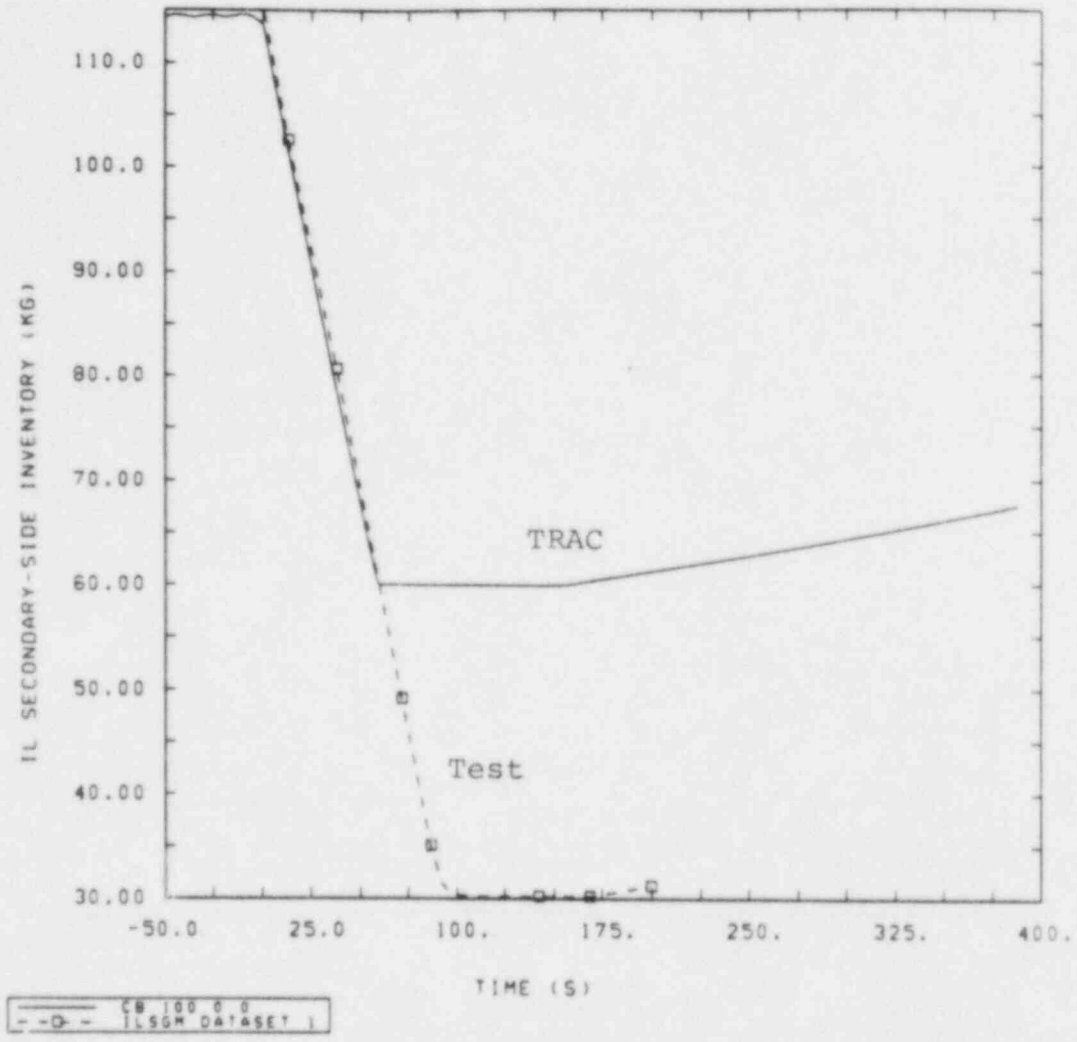


Figure 5.0.5 IL Secondary-Side Inventory, S-SF-3 Base Case Transient

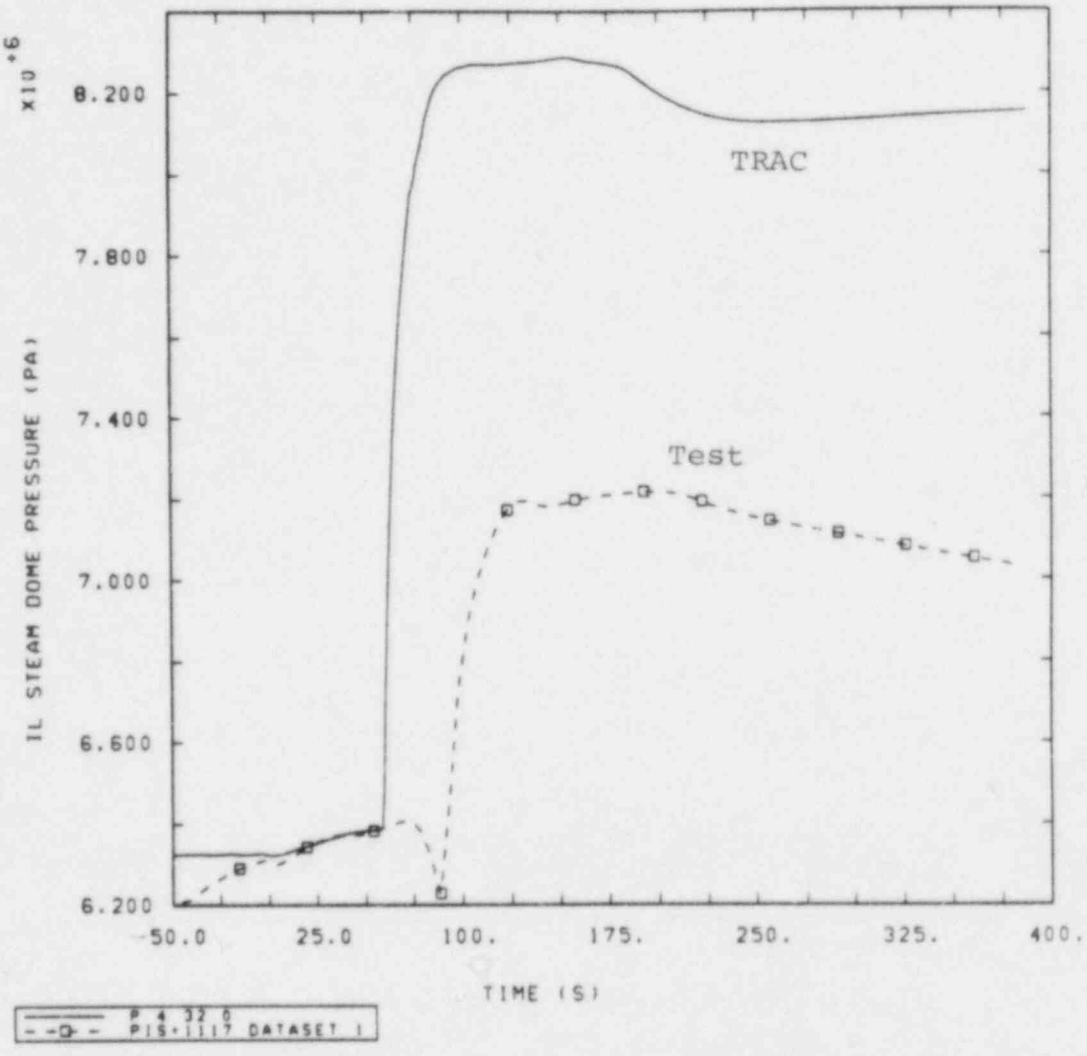


Figure 5.0.6 IL Steam Dome Pressure, S-SF-3 Base Case Transient

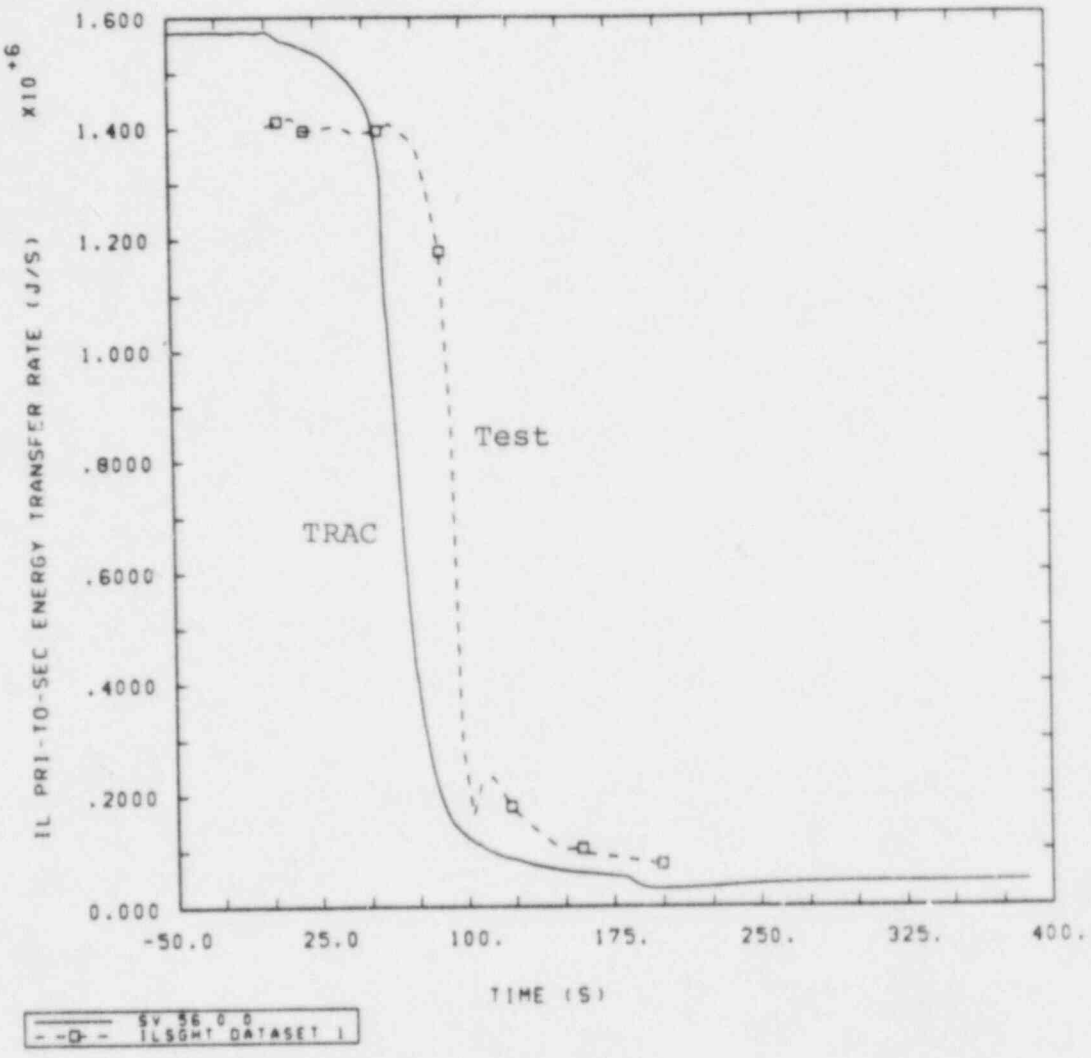


Figure 5.0.7 IL Primary-to-Secondary Heat Transfer Rate, S-SF-3 Base Case Transient

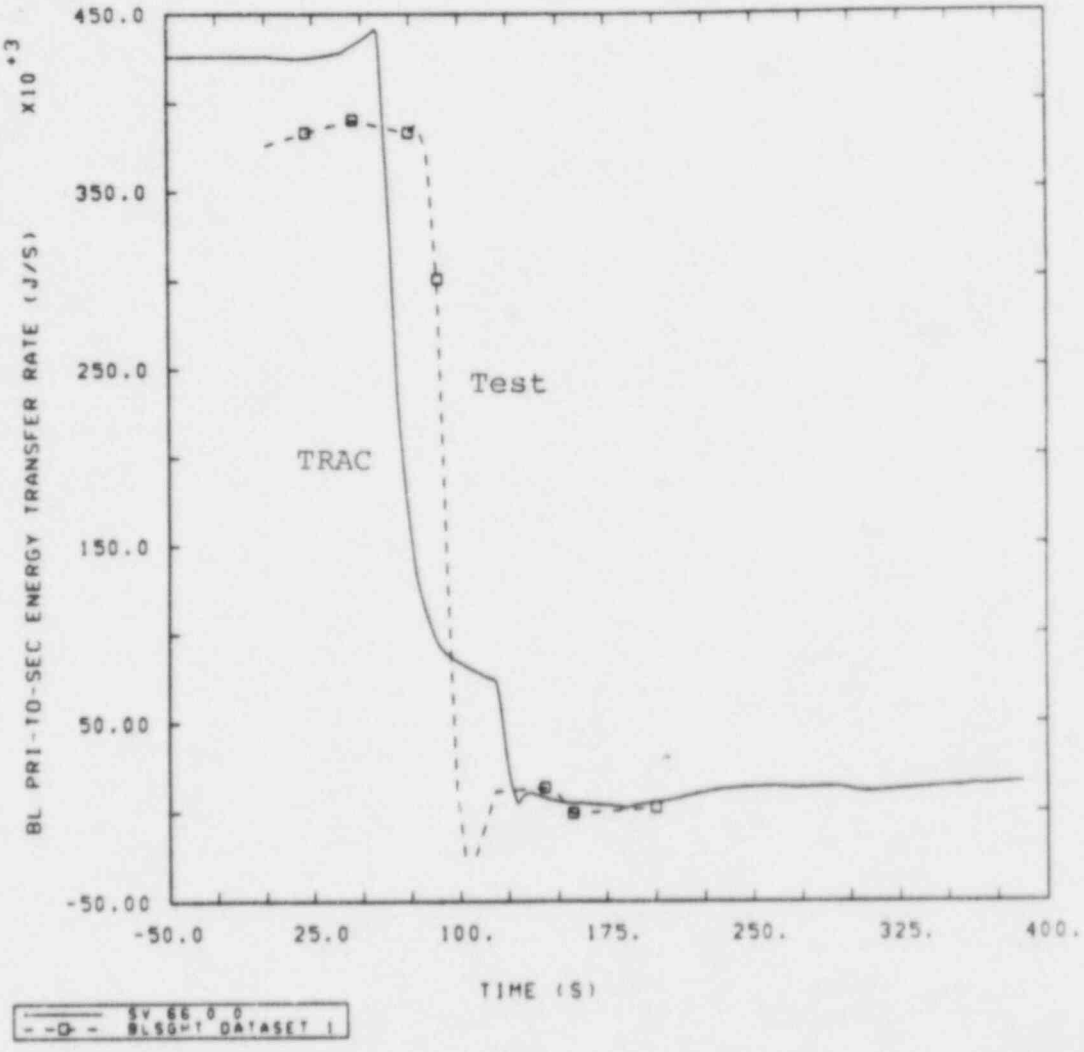


Figure 5.0.8 BL Primary-to-Secondary Heat Transfer Rate, S-SF-3 Base Case Transient

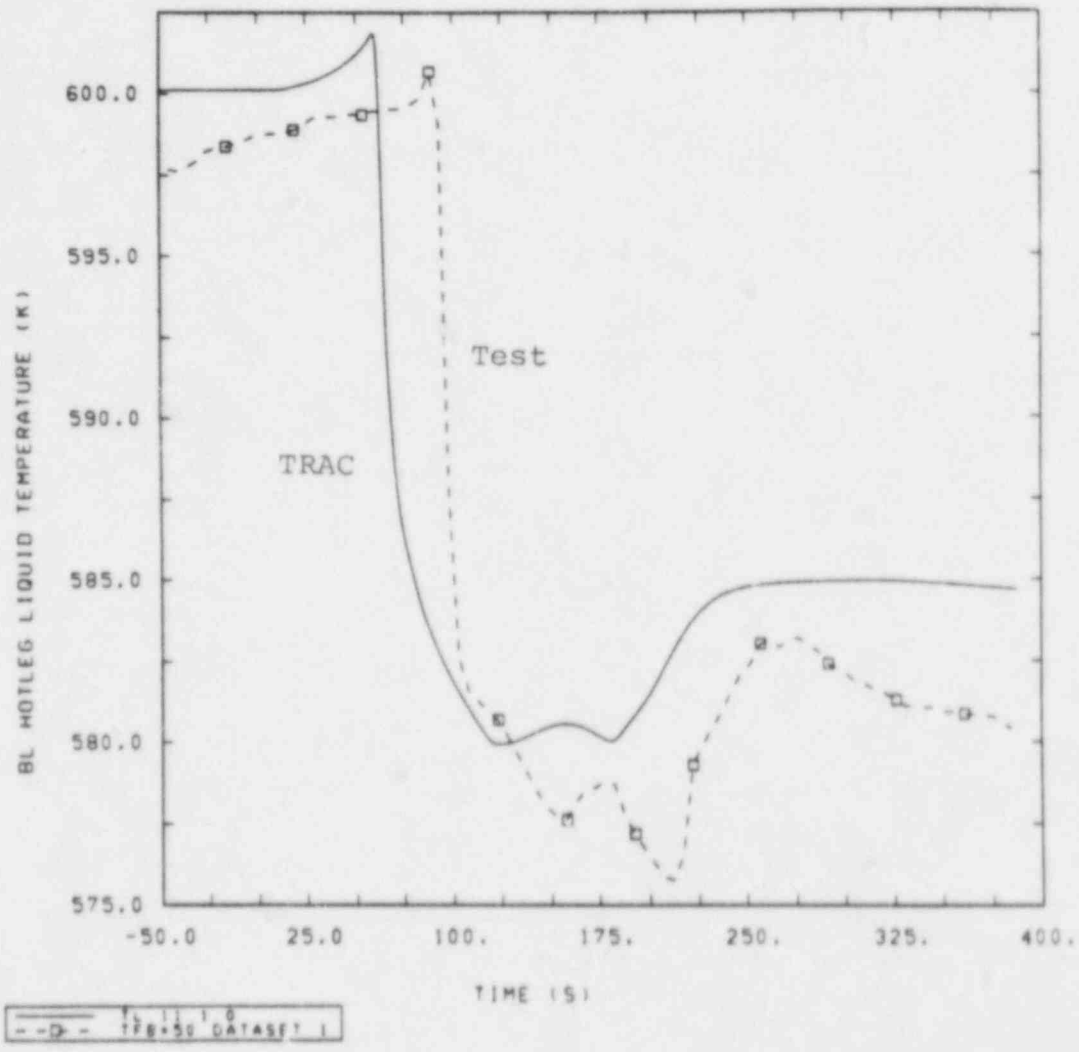


Figure 5.0.9 BL Hot-Leg Liquid Temperature, S-SF-3 Base Case Transient

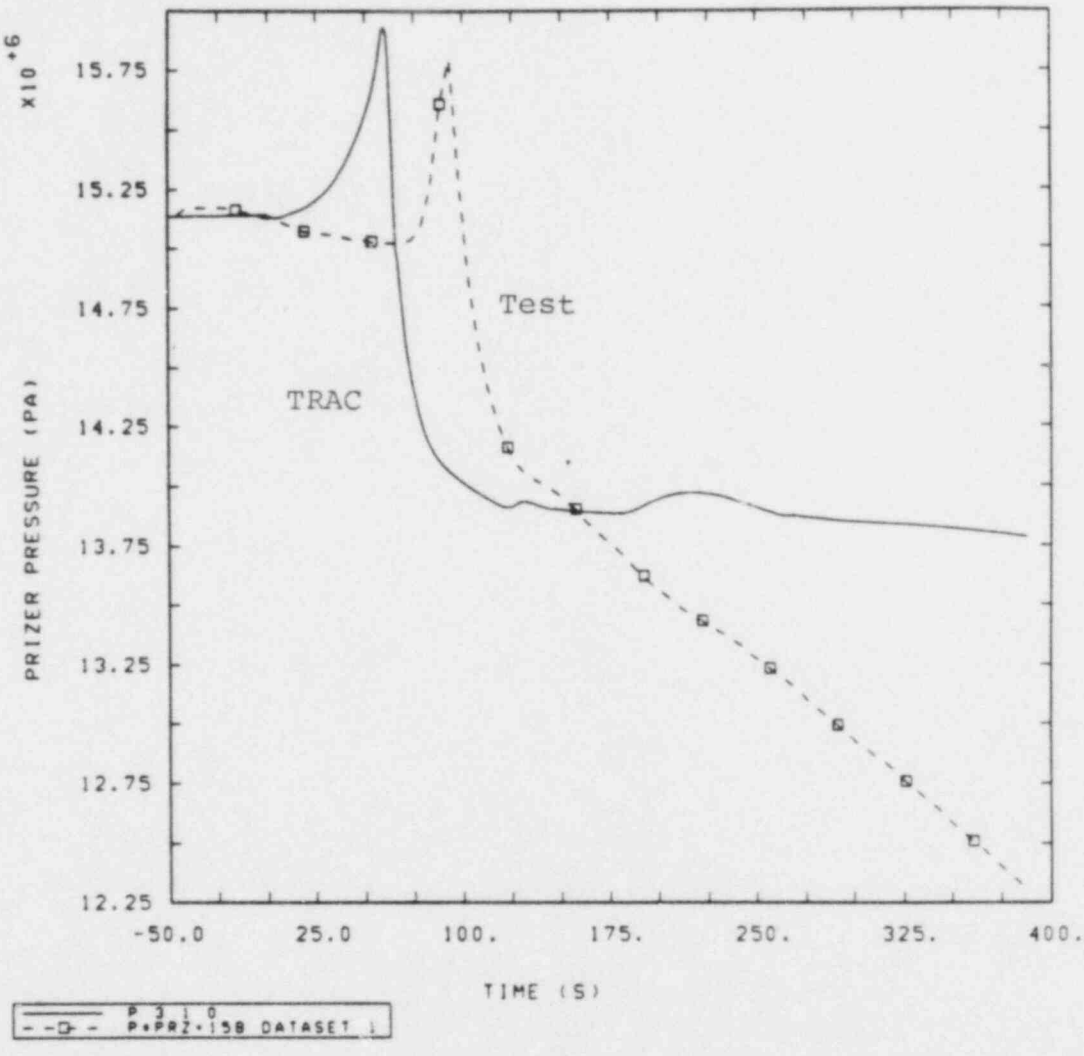


Figure 5.0.10 Pressurizer Pressure, S-SF-3 Base Case Transient

## 6.0 STEADY-STATE AND TRANSIENT PARAMETRIC CASES

We observed in the base case transient calculation that S-SF-3 was not so much a feedwater-line break transient as it was a loss-of-feedwater transient. The dominant phenomenon was observed to be the primary-to-secondary heat transfer degradation that occurred as a result of feedwater termination at the initiation of the transient. The small break in the BL feedwater line had little effect on the primary-side response, especially before around 100 s, the period of most interest. Additional work therefore, focused on investigating the heat transfer degradation phenomenon.

The base case calculation just described was run with an input model containing a 3-D VESSEL component and ran relatively slowly due to a Courant time-step limitation in the vessel. The slow running time imposed by the 3-D vessel made it desirable to develop a model using a 1-D CORE component which uses a numerical technique (the two-step solution algorithm) that does not possess a Courant limit restriction.

At the time this work was being done, the PLENUM component allowing multiple connections to a single cell was not yet available. This component allows one to easily model (compared to using only TEE components) the bypass flow paths in the vessel. Therefore, an input model was prepared using the 1-D CORE component to model the vessel, excluding the downcomer-to-upper head connection (bypass line), the support columns, the guide tube, and the upper head. These regions were excluded to greatly simplify the model. The lack of the bypass line, support columns, and guide tube would not significantly affect the transient because the primary side remains liquid full, but the lack of the upper head would affect the primary-side pressure response. This model was developed, however, to investigate only the secondary-side response during the first 90 s of this transient. This is the period of interest in which primary-to-secondary heat transfer degradation occurs, as mentioned previously. This model contained a total of 202 mesh cells (all 1-D). Calculations with this model ran with a time step of about 0.5 s compared to only 0.05 s for the calculation with the model containing the 3-D vessel. This made it much less costly to perform parametric calculations.

A steady-state calculation was run using this simple 1-D model in addition to the calculation using the 3-D vessel. The results of this calculation agree well with those from the base case 3-D vessel calculation, as summarized in Table 6.0.1 which lists some selected steady-state conditions. A base case transient calculation was also performed with this model and again the results agreed well with those from the calculation using the 3-D vessel (generally within about 5% for the temperatures and pressures). However, the intent of the 1-D model calculation was not to replace the 3-D model assessment calculation, but rather to allow a more economical means of investigating the effects of changes in initial conditions or geometry.

Table 6.0.1. S-SF-3 Steady-State Results (1-D)

| Parameter | Experiment | TRAC 3-D Model | TRAC 1-D Model |
|---|---|---|---|
| Fluid Temperatures (K): | | | |
| IL Hot Leg | 598±2.2 | 600.9 | 600.8 |
| IL Cold Leg | 563±2.2 | 569.6 | 569.5 |
| Fluid Temperatures (K): | | | |
| BL Hot Leg | 599±2.2 | 600.1 | 600.8 |
| BL Cold Leg | 561±2.2 | 566.5 | 566.7 |
| Secondary-Side Inventories (kg): | | | |
| IL | 115 | 115.0 | 114.3 |
| BL | 126 | 126.9 | 121.9 |

### 6.1 IL Secondary-Side Inventory

It is implied in reference 3 that there is a great deal of uncertainty in determining the steady-state secondary-side steam generator inventories; it would therefore be informative to know how sensitive the transient results are to this parameter. Also, it is not clear if the reported inventory represents the liquid and vapor mass or just that of the liquid. Our TRAC calculation uses the total liquid and vapor mass to determine the inventory and the vapor mass is approximately 7 kg of the total when using the reported IL inventory of 114 kg. If the liquid inventory only were used in the calculation, the total mass would be increased by 7 kg.

A parametric case was run using the 1-D model in which the steady-state IL secondary-side inventory was increased from the reported value of 114 kg to 134 kg. The value of 134 kg was chosen arbitrarily. The "extra" 20 kg of liquid was added to the secondary-side inventory during steady state; the distribution of that inventory was determined by TRAC. (When performing the calculation with an inventory of 134 kg, it was necessary to use a "large area" separator model, as was done on the broken loop, instead of the separator-K model. The separator-K model just did not work smoothly with the larger inventory. The 1-D model calculation with 114 kg inventory was rerun using the "large area" separator also to be consistent.)

In the "all 1-D" transient calculation, reactor scram occurred at 62 s when the reported inventory was used (i.e., the same inventory as used for the base case 3-D calculation). When the higher inventory of 134 kg was used, heat transfer degradation was delayed and scram occurred at 82 s. Figure 6.1.1 shows the IL primary-to-secondary heat transfer rate for both 1-D model transient calculations and demonstrates this delay when the higher inventory was used. The effect of this delay on the pressurizer pressure is shown in Figure 6.1.2. (The figures for the S-SF-3 parametric calculations do not contain comparisons to data because, as mentioned, this simplified model was developed to economically investigate the secondary-side response to various input changes. Only comparisons to other calculations using this model are legitimate.)

This calculation demonstrates that the system response for this transient is very sensitive to the initial inventory; an increase of 20 kg in the IL secondary side delays reactor scram by 20 s. The time of reactor scram in the base case calculation was off by 26 s; part of this error may be due to inventory uncertainty.

### 6.2 Break Geometry

Additional information concerning the feedwater-line break geometry was obtained from INEL [15] after this analysis was initiated. A parametric case was run in which this information was incorporated into the TRAC input model. Modifications to the geometry included changing the break pipe diameter from 1.5 inches to 2.0 inches, addition of the appropriate area change at the connection between the break pipe and the downcomer, and modifying the break-pipe elevations to reflect its approximately 15 degree downward slope. None of these changes had any significant effect on the predicted break flow rate, which was still underpredicted by almost a factor of two. Because these minor changes had no effect on the transient, we felt it was not worth rerunning the base case calculation.

### 6.3 Flow Shutter Geometry

The base case calculation indirectly indicated that the fluid distribution on the secondary side influences the heat transfer degradation during the transient. We therefore closely examined the calculated and measured steam generator results to determine if there was any input model deficiency that might change the fluid distribution. One such possibility we discovered involved the flow shutter (the connection between the boiler and the downcomer). To address this, an additional parametric case was run in which a modification was made to the flow area of the flow shutter. The experimental data indicates a pressure increase during steady state at this location, whereas a pressure drop was calculated by TRAC. The flow area was changed to reflect the relatively large flow area of the four slots at the bottom of the annular downcomer region instead of the area of the downcomer channels (see Figure A1.7). This resulted in the calculation of a pressure increase reasonably close to the experimental data. Also, the calculated total pressure drop from the top of the steam dome to the bottom of the downcomer was in good agreement with the measured value. However, this says nothing about the separate pressure drops due to flow effects and elevation head. The transient was rerun starting from this modified steady state with very little change in the results. Again, because this modification did not make any difference in the results, we did not rerun the base case calculation.

### 6.4 Recirculation Ratio

Another discrepancy discovered between the calculated and measured secondary-side results involved the IL steam generator downcomer fluid temperature. We observed that this temperature in the experiment was about 10 K less than that calculated by TRAC during the steady state. This provides further evidence that the calculated secondary-side fluid distribution during steady state is incorrect. Also, the large-K steam separator model in TRAC provides 100% separation efficiency, whereas the actual separator efficiency is less than this. It can therefore be assumed that the recirculation ratio in the TRAC calculation is incorrect. Unfortunately, both the separation efficiency and the recirculation ratio in the experiment are unknown.

A rough approximation of the recirculation ratio was obtained by performing an energy balance for the steady state using the measured feedwater flow rate (1.0 kg/s), feedwater temperature (528 K), and downcomer temperature (552 K). This balance indicated that about 0.75 kg/s of saturated liquid was flowing down the downcomer in the test, giving a recirculation ratio (downcomer flow rate divided by the feedwater flow rate) of 0.75. About 2.5 kg/s of liquid was flowing down the downcomer in the TRAC calculation (giving a recirculation ratio of about 2.6) indicating a large discrepancy in the steady-state recirculation ratio, which would influence the heat transfer degradation during the transient.

This large possible discrepancy in the recirculation ratio indicates that the calculated fluid distribution in the secondary side during steady state is grossly wrong. A possible reason for this is that the vapor generated in the boiler is entraining far too much liquid into the steam dome and downcomer. A steady-state calculation was performed in which the flow areas in the boiler were increased by a factor of 10. This resulted in much less entrainment and led to a greatly reduced

downcomer flow similar to that inferred from the experimental data. Of course, the exaggerated flow areas eliminated any chance of correctly predicting the flow-related pressure losses. This calculation was performed only to try to demonstrate the strong influence of entrainment on the recirculation ratio. (Attempts to decrease the entrainment by modifying the entrainment model in TRAC were unsuccessful.)

This calculation suggests that perhaps the distribution of the initial inventory is as important as the inventory itself. It may not be an inadequacy of TRAC's heat transfer model that causes the early calculated heat transfer degradation but rather a combination of initial inventory uncertainty along with a misdistribution of that inventory. The possible misdistribution of the inventory could be caused by a code-model or an input-model deficiency. Unfortunately, insufficient data is available to determine the actual steady-state inventory distribution.

### 6.5 Vessel Structure

After the base case and parametric calculations had been completed for the SF series of calculations, we discovered during the S-IB-3 calculation [13] that the modeling of the vessel heat slabs probably was not representative of the test and could be improved. In the Semiscale vessel and downcomer, a honeycomb insulation, between the outer walls and the fluid, effectively reduces the transfer of energy between the vessel heat structure and the fluid. The original input model did not account for this insulation. Therefore, the 1-D input model was modified, with the assumption that the honeycomb structure provided complete insulation. (Not all of the structure in the vessel was insulated.) We reran the base case calculation using this modified model and found that the effect of this change on the transient was negligible.

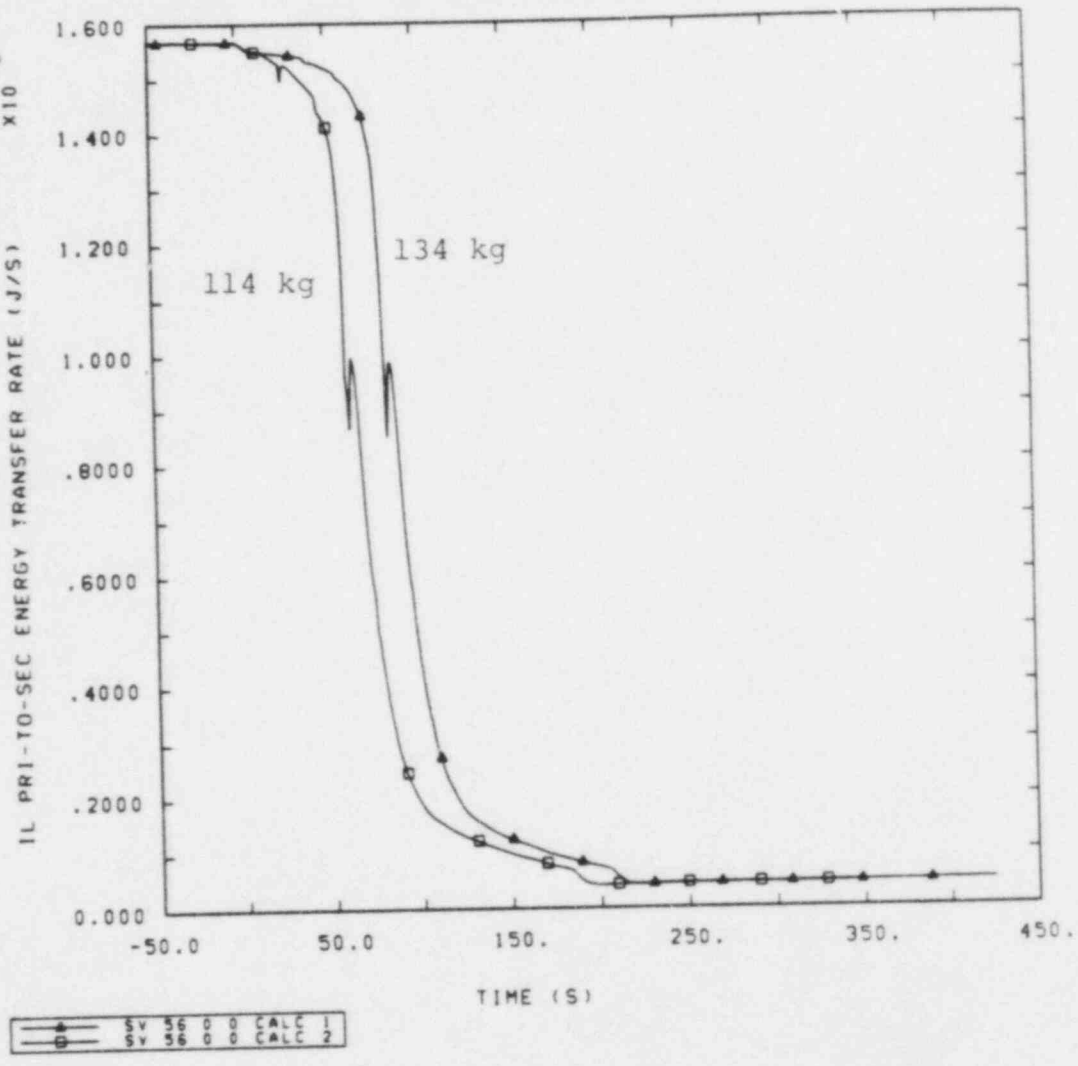


Figure 6.1.1 IL Primary-to-Secondary Heat Transfer Rate for 1-D Model Calculation, S-SF-3 IL Inventory Parametric Transient

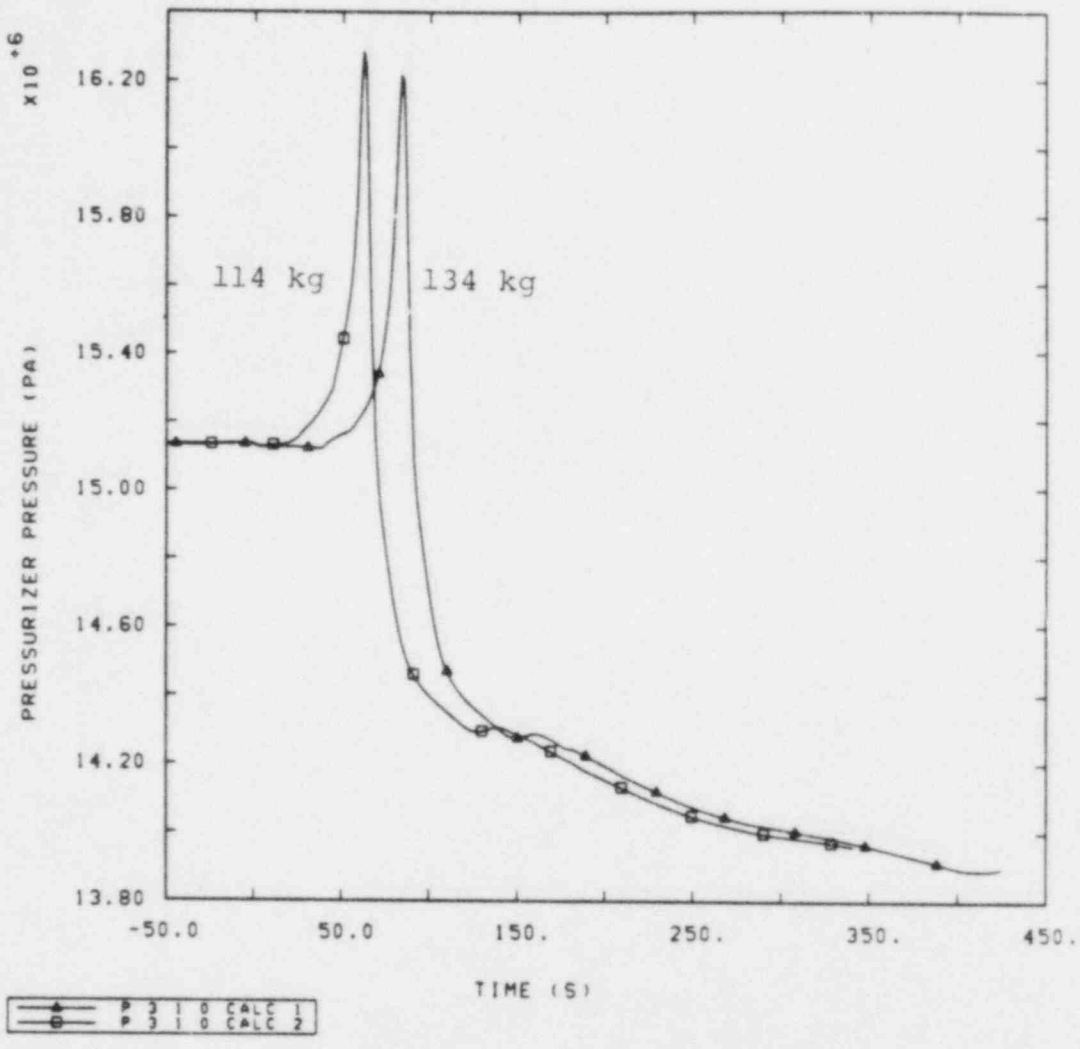


Figure 6.1.2 Pressurizer Pressure for 1-D Model Calculation, S-SF-3 IL Inventory Parametric Transient

## 7.0 S-SF-3 CONCLUSIONS

With respect to the steady-state calculations using both the base case model and the "all 1-D" model, the agreement with the experimental data is good for the major primary-side and some secondary-side parameters, such as the temperatures and flow rates. However, there is evidence that the recirculation ratio and the fluid distribution on the secondary side is incorrect, possibly due to overprediction of entrainment. Although these discrepancies do not prevent the calculation of a good steady state, they probably do have a large influence on the transient with respect to prediction of the heat transfer degradation. Also, the problems encountered with the steam separator model indicate that a better separator model would be very beneficial to the code user. The problems with the separator, however, may have been exacerbated by the possible overprediction of entrainment.

The results of the transient calculation indicate that the trends of the test were calculated reasonably well, but the timing was not. Specifically, the initiation of heat transfer degradation was not correctly predicted, which affected the rest of the calculation. Refinements in the input model involving the flow shutter geometry, break geometry, and the vessel heat slabs did not affect the calculated transient response. However, changes in the steam generator secondary-side inventory did influence the response, indicating that uncertainties associated with that quantity may account for part of the calculated heat transfer timing discrepancy. A steady-state parametric calculation with reduced entrainment indicated that perhaps the interfacial drag was not being predicted correctly for this test, which also might affect the heat transfer degradation during the transient.

In all cases, the break flow rate was not calculated correctly, but this did not significantly affect the transient response because of the small size of the break. Also, it was not surprising that the break flow rate was not calculated correctly for this test because similar difficulties were encountered by analysts at INEL using the RELAP5 code [7].

Insufficient experimental data, particularly for the secondary side, precludes making any definite conclusions about TRAC's ability to predict the timing and magnitude of heat transfer degradation. It can be inferred, however, that the calculated distribution of fluid on the secondary side is incorrect and this greatly affects the heat transfer degradation during the transient. Possible reasons for the misdistribution include overprediction of entrainment in the boiler and inadequate geometric description and modeling of the steam generators.

## 8.0 S-SF-5 STEADY-STATE CALCULATION

The base case S-SF-3 input deck, containing the 3-D vessel, was modified for the S-SF-5 steady-state and transient calculations. Modifications included changes to the control blocks, trip data, and initial conditions to reflect the S-SF-5 test. No changes to the components were required because the S-SF-3 input deck was constructed with all the necessary components for either a feedwater-line or a steam-line break. It was necessary, however, to remove the steam separators from the input model for the S-SF-5 transient calculation because liquid would accumulate in the cell beneath the separator until a large pressure pulse acted to expel that liquid. The separator models were not needed for the S-SF-5 steady state because the core power was only 30 kW; therefore, there was no liquid entrained out of the steam generator because of the extremely low secondary-side steam generation rate. For the transient, the test data indicated that the exit steam quality for the steam-line break flow was very high. In the calculation, the exit quality was also very high during most of the transient. Therefore, we felt that removal of the separators did not strongly affect the results.

The S-SF-5 boundary conditions used in the TRAC input model are given in Table 8.0.1. Table 8.0.2 compares some of the measured steady-state results to those calculated by TRAC. (The feedwater flow rates were not measured in the test.) The results agree reasonably well with experimental data. Because of the low power level for this test, the uncertainties of the temperature readings are significant and make it difficult to make a definite evaluation of the comparison to TRAC results. As was the case with the S-SF-3 steady state, the reported core power is not consistent with the power calculated by multiplying the loop flows by the loop enthalpy differences. Measurement uncertainties in the fluid temperatures and mass flow rates account for this inconsistency.

Although the core power was 30 kW, a total of 150.3 kW of power was supplied to the primary side during the steady state. The additional 120.3 kW of power was supplied by guard heaters attached to the primary-side loops and the vessel, and by the electrically-heated core to account for the large environmental heat losses. (Recall that the system was assumed to be adiabatic for the TRAC input model.) It is interesting to note that a 1% error in this augmented power would be equivalent to a 4% error in the core power which in turn would translate to approximately a 4% error in the temperature difference between the hot and cold legs. This illustrates the uncertainty introduced by the very low power in conjunction with the large environmental heat losses.

Table 8.0.1. S-SF-5 Boundary Conditions

| | |
|---|---|
| Core Power (kW): | 30.0 |
| Pressurizer Pressure (MPa): | 15.63 |
| Pressurizer Liquid Mass (kg): | 11.4 |
| Loop Flow Rates (kg/s): | |
| IL | 7.13 |
| BL | 2.44 |
| Secondary-Side Pressures (MPa): | |
| IL | 6.84 |
| BL | 6.43 |
| Feedwater Temperatures (K): | |
| IL | 503.0 |
| BL | 553.0 |
| Auxiliary Feedwater Temperatures (K): | |
| IL | 293.3 |
| BL | 293.3 |
| HPI Liquid Temperature (K): | 298.0 |

Table 8.0.2. S-SF-5 Steady-State Results

| Parameter | Measured | Calculated |
|---|---|---|
| Fluid Temperatures (K): | | |
| IL Cold Leg | 557±2.2 | 558.2 |
| BL Cold Leg | 555±2.2 | 556.4 |
| Fluid Temperatures (K): | | |
| IL Hot Leg | 559±2.2 | 558.3 |
| BL Hot Leg | 560±2.2 | 558.3 |
| Secondary-Side Inventories (kg): | | |
| IL | 118.1 | 118.9 |
| BL | 42.8 | 42.4 |
| Pump Speeds (rad/s): | | |
| IL | 207±5 | 201.8 |
| BL | 1034±21 | 1406.0 |
| Feedwater Flows (kg/s): | | |
| IL | unavailable | 0.00775 |
| BL | unavailable | 0.01047 |
| Leakage (m**3/s): | 1.1E-5 | 1.1E-5 |

## 9.0 S-SF-5 BASE CASE TRANSIENT CALCULATION

As mentioned in Section 6.5, two different methods of modeling the vessel heat slabs were tried and this did not make any difference in the S-SF-3 transient calculations. However, the effect of this change for the S-SF-5 transient calculations was significant enough to warrant redoing the S-SF-5 calculations with the revised model; it is these calculations using the revised model (with the 3-D vessel) that are discussed in Sections 9.0 through 10.3.

In the revised model, the honeycomb structure provided complete insulation, whereas, in the original model, it provided no insulation. The revised model was chosen for the base case because we felt that this approach was a more realistic representation, even though the true insulating ability of the honeycomb structure probably lies somewhere in between the two bounds. No data was available to help us determine the true insulating ability.

The steam-line break transient calculation was run beginning from the steady-state calculation described in Section 8.0. Core power remained constant and the coolant pumps remained running throughout the transient. Also, the auxiliary feedwater flow was input as a flow versus time-after-trip table as specified in the experiment and HPI flow was modeled as a pressure-dependent boundary condition.

The S-SF-5 transient sequences of events for both the calculation and the experiment are given in Table 9.0.1. The primary-side low-pressure signal was programmed to occur 25 s after the pressurizer pressure dropped below 14.41 MPa. The BL low-pressure signal was programmed to occur when the BL secondary-side pressure dropped below 4.13 MPa. The table shows that both low-pressure signals were calculated to occur too early. Receipt of the primary-side low-pressure signal activated HPI flow and receipt of the secondary-side low-pressure signal activated AFW flow and steam-line valve closure. About 18 s was required (according to the experimental data) for the IL steam-line valve to close and end IL secondary-side blowdown.

Figures 9.0.1 through 9.0.10 illustrate the secondary-side response to the steam-line break. The steam-line break flow rates for both steam generators are shown in Figures 9.0.1 and 9.0.2. With discharge coefficients of 1.0, the break flow for the broken loop is about 40% high while the break flow for the intact loop is in fairly good agreement with the data (about 8% low). (The RELAP5 post-test calculations [8] required two-phase discharge coefficients of 0.84 for the intact loop and 0.55 for the broken loop in order to match the data.) The flow spike, from about 5 to 20 s in the calculation for the intact loop, was the result of the level swell that occurred during blowdown along with the fact that the steam separators were not modeled. During this time, liquid that would have been separated from the steam was flowing out the break. This did not happen in the broken loop because the initial water level was only about one-third that of the intact loop.

The effect of this flow spike on the secondary-side depressurization and the primary-to-secondary heat transfer was not significant because of the short duration of the spike and the relatively small amount of liquid lost. The volumetric flow during this spike actually decreased, as shown in Figure 9.0.3; therefore, there was no sudden depressurization due to the mass flow rate spike. Although the liquid lost

would no longer be available for energy removal, it really didn't matter because the heat transfer was overpredicted and because there was a large amount of liquid remaining after the IL steam-line valve closed. (An attempt was made to model the separator on the intact loop; this attempt was unsuccessful because liquid accumulated in the steam dome during blowdown, resulting in a large pressure spike.)

The BL steam dome pressure, shown in Figure 9.0.4, decreased slightly faster in the calculation than in the experiment as a result of the overprediction of the break flow. There was good agreement between the calculation and experiment for the IL steam dome pressure, as shown in Figure 9.0.5. The IL steam-line valve began to close at around 62 s in the calculation, at which time the pressure began to increase. The valve began closing earlier in the calculation than in the experiment because the calculated BL steam dome pressure was decreasing faster than in the experiment.

Figure 9.0.6 shows the BL secondary-side inventories for the calculation and the experiment. Because the BL break flow was overpredicted, the inventory was dropping somewhat faster in the calculation than in the experiment. The inventories for the intact loop are shown in Figure 9.0.7; again, agreement between the calculation and experiment is good until the time of IL steam-line valve closure.

The fluid temperatures in the downcomers (about 3.0 m from the bottom) of both the BL and IL steam generators are plotted in Figures 9.0.8 and 9.0.9, respectively. Both the liquid and vapor temperatures for the calculation are included. The agreement for the broken loop is fairly good. At about 100 s, the downcomer is almost empty in the calculation (the vapor fraction is about 0.98) at this elevation. The calculated liquid temperature, therefore, reflects the saturation temperature and the vapor is superheated due to the heat transfer from the hot metal walls in the calculation. The slopes of the curves for the intact loop are about the same for the calculation and the experiment; the magnitudes differ, however, even during the steady state.

During the steady-state calculation, energy was being transferred from the boiler to the downcomer fluid via the heat structure used to model the downcomer wall (between the boiler and downcomer). In the test, the boiler filler pieces (filled mostly with air) apparently provided sufficient insulation to prevent the downcomer wall and downcomer fluid from heating. (In a full-power steady state, the downcomer fluid is heated by the flow of hot steam from the boiler (recirculation); the S-SF-5 steady state, however, was run at hot zero power and therefore, there was no such recirculation flow.)

To investigate the possibility of the filler pieces providing insulation, the calculation was rerun with the downcomer wall area reduced by an arbitrary factor of 1000.0. This had the effect of preventing the downcomer wall from heating during the steady state. The calculated downcomer fluid temperature for this case, shown in Figure 9.0.10, agreed much better with the measured value, especially during the steady state. Also, after IL steam-line valve closure in the transient, the cooling capacity of the auxiliary feedwater was not being depleted by the stored energy of the downcomer wall. Overall, the effect of reducing the wall area in the calculation on the steady-state and transient responses was negligible because of the relatively small amount of energy involved. (The S-SF-3 calculations also showed no significant effect from this change.)

Figures 9.0.11 through 9.0.22 demonstrate the primary-side response to the secondary-side steam-line break. Before the IL steam-line valve closure, the combined IL and BL primary-to-secondary heat transfer was overpredicted, as demonstrated in Figures 9.0.11 and 9.0.12, which show the measured and calculated heat transfer rates for the intact loop and broken loop, respectively. The heat transfer rates were computed by multiplying the primary-side mass flow rate by the liquid's specific heat times the temperature difference across the steam generator primary-side inlet and outlet. This method of computing the heat transfer rate is consistent with the way it was computed for the test.

Due to the early-time overprediction of the heat transfer, the primary-side fluid cooled too rapidly and the resulting fluid contraction caused the calculated pressure to drop faster than the measured pressure, as shown in Figure 9.0.13.

The IL and BL hot- and cold-leg fluid temperatures, given in Figures 9.0.14 through 9.0.17, demonstrate the primary-side fluid overcooling. Because the coolant pumps remained running throughout the transient, the loop volumetric flows remained constant although the loop mass flow rates slowly increased as the primary-side liquid cooled. The difference between the calculated and measured loop volumetric flows was less than 1% while the difference between the calculated and measured loop mass flow rates was within about 4%.

After the IL steam-line valve closure, the BL heat transfer was overpredicted but the IL heat transfer was underpredicted. (The IL heat transfer drops rapidly at about 100 s due to closure of the steam-line valve, thus ending IL secondary-side blowdown.) In fact, the calculated IL heat transfer dropped below zero, indicating secondary-to-primary heat transfer. The reason this occurred is related to the modeling of the filler pieces on the secondary side, as discussed earlier. With the base case model, in which the filler pieces were not modeled as perfect insulators, the cooling capacity of the auxiliary feedwater was being depleted by the stored energy in the downcomer wall; thus, the fluid temperature on the secondary side was not cooled by the auxiliary feedwater. When the filler pieces were assumed to provide perfect insulation, as the data indirectly indicates, the heat transfer did not reverse because the cold auxiliary feedwater reduced the secondary-side fluid temperature below that of the primary-side fluid. The reverse heat transfer in the base case calculation, however, did not have a significant effect on the primary-side response because of the relatively small amount of energy involved.

It is interesting to note that the measured heat transfer after valve closure was about 100 kW, which is greater than the energy removal capacity of the auxiliary feedwater (60 kW). This discrepancy is probably due to the heat losses to the environment (approximately 6 kW for each steam generator [3]) along with the temperature measurement uncertainty associated with the computation of the measured heat transfer rate. (Recall that the measured heat transfer rate was computed by multiplying the primary-side mass flow rate by the liquid's specific heat by the temperature difference across the steam generator primary-side inlet and outlet; the importance of the measurement error is emphasized by the very small temperature difference that exists after steam-line valve closure.)

In an overcooling transient such as this, the cooling of the primary-side fluid is also influenced by the amount of energy transferred to the fluid from the

primary-side structure during the transient. The heat transfer rates from the internal vessel structure (not all structure was insulated) and from the fuel rods (the dominant sources in the calculation) are given in Figures 9.0.18 and 9.0.19, respectively. These quantities were not measured during the experiment but the calculated values are included here to give the reader an idea of their magnitude.

After IL steam-line valve closure, the calculated pressure was increasing while the measured pressure was slowly decreasing as was shown in Figure 9.13. The following analysis was performed to help us better understand the reason for this discrepancy.

Whether the primary-side pressure increases or decreases depends on the net rate of change of the primary-side fluid volume. This net change can be expressed as the sum of four terms:

(1) rate of volume change due to fluid contraction or expansion,
(2) rate of volume change due to primary-side leakage,
(3) rate of volume change due to HPI flow, and
(4) rate of volume change due to phase change (vaporization or condensation)

If the primary-side fluid temperature is decreasing, the fluid contracts and the first term is negative. The second term is always negative while the third term is always positive. The fourth term depends on the first three terms. If the sum of the first three terms is less than zero, the pressure will decrease and as a result, some of the saturated liquid in the pressurizer will vaporize; this will slow the rate of depressurization. Contrariwise, if the sum of the first three terms is positive, the pressure will increase and, as a result, some of the vapor in the pressurizer will condense and slow the rate of pressurization. (This term can also be affected by pressurizer environmental heat losses. If the losses are large enough, cooling of the pressurizer walls could be sufficient to greatly enhance vapor condensation in the pressurizer. Because the pressurizer was insulated, we assumed that no such heat losses occurred; there was no measurement of the pressurizer wall temperatures to verify this, however. Also, pressurizer heaters were not used during the transient tests.) Because the fourth term only slows the rate of pressurization or depressurization, the sum of the first three terms can be used to indicate if the primary-side pressure is increasing or decreasing.

After IL steam-line valve closure, the calculated primary-side pressure increased; this is consistent with the net rate of change of the primary-side fluid volume as calculated according to the preceding prescription. Application of this prescription using data from the test indicates that the measured pressure should also be increasing, contrary to the measured response. A possible explanation for this discrepancy is that the leakage rate, determined only during the steady-state portion of the experiment, was much larger during the transient.

Figure 9.0.20 shows the pressurizer volumetric flow for the experiment and the calculation. As mentioned, the rate of change of the primary-side fluid volume is greater in the calculation than in the experiment before the time of IL steam-line valve closure. After closure, the flow continued out of the pressurizer in the

experiment. If the above prescription is used with the net rate of change of fluid volume set equal to the measured pressurizer outflow, the leakage rate would have to be about 7.0 times greater than the reported steady-state value for the prescription to balance.

If the pressurizer volumetric outflow is instead determined by multiplying the pressurizer fluid cross-sectional area by the slope of the pressurizer water level curve (Figure 9.0.21), and the above computation repeated, the leakage would have to be about 3.5 times greater for the prescription to balance. (A calibration error existed in the measured water level curve; this curve is for trend information only.) Based on either computation, it seems that leakage must have increased during the experiment, to a value greater than the steady-state value, to account for the decreasing pressure.

Application of the rate-of-change of volume prescription just described involved a good deal of uncertainty because of the approximation required to estimate the contraction/expansion term. This term can be calculated as the mass of the primary-side fluid multiplied by the rate-of-change of the primary-side fluid specific volume. The rate-of-change of the specific volume can be estimated from the slope of a fluid temperature-versus-time curve along with the equation of state to convert the temperatures to specific volumes. Of course, such a curve for the entire primary system during the experiment does not exist. Therefore, an average slope was calculated using the temperature plots from several different locations in the primary system. It was also necessary to approximate the mass of the primary-side fluid.

Despite the uncertainty of this method, use of the prescription provided insight into the sensitivity of the prediction of the primary-side pressure response. Before the time of IL steam-line valve closure, the contraction term was the dominant term in the prescription. After valve closure, this term was small compared to the effects of the leakage and HPI terms. The calculated HPI flow agrees reasonably well with the measured flow as shown in Figure 9.0.22. The flow began earlier in the calculation because the pressure was calculated to drop too rapidly, thereby causing the low-pressure trip signal to be reached too soon. (The initial flow spike seen in the experiment is probably due to a slug of cold liquid in the injection lines.) Because the leakage is of the same order of magnitude as the HPI flow, the system response is a strong function of the leakage, especially after IL steam-line valve closure.

Table 9.0.1. S-SF-5 Transient Sequence of Events

| Event | Time (s) Experiment | Calculation |
|---|---|---|
| Close Feedwater Valves (3 s to close) | -2 | -2 |
| Initiate Steam-Line Break, Terminate Makeup Flow | 0 | 0 |
| Primary-Side | | |
| Low-Pressure Signal: Initiate HPI Flow | 70 | 51 |
| BL Secondary-Side Low-Pressure Signal: Initiate IL and BL AFW, Close IL Steam-Line Valve | 80 | 62 |

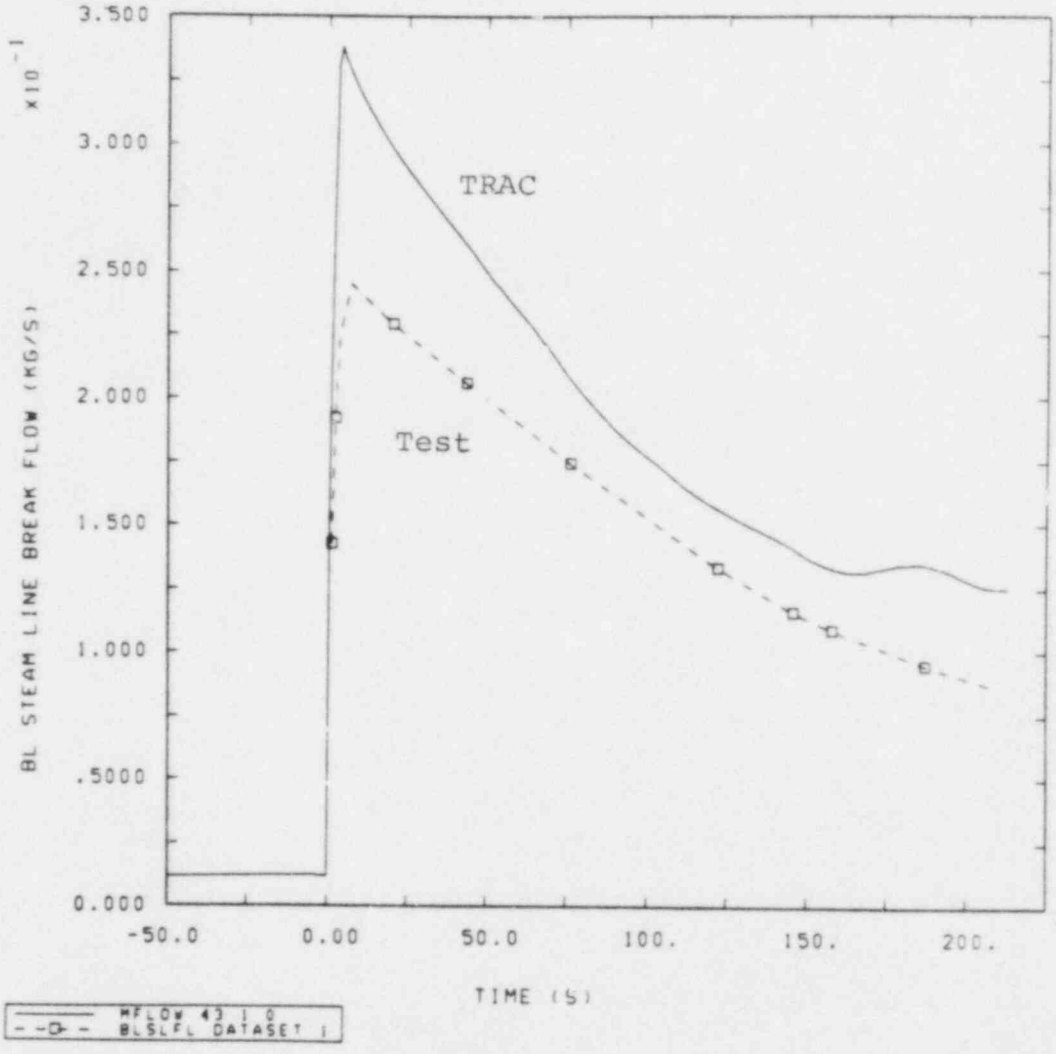


Figure 9.0.1 BL Steam-Line Break Flow Rate, S-SF-5 Base Case Transient

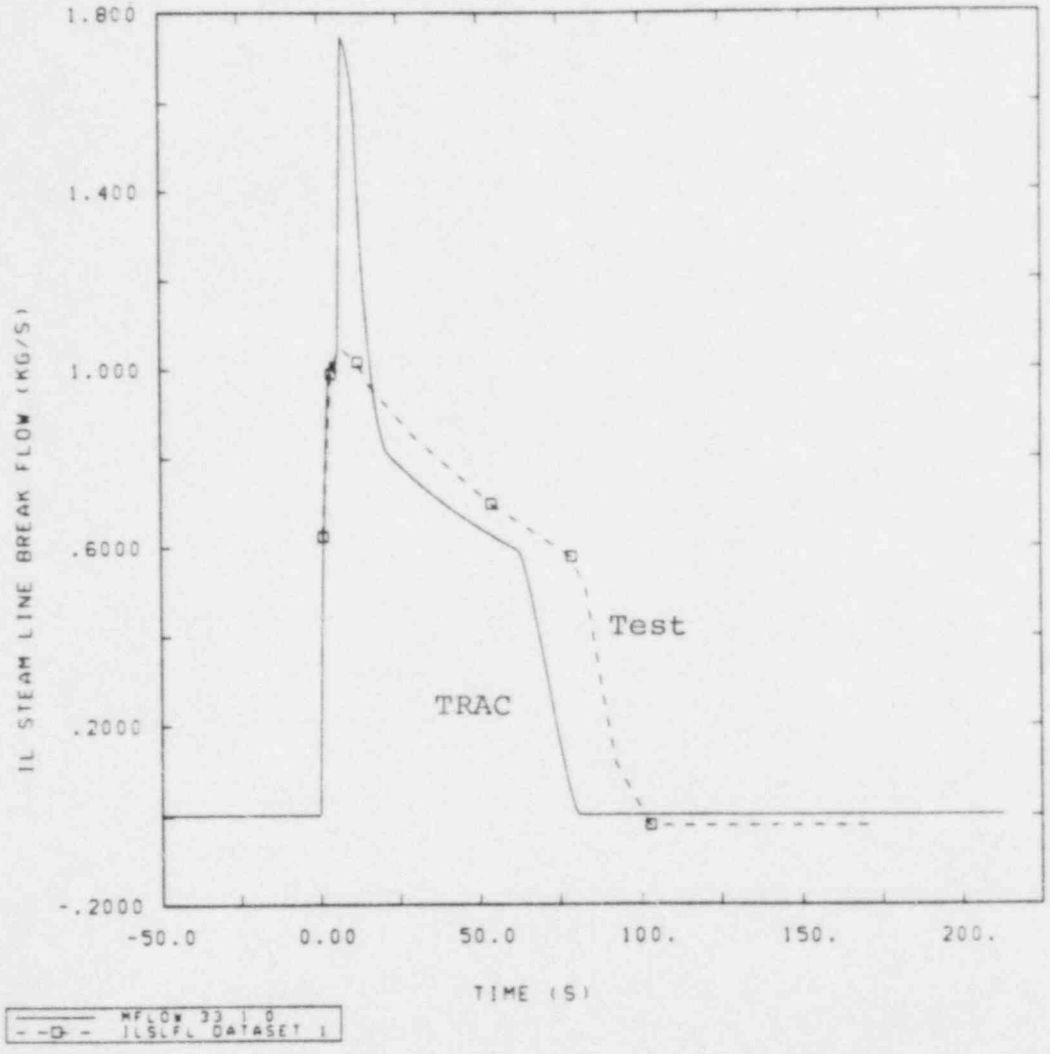


Figure 9.0.2 IL Steam-Line Break Flow Rate, S-SF-5 Base Case Transient

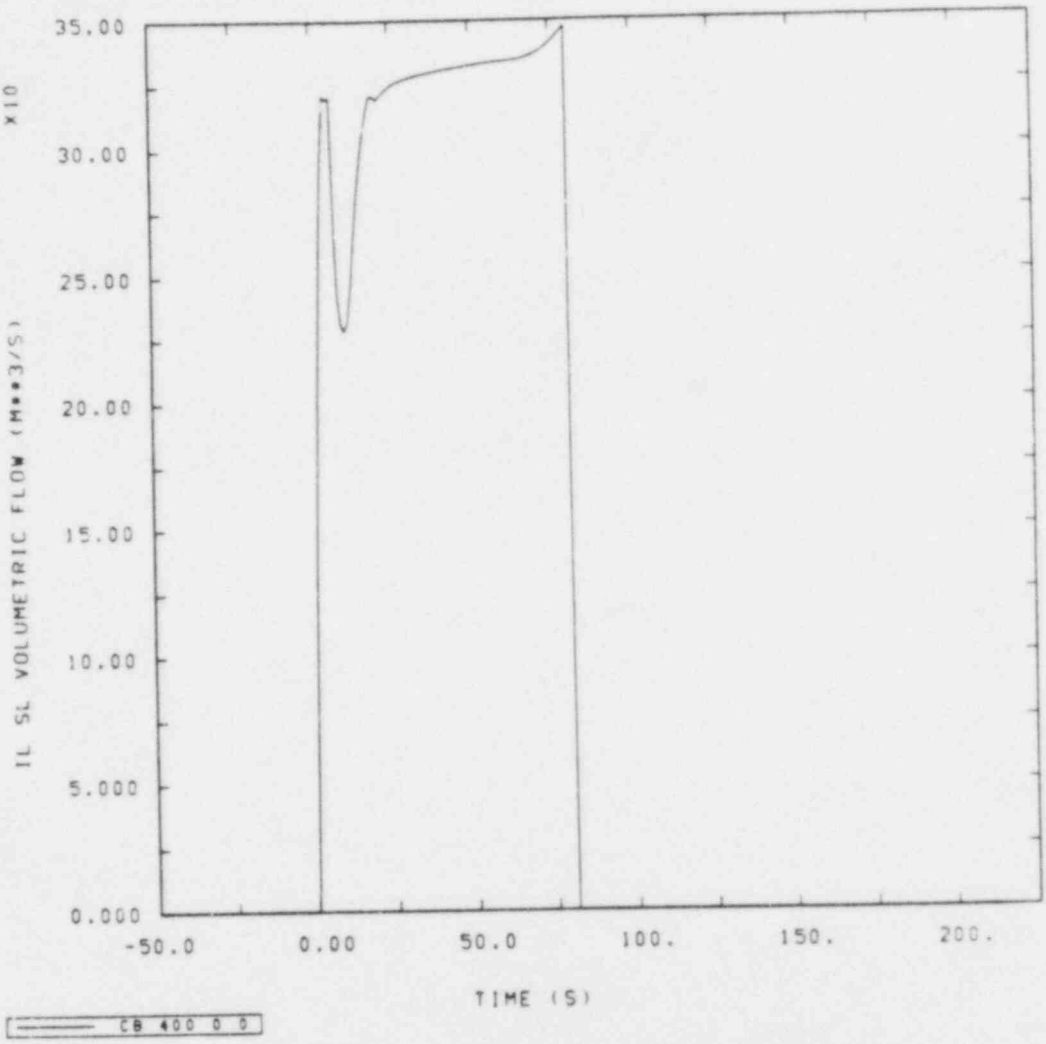


Figure 9.0.3 IL Steam-Line Volumetric Flow Rate, S-SF-5 Base Case Transient

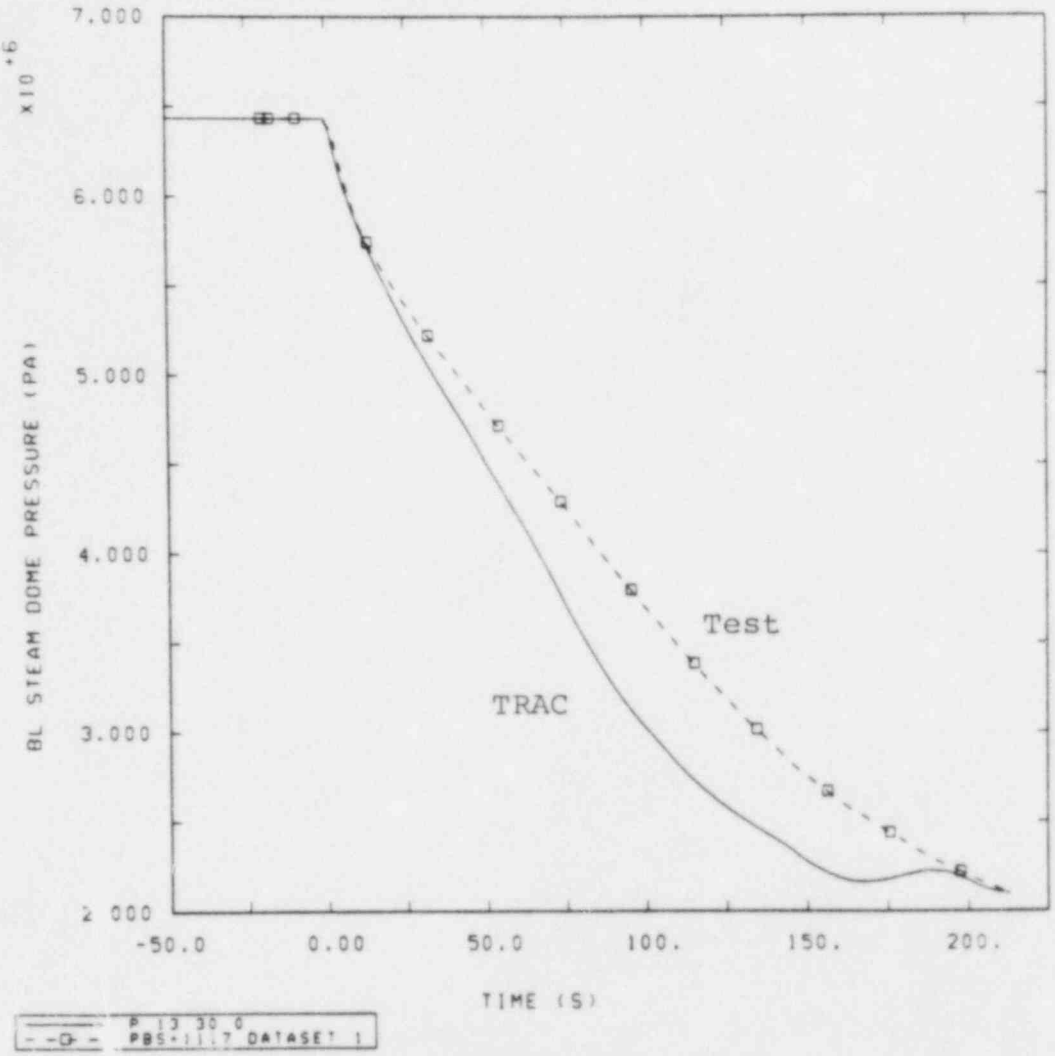


Figure 9.0.4 BL Steam Dome Pressure, S-SF-5 Base Case Transient

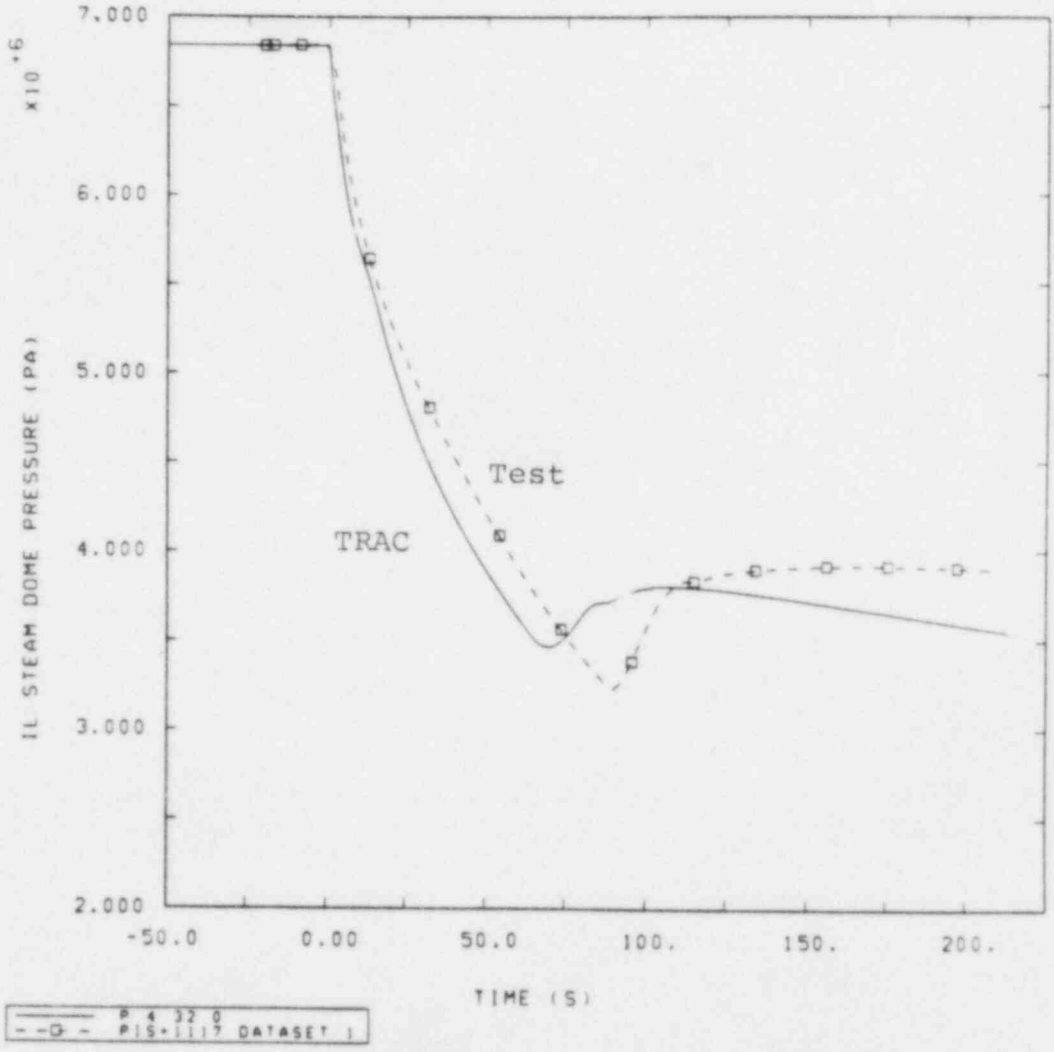


Figure 9.0.5 IL Steam Dome Pressure, S-SF-5 Base Case Transient

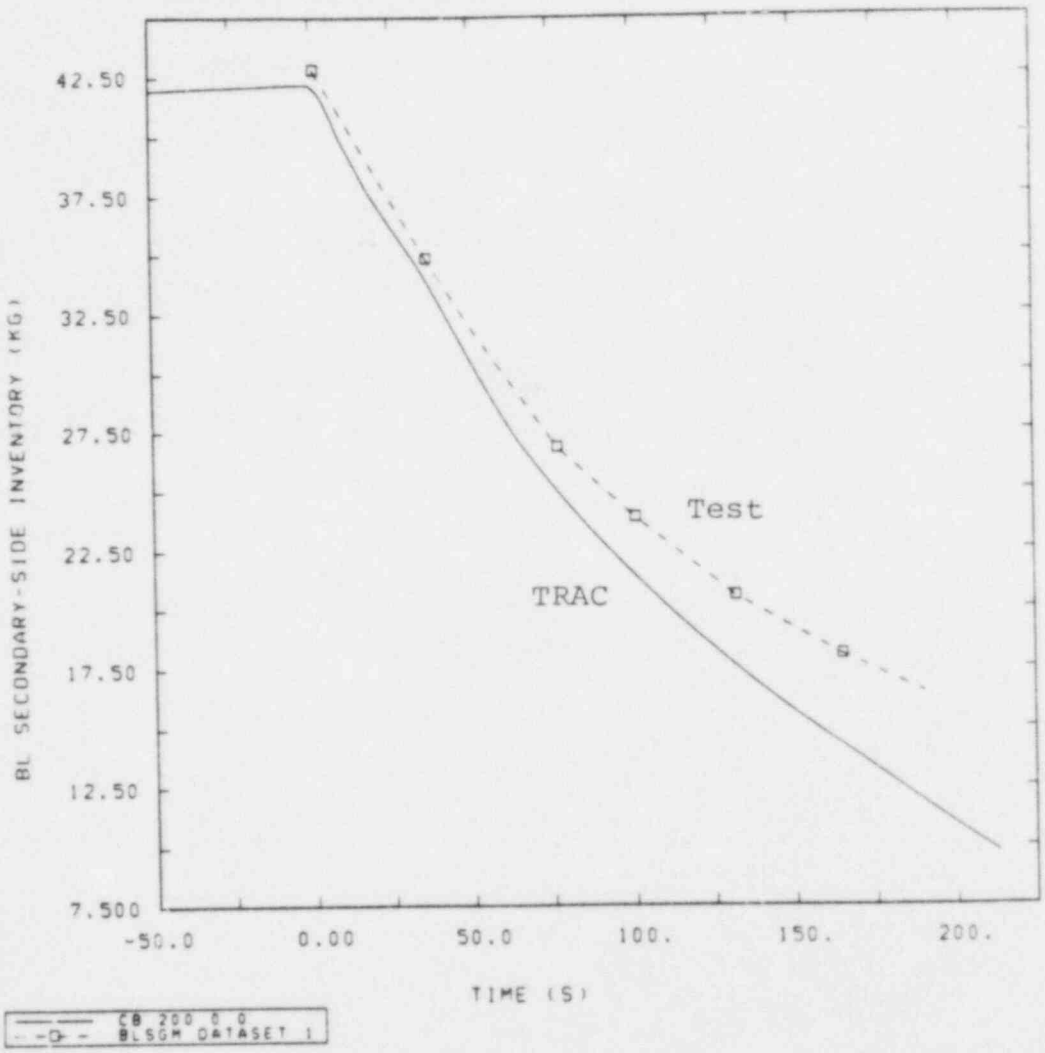


Figure 9.0.6 BL Secondary-Side Inventory, S-SF-5 Base Case Transient

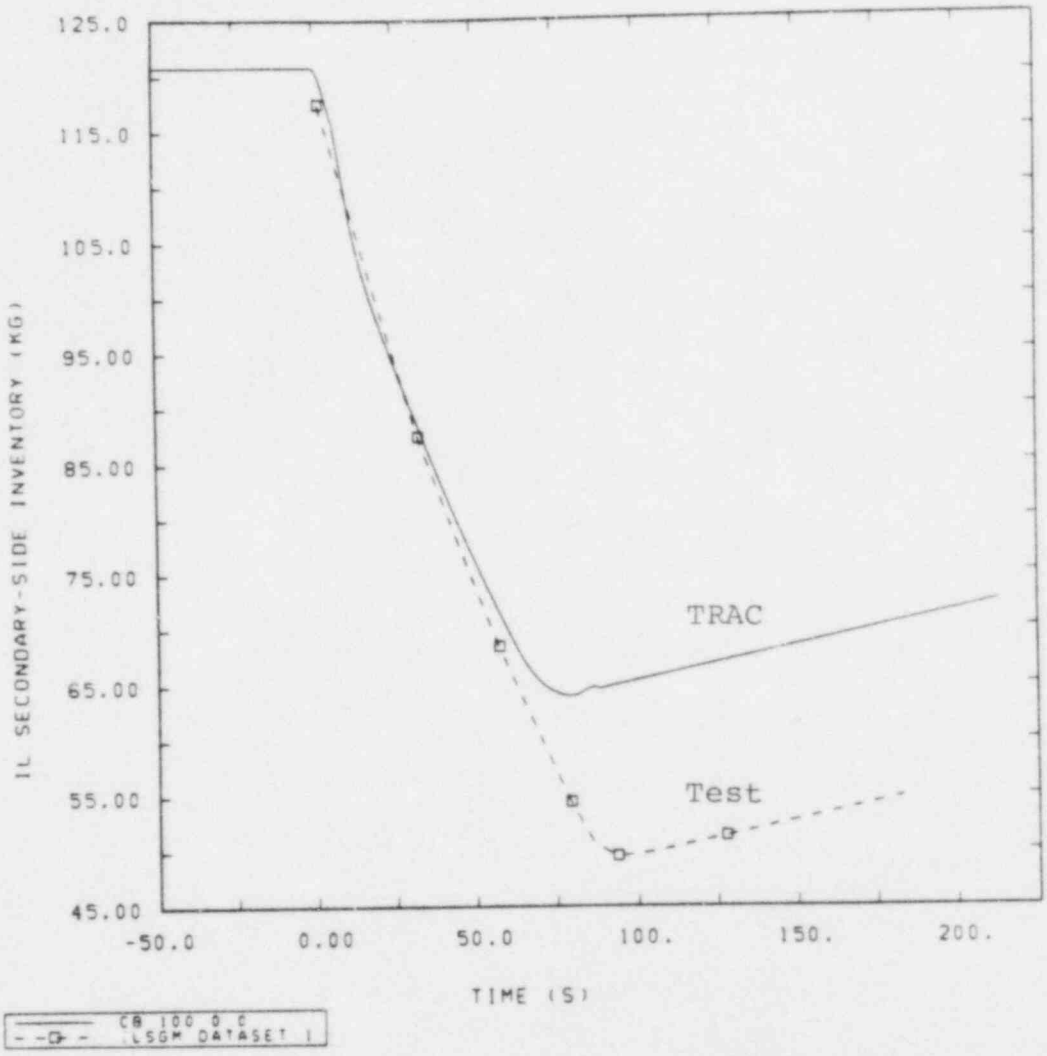


Figure 9.0.7 IL Secondary-Side Inventory, S-SF-5 Base Case Transient

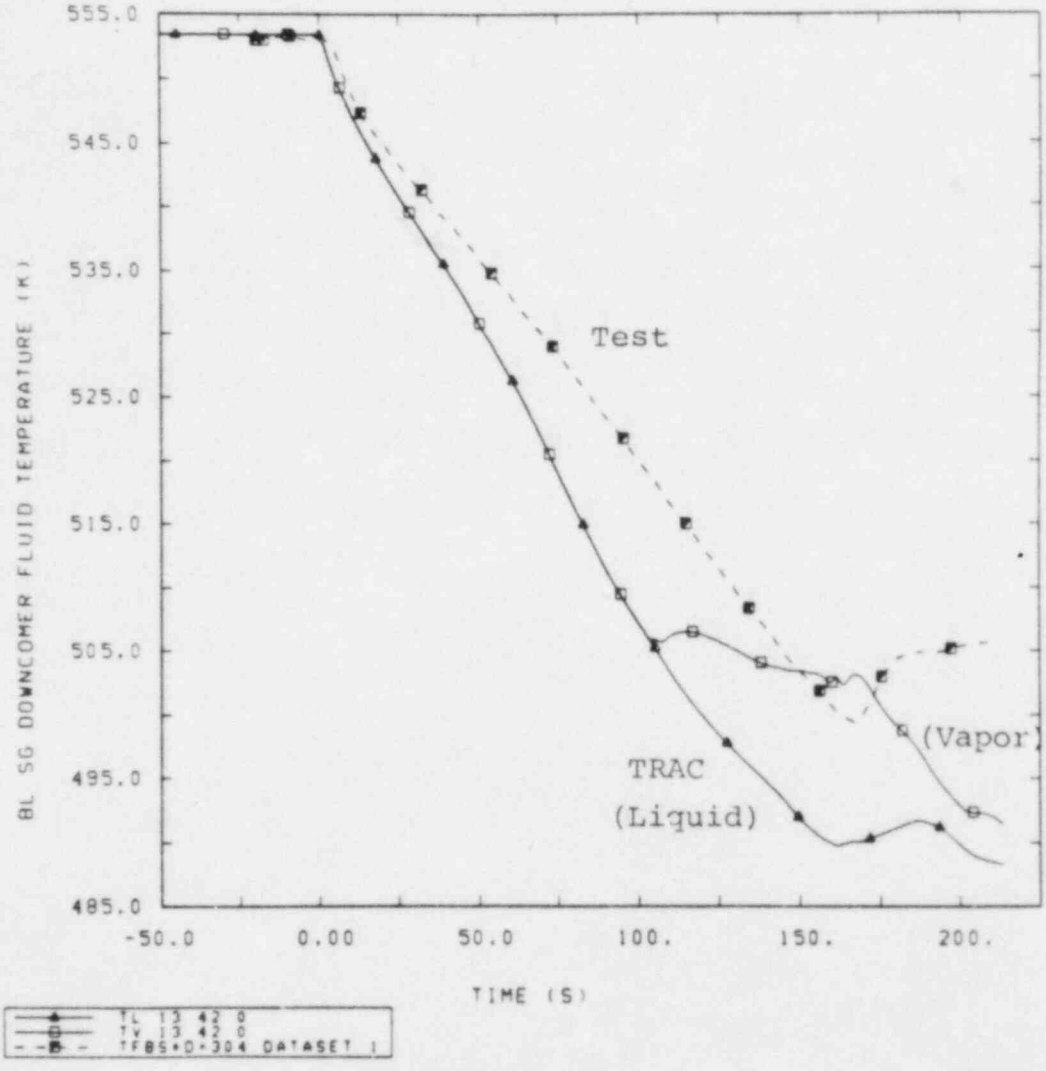


Figure 9.0.8 BL Steam Generator Downcomer Fluid Temperature, S-SF-5 Base Case Transient

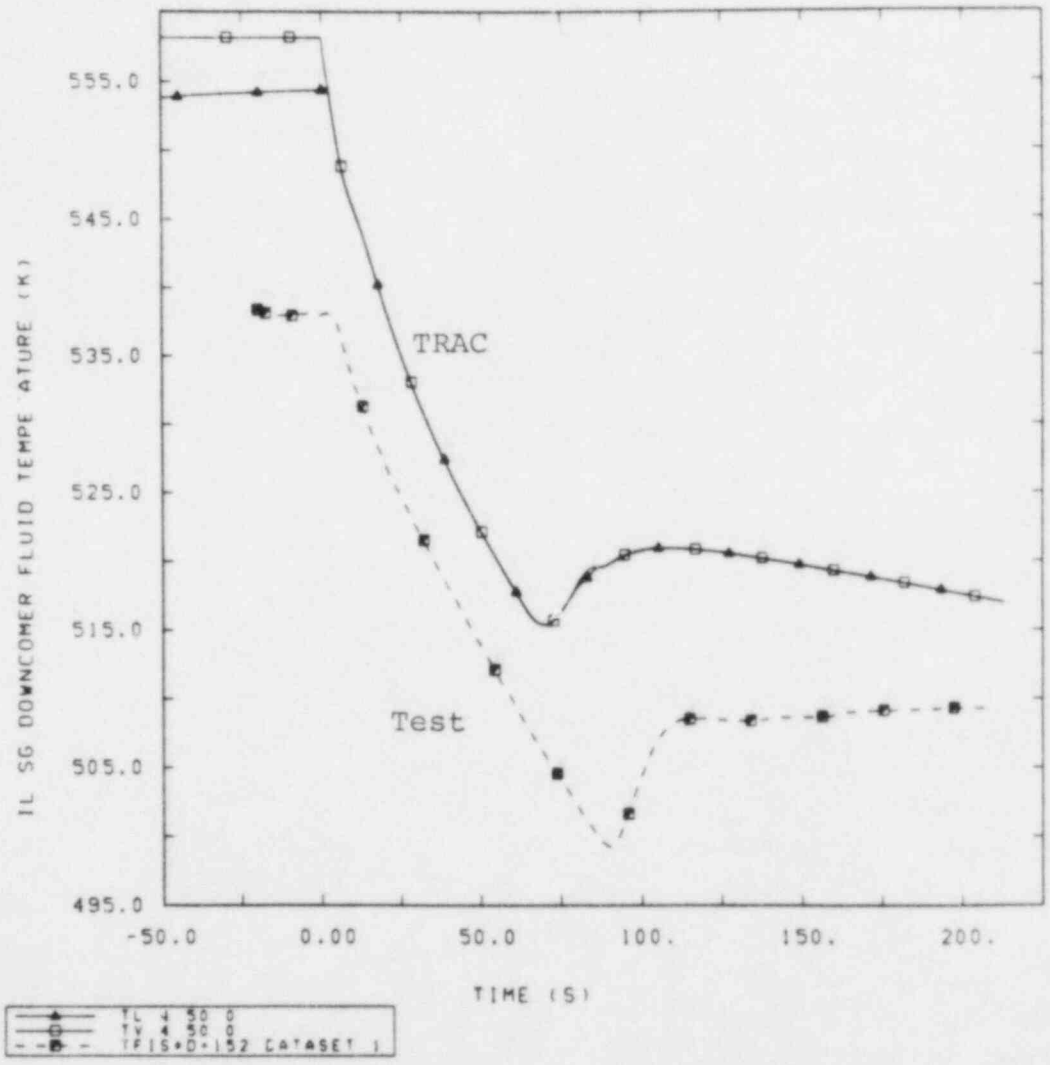


Figure 9.0.9 IL Steam Generator Downcomer Fluid Temperature, S-SF-5 Base Case Transient

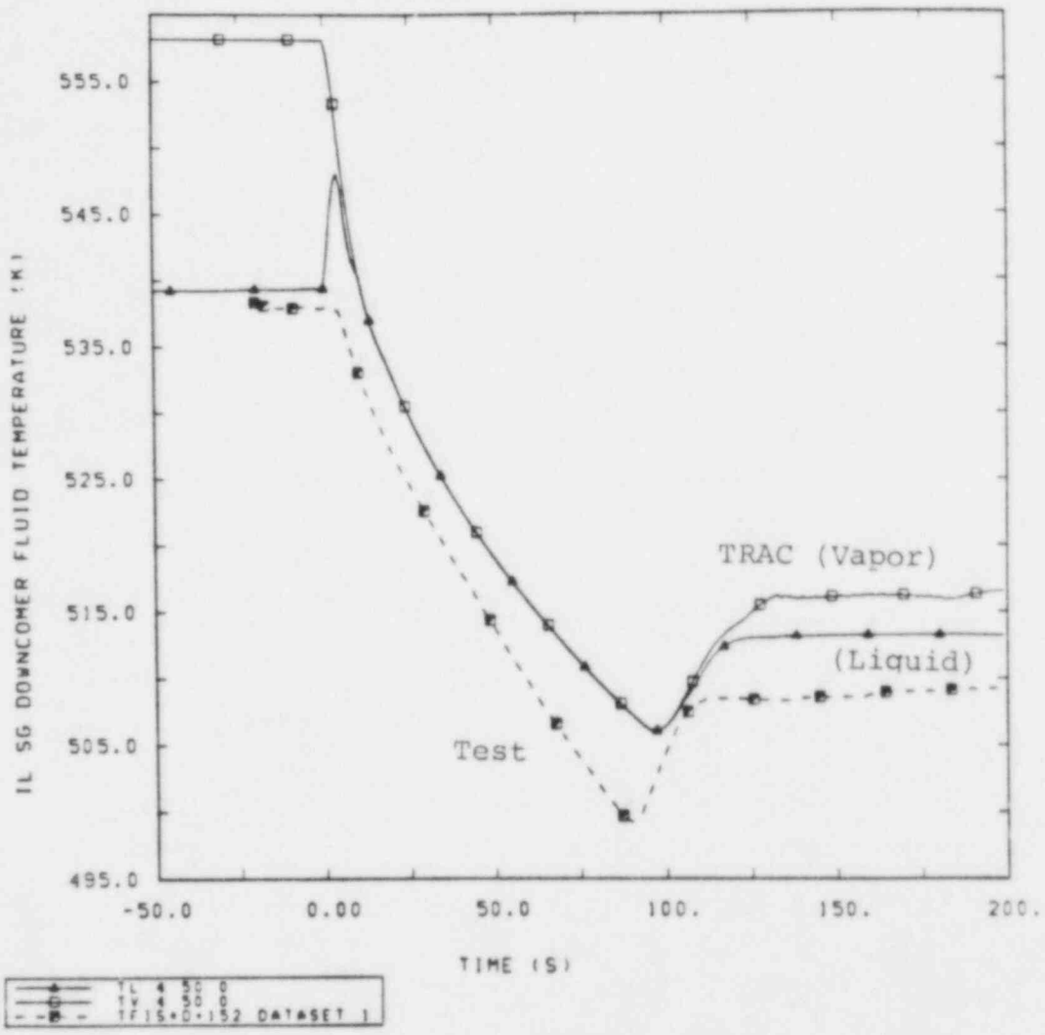


Figure 9.0.10 IL Steam Generator Downcomer Fluid Temperature, S-SF-5 Base Case Transient with modified filler piece heat slab

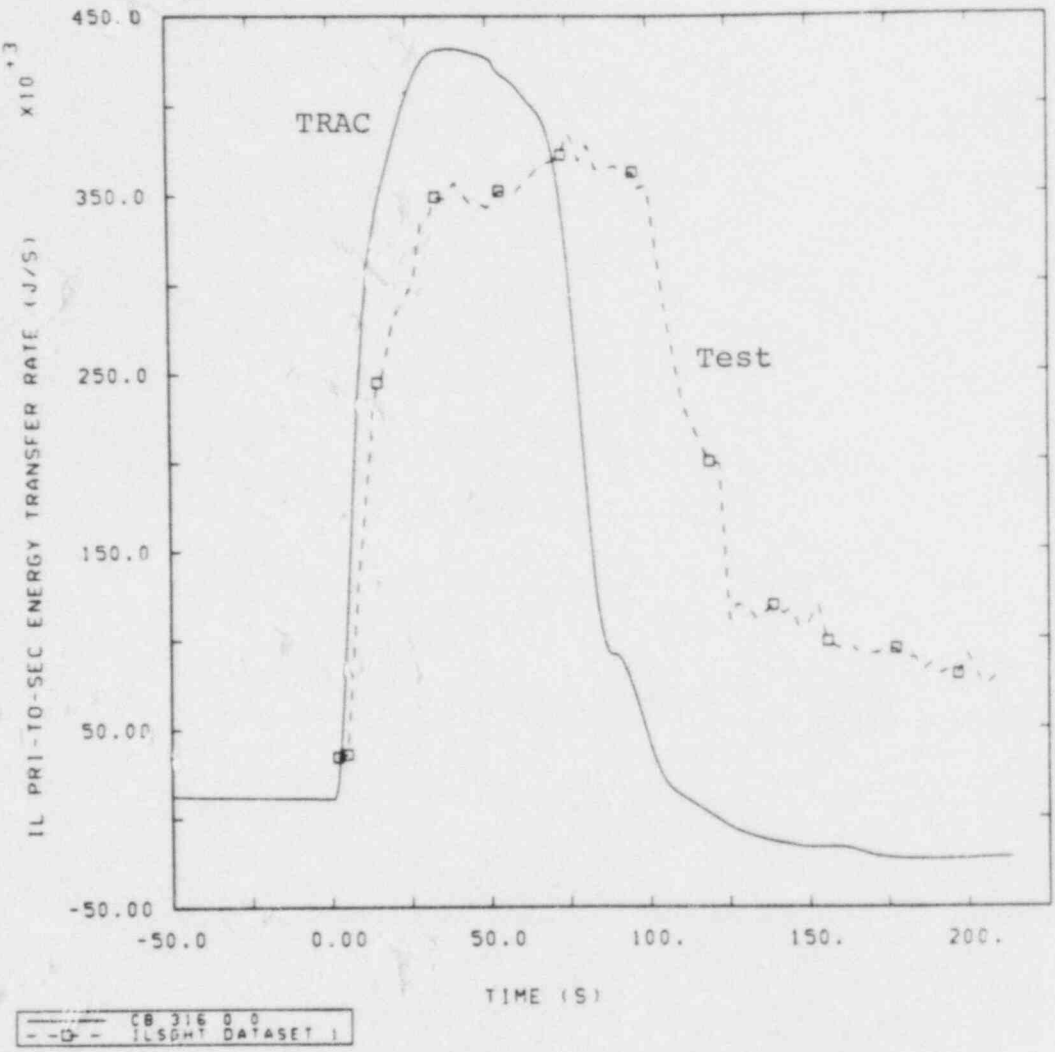


Figure 9.0.11 IL Primary-to-Secondary Heat Transfer Rate, S-SF-5 Base Case Transient

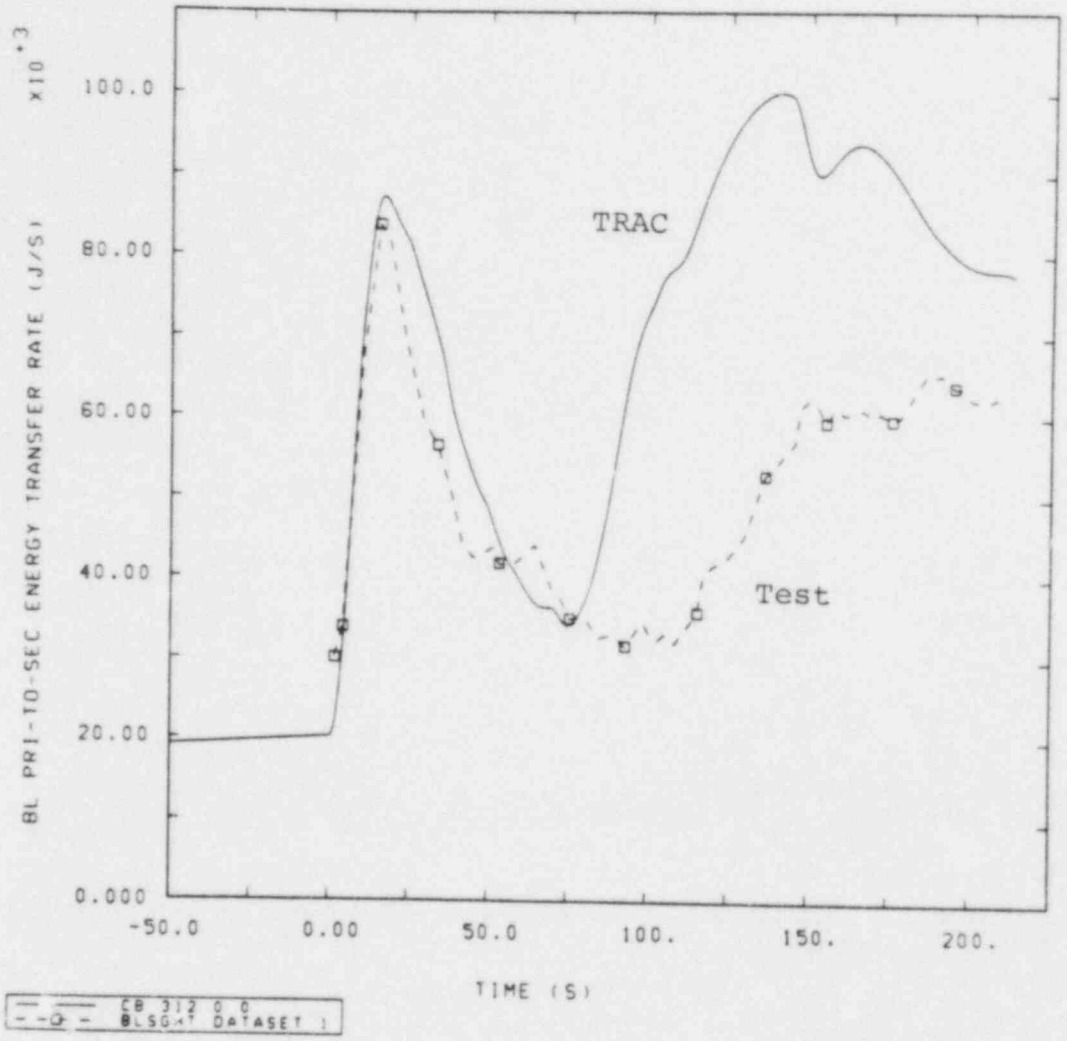


Figure 9.0.12 BL Primary-to-Secondary Heat Transfer Rate, S-SF-5 Base Case Transient

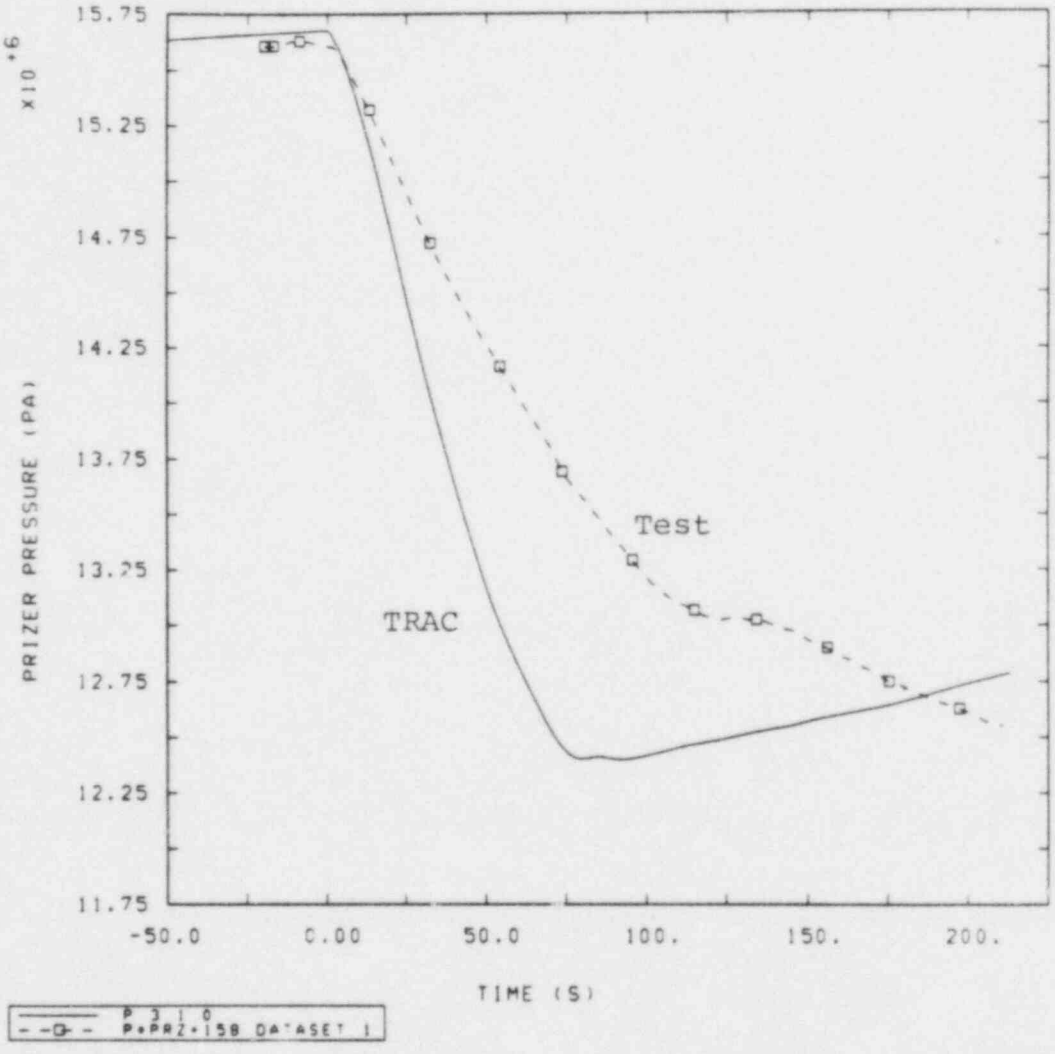


Figure 9.0.13 Pressurizer Pressure, S-SF-5 Base Case Transient

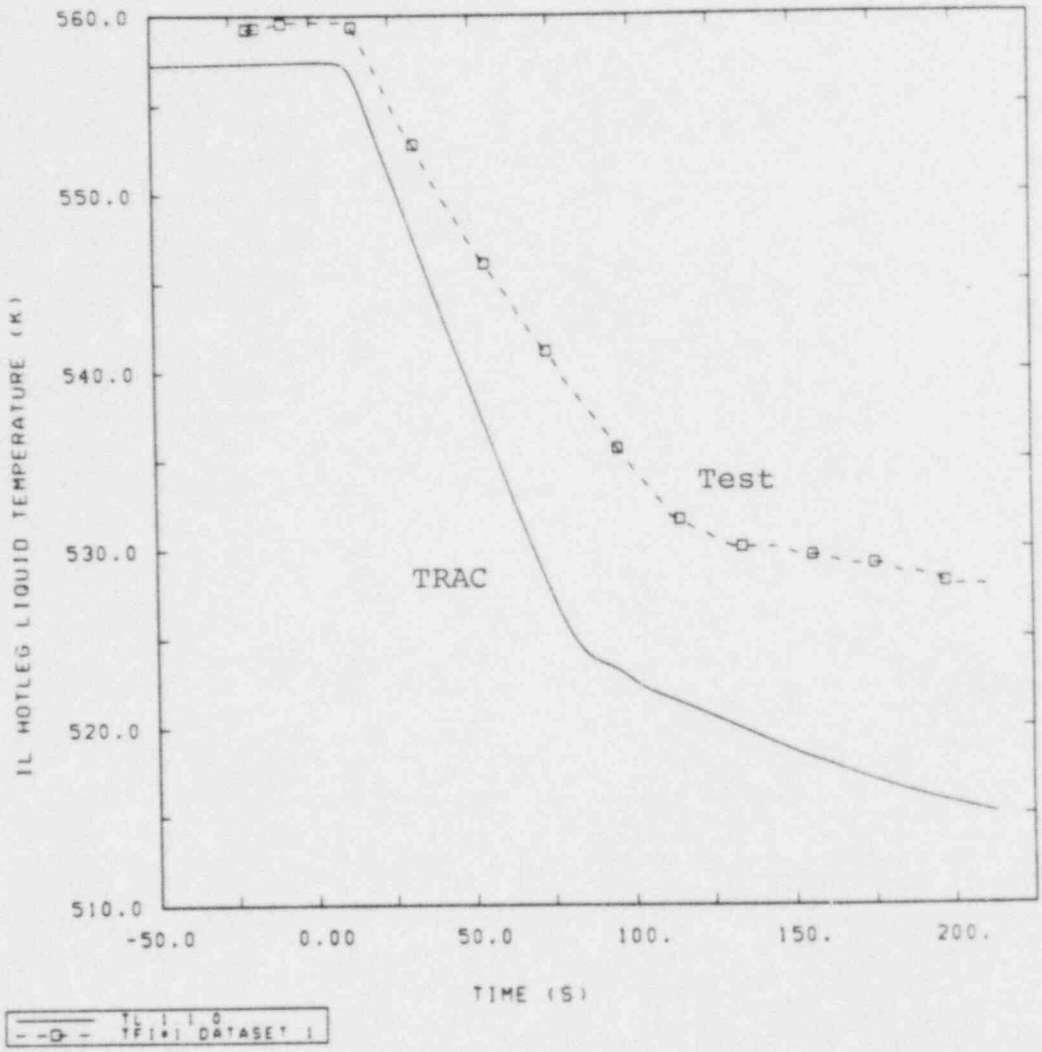


Figure 9.0.14 IL Hot-Leg Liquid Temperature, S-SF-5 Base Case Transient

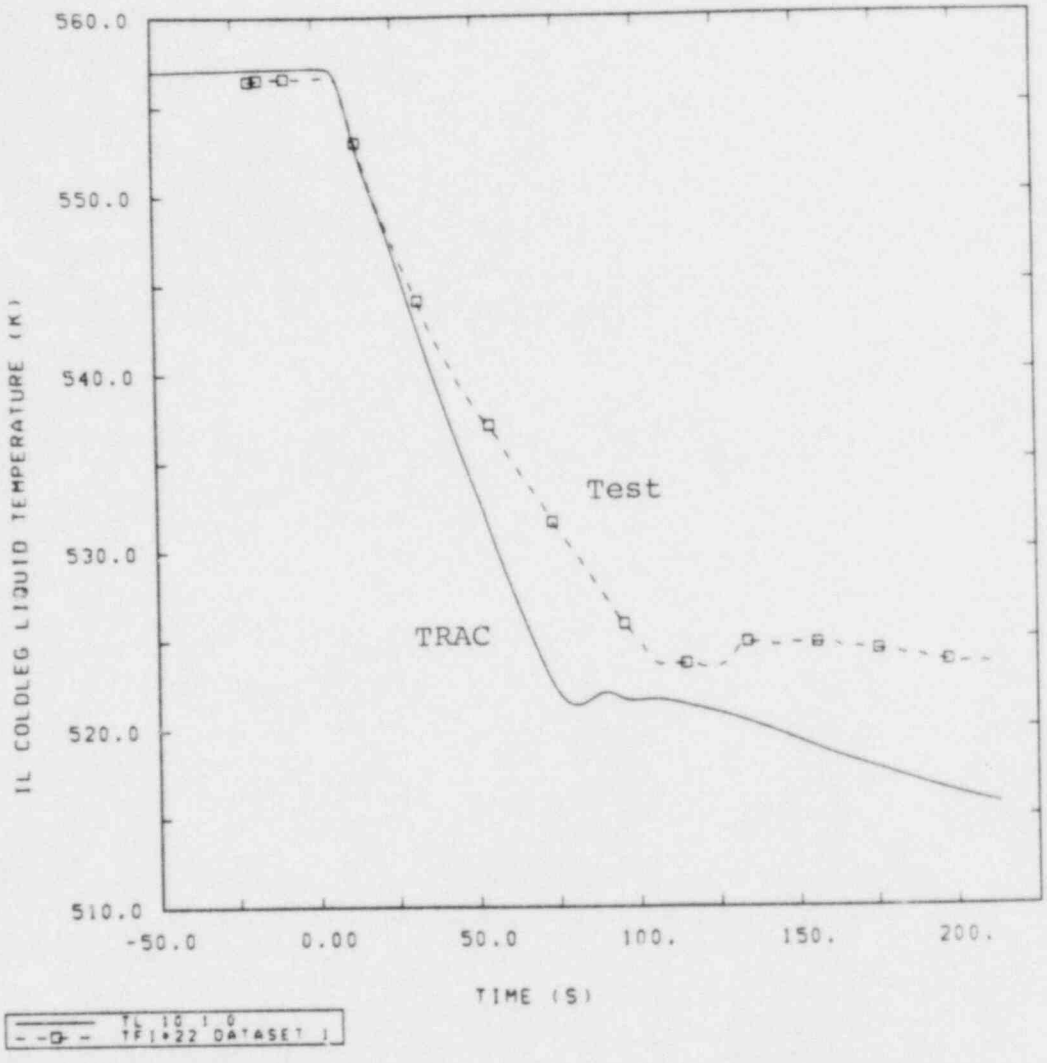


Figure 9.0.15 IL Cold-Leg Liquid Temperature, S-SF-5 Base Case Transient

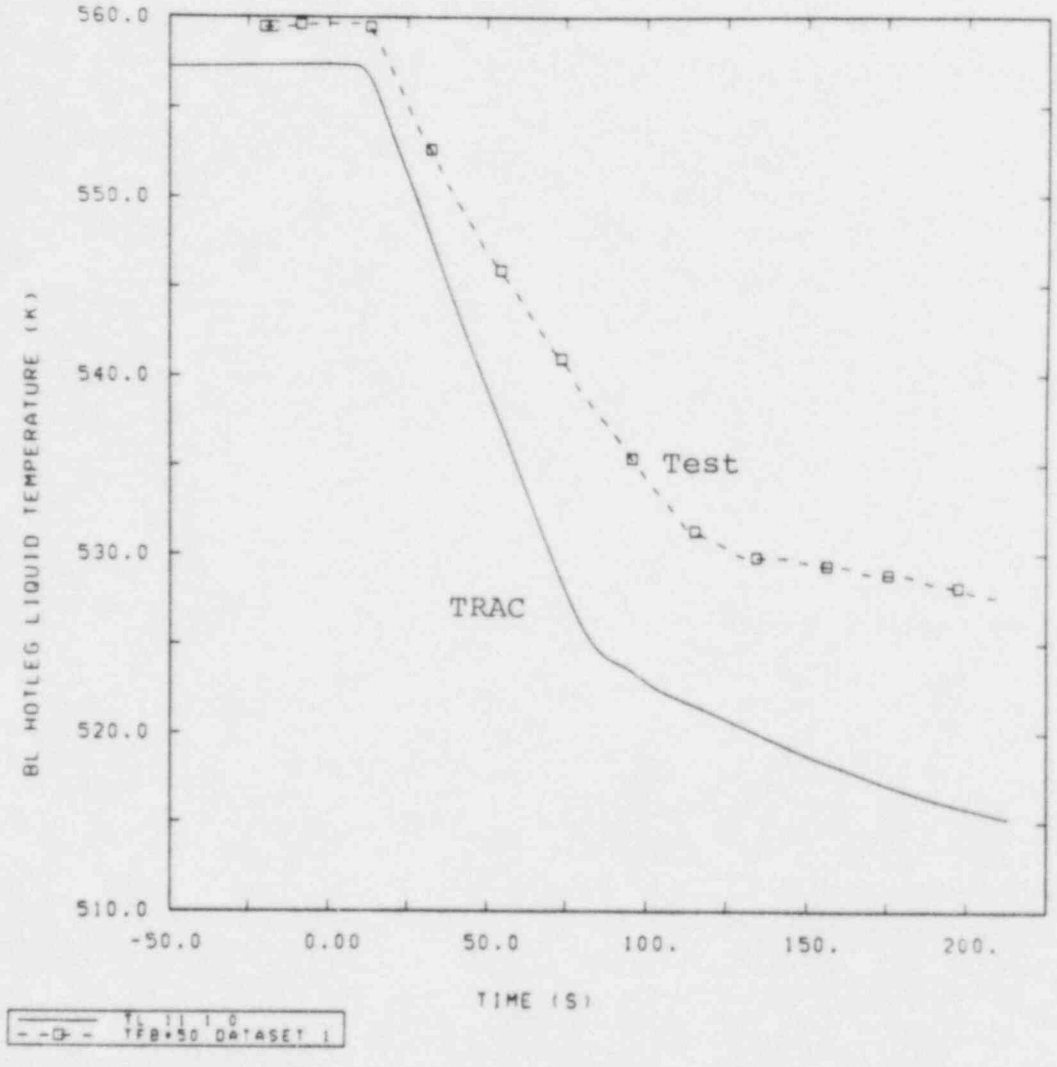


Figure 9.0.16 BL Hot-Leg Liquid Temperature, S-SF-5 Base Case Transient

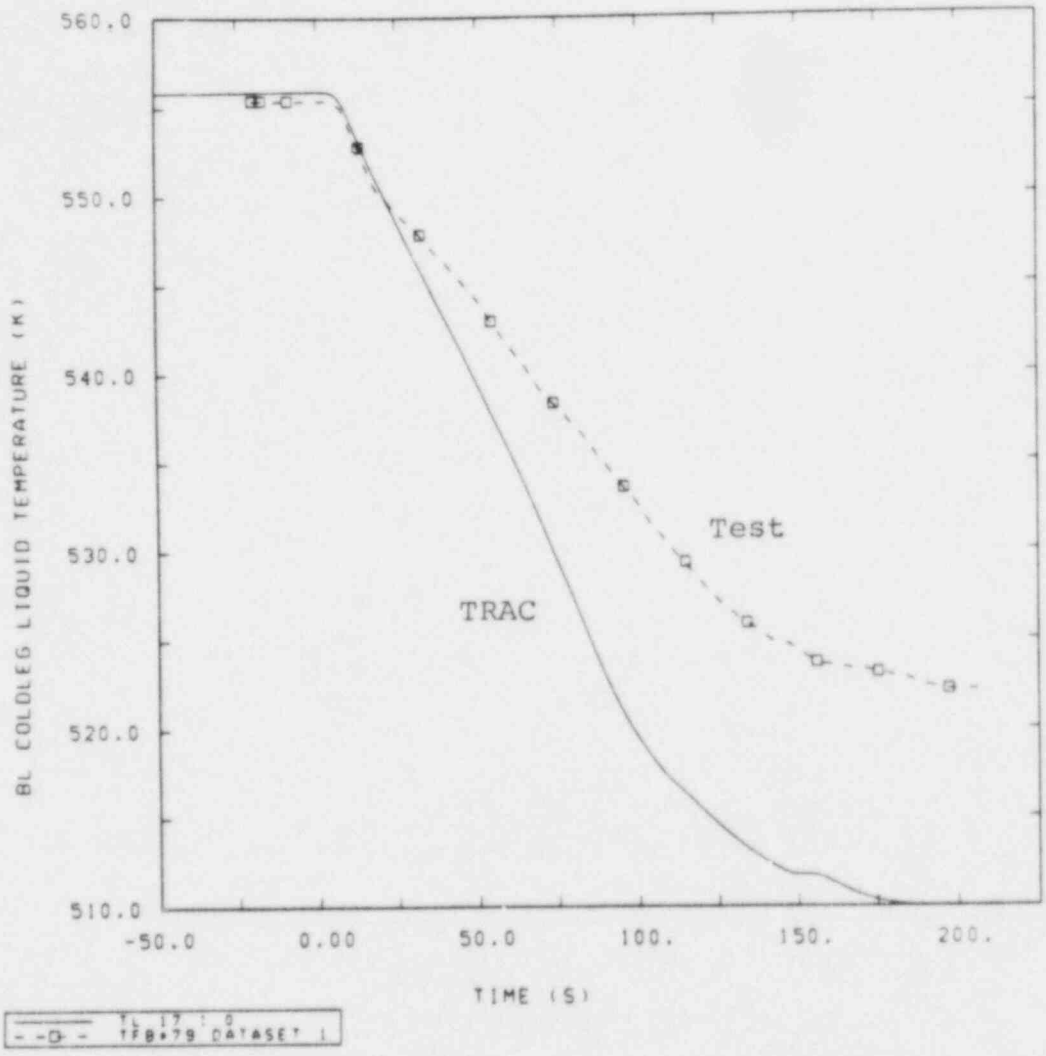


Figure 9.0.17 BL Cold-Leg Liquid Temperature, S-SF-5 Base Case Transient

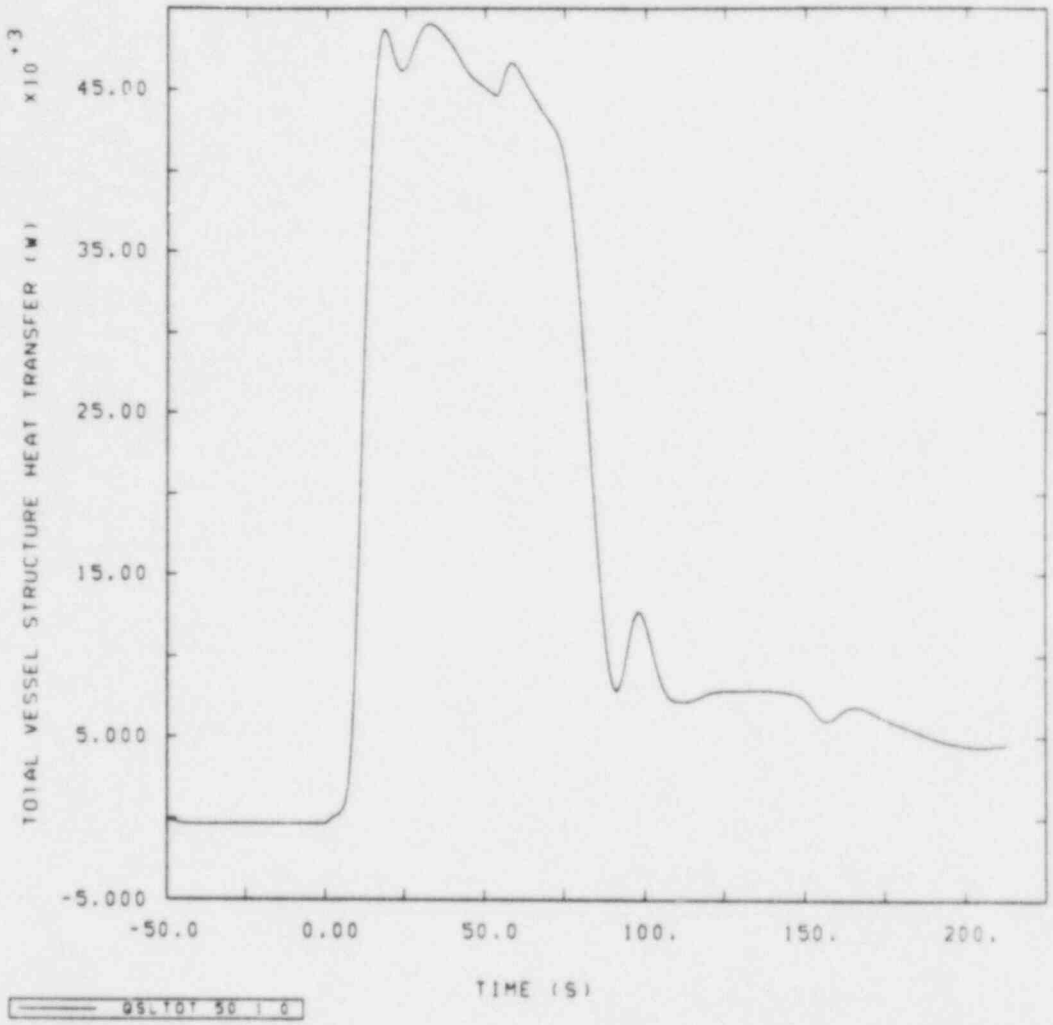


Figure 9.0.18 Total Vessel Structure Heat Transfer, S-SF-5 Base Case Transient

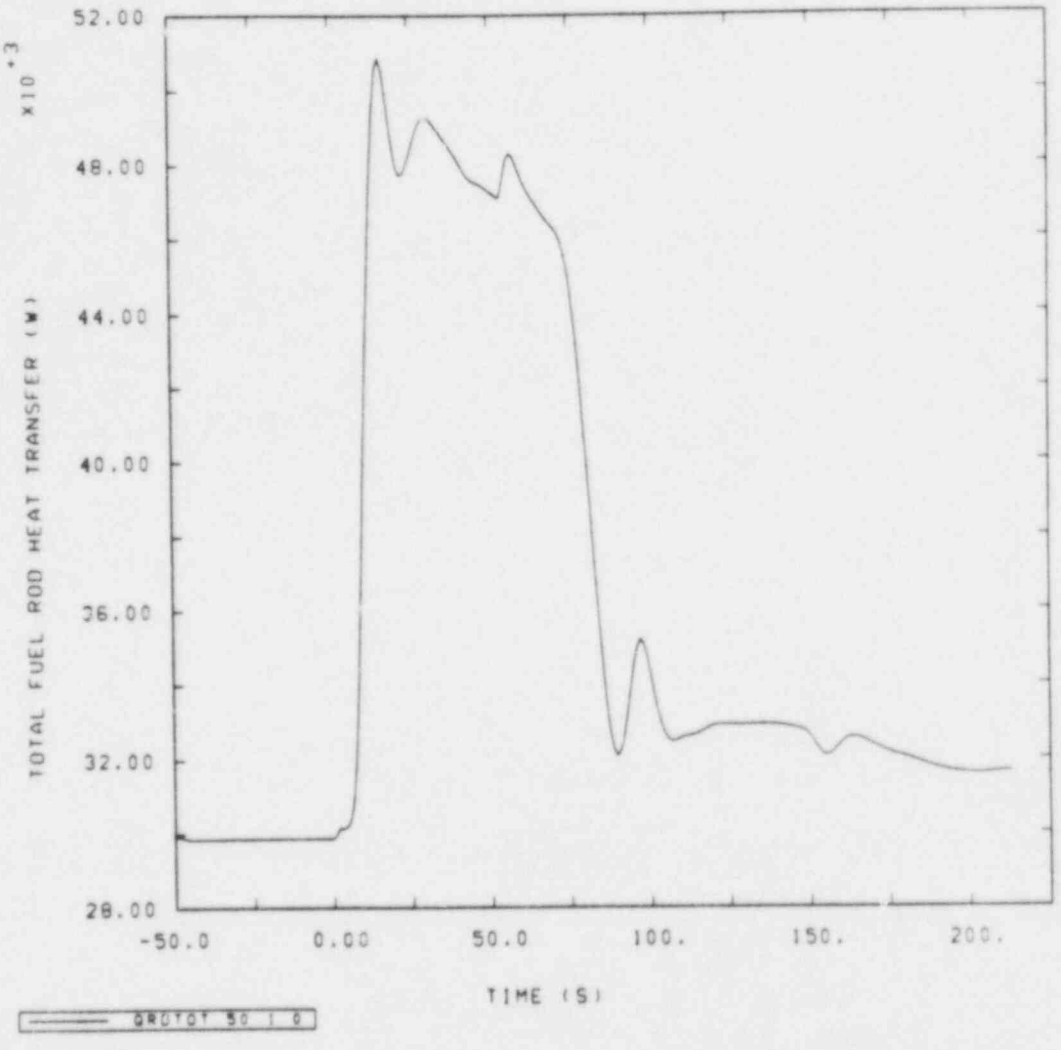


Figure 9.0.19 Total Fuel Rod Heat Transfer, S-SF-5 Base Case Transient

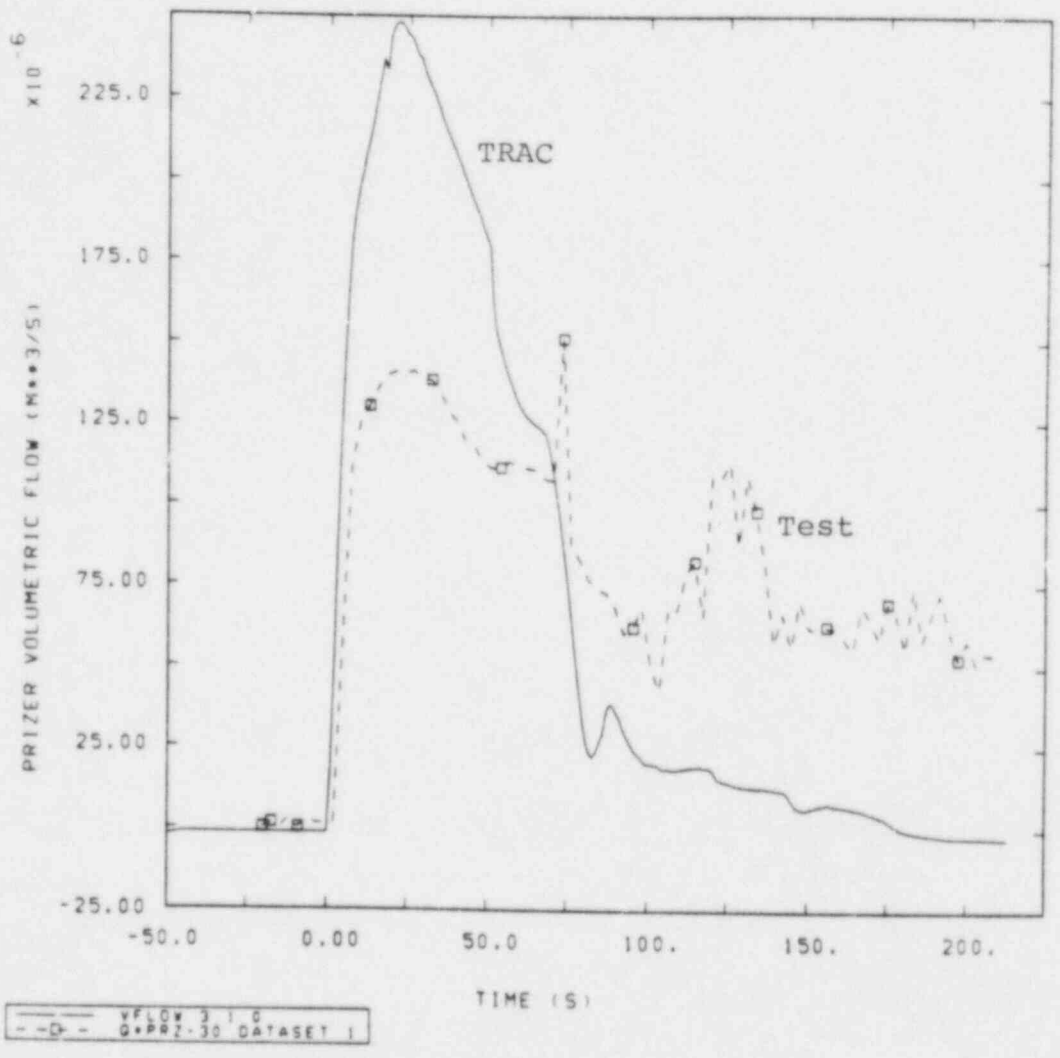


Figure 9.0.20 Pressurizer Volumetric Flow Rate, S-SF-5 Base Case Transient

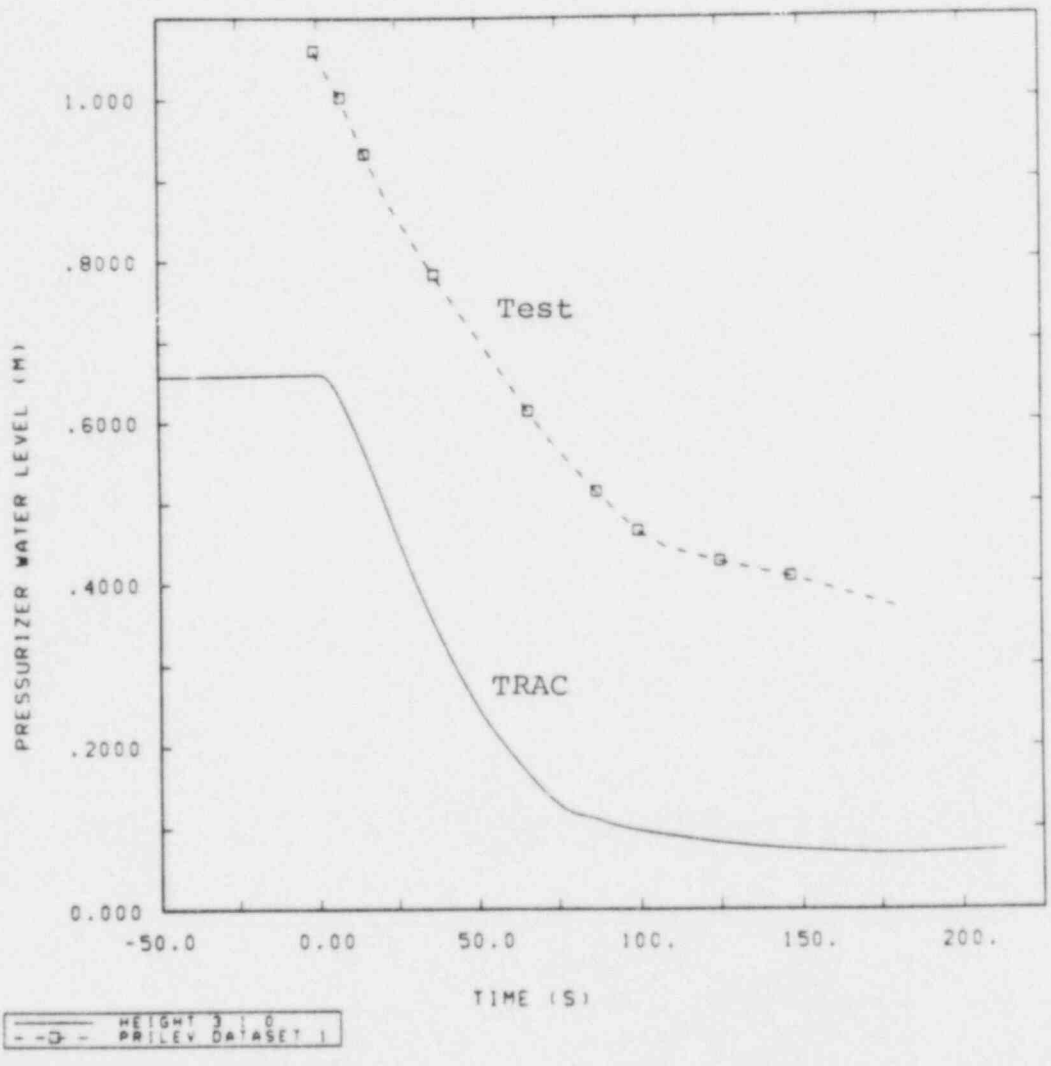


Figure 9.0.21 Pressurizer Water Level, S-SF-5 Base Case Transient

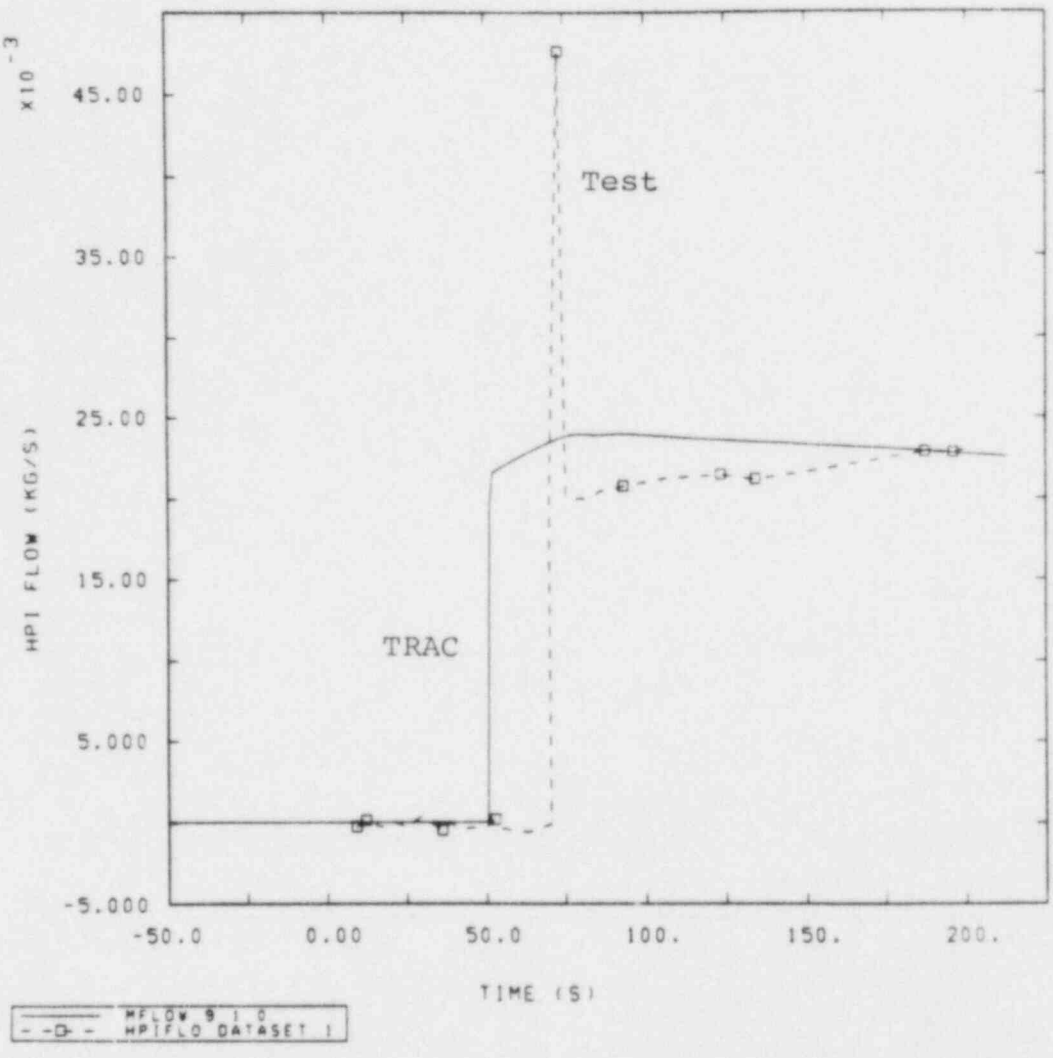


Figure 9.0.22 HPI Flow Rate, S-SF-5 Base Case Transient

## 10.0 TRANSIENT PARAMETRIC CASES

Several parametric cases were performed, using the base case 3-D model, to increase our understanding of the test and the calculated response. These cases help to illustrate the sensitivity of the results to the break flow, leakage, and vessel stored energy.

### 10.1 BL Steam-Line Break Discharge Coefficient

For the base case calculation, the calculated IL steam-line break flow agreed fairly well with that in the experiment while the calculated BL steam-line break flow was about 40% too high. As a result, the BL primary-to-secondary heat transfer was overpredicted. To determine the impact of this overprediction on the transient response, a parametric calculation was performed in which a two-phase discharge coefficient of 0.7 was applied to the BL steam-line break. Based on the base case calculation, we determined that this value would result in the correct break flow as measured in the test. Figure 10.1.1 shows that a good agreement was achieved.

With the correct break flow, the calculated BL primary-to-secondary heat transfer was underpredicted. However, because the IL primary-to-secondary heat transfer was overpredicted (even though the correct break flow was calculated), the primary-side pressure was still calculated to decrease too fast, as shown in Figure 10.1.2. Also, because the IL steam-line valve closure was delayed, due to the lower BL break flow, the primary-side pressure dropped to a lower value than in the base case calculation. We do not understand why the calculated heat transfer is too low in the BL steam generator and too high in the IL steam generator, even though the break flow is approximately correct for both. There are no major design or operating differences between the two steam generators of which we are aware, other than the number of tubes and the lower initial inventory for the BL steam generator. Also, the input models for both are very similar. A possible explanation is that the effective tube wall areas for the steam generators are different than the actual wall areas.

### 10.2 IL Steam-Line Break Discharge Coefficient

Although the calculated IL steam-line break flow agreed reasonably well with the measured flow, a parametric calculation was performed in which a two-phase discharge coefficient of 0.75 was applied to the IL steam-line break. (A discharge coefficient of 0.7 was used for the broken loop.) This IL value was chosen in an attempt to decrease the IL heat transfer rate to that of the experiment. In this way, we could better assess TRAC's ability to calculate the primary-side response.

Figure 10.2.1 shows the resulting decrease in the IL break flow in this parametric calculation. (Recall that the flow spike in the calculated flow is due to a level swell in the boiler such that a small amount of liquid was being carried out the break with the vapor.) Although the break flow is no longer in good agreement with the data, the calculated IL heat transfer rate is much closer to that of the test, as shown in Figure 10.2.2. (The calculated heat transfer rate is still too low after 125 s because of the way the filler pieces were modeled as discussed in Section 9.0.)

With this improved prediction of heat transfer, the calculated hot- and cold-leg temperatures (Figures 10.2.3 through 10.2.6) exhibit somewhat better agreement with the data. As a result, the prediction of the pressurizer pressure, shown in Figure 10.2.7, is also in better agreement with the test. However, the pressure still decreased a little too fast before IL steam-line valve closure. The primary-side low pressure signal occurred at 56 s, compared to 70 s in the test, and 51 s in the base case. Also, the pressure continued to rise after closure, as it did in the base case calculation, contrary to the measured response.

10.3 Primary-Side Leakage

In an attempt to better predict the pressure decrease following IL steam-line valve closure, the calculation of Section 10.2 was repeated with an increased value of primary-side leakage. In the discussion of the base case (Section 9.0), we estimated (using the plot of pressurizer volumetric flow) that the leakage during the experiment would have to be about 7 times greater than the reported steady-state leakage to account for the decreasing pressure in the test after valve closure. Based on the plot of the pressurizer water level, we estimated that the leakage would have to be about 3.5 times as great.

The calculation of Section 10.2 was repeated using a leakage rate 3.5 times greater than reported. The increased leakage, along with the overprediction of the primary-side fluid contraction, was sufficient to empty the pressurizer by 100 s. The primary side then rapidly depressurized because the free surface area of the saturated fluid in the system decreased significantly as the fluid level dropped into the pressurizer surge line; i.e., the vaporization of saturated fluid in the pressurizer ended. The early emptying of the pressurizer prevented us from evaluating the effect of leakage. We avoided this problem by then increasing the initial pressurizer water level by about 0.3 m and rerunning the calculation.

Increasing the leakage by a factor of 3.5 resulted in the pressurizer emptying at about the same rate as in the experiment after IL valve closure, as exhibited in Figure 10.3.1. (Recall that the measured water level is for trend information only.) The calculated pressurizer pressure, shown in Figure 10.3.2, was slowly decreasing after valve closure, which is a better prediction than in the other cases. But because of the increased leakage, the pressure before valve closure decreased faster and a somewhat worse agreement with data resulted. Perhaps in the experiment, leakage was low initially and then greatly increased after around 100 s. The fact that leakage occurs during the experiment, and that only the steady-state value is known, complicates the assessment of TRAC's ability to predict the primary-side response.

10.4 Vessel Structure

As mentioned earlier, the SF calculations were originally performed with an input model that did not account for the honeycomb insulation in the vessel. Results from one of those calculations are presented here as a parametric case to demonstrate the importance of the heat slab stored energy on the steam-line break transients.

This calculation was very similar to the one described in Section 10.3, except the honeycomb insulation was not accounted for and an IL steam-line break discharge coefficient of 0.55 was necessary to achieve the correct IL secondary-side heat transfer rate. A leakage rate 3.5 times greater than the reported steady-state leakage was used and a discharge coefficient of 0.7 was used for the broken loop.

With the vessel insulation unaccounted for, the heat transfer rate from the vessel structure was about 6 times as large as when the honeycomb structure was assumed to provide complete insulation (not all of the structure in the vessel was insulated). Because the vessel structure heat transfer was not measured during the test, we do not know exactly how effective the honeycomb insulation really was.

The results for this calculation are in better agreement with data than any of the other S-SF-5 calculations performed. Figures 10.4.1 through 10.4.4 show that the calculated loop liquid temperatures are very close to those of the test. Despite this good agreement with temperatures, the pressurizer pressure, shown in Figure 10.4.5, was still predicted to drop too fast before IL steam-line valve closure and to not decrease fast enough after valve closure. A possible reason for the different rates of pressure change between the calculation and the test before valve closure involves the rate of phase change in the pressurizer. In TRAC, the phase change rate is a function of empirically-determined interfacial heat transfer coefficients and areas; the calculated coefficients and areas may not be appropriate for this transient. Our TRAC assessment calculations for the NEPTUNUS pressurizer tests [16] support this hypothesis, although that test also included the effects of pressurizer sprays.

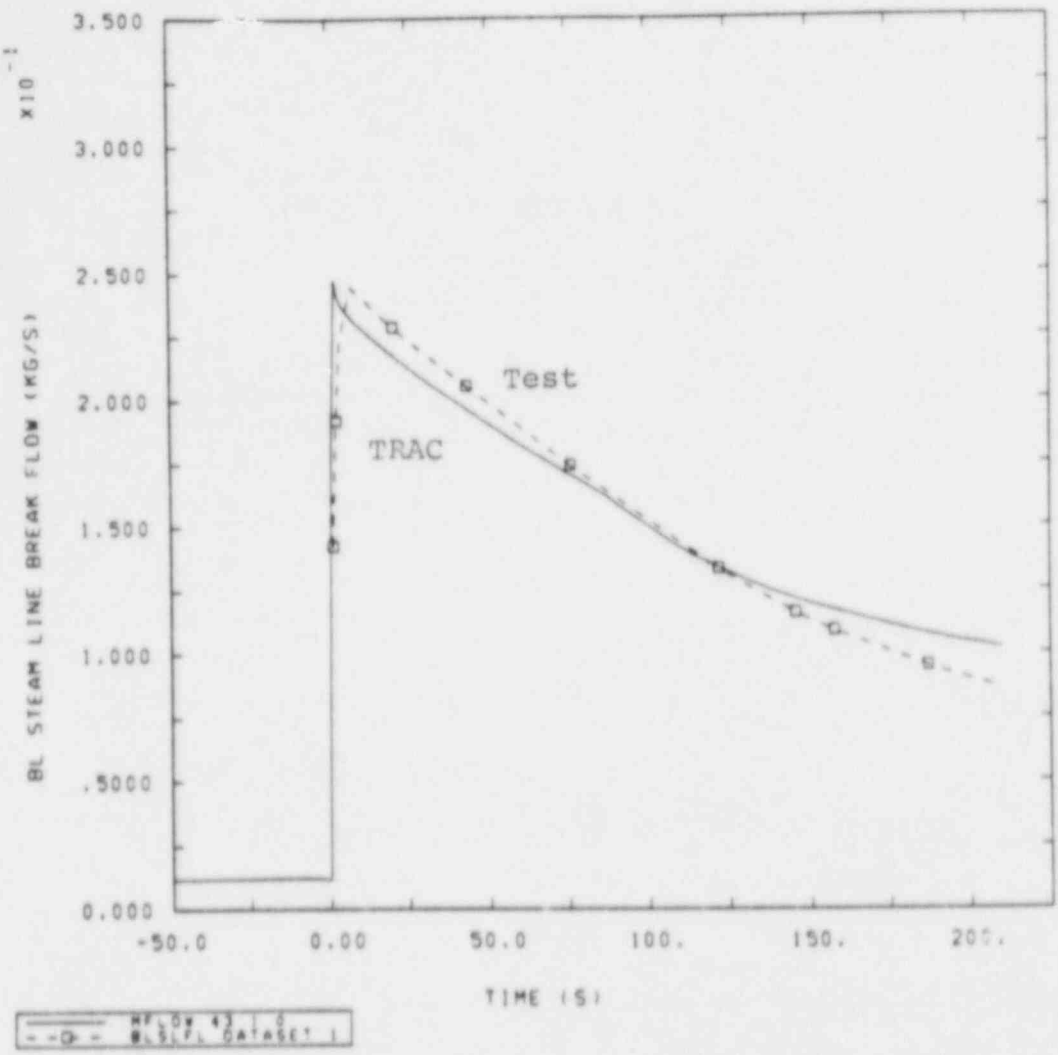


Figure 10.1.1 BL Steam-Line Break Flow Rate, S-SF-5 BL Discharge Coefficient Parametric Transient

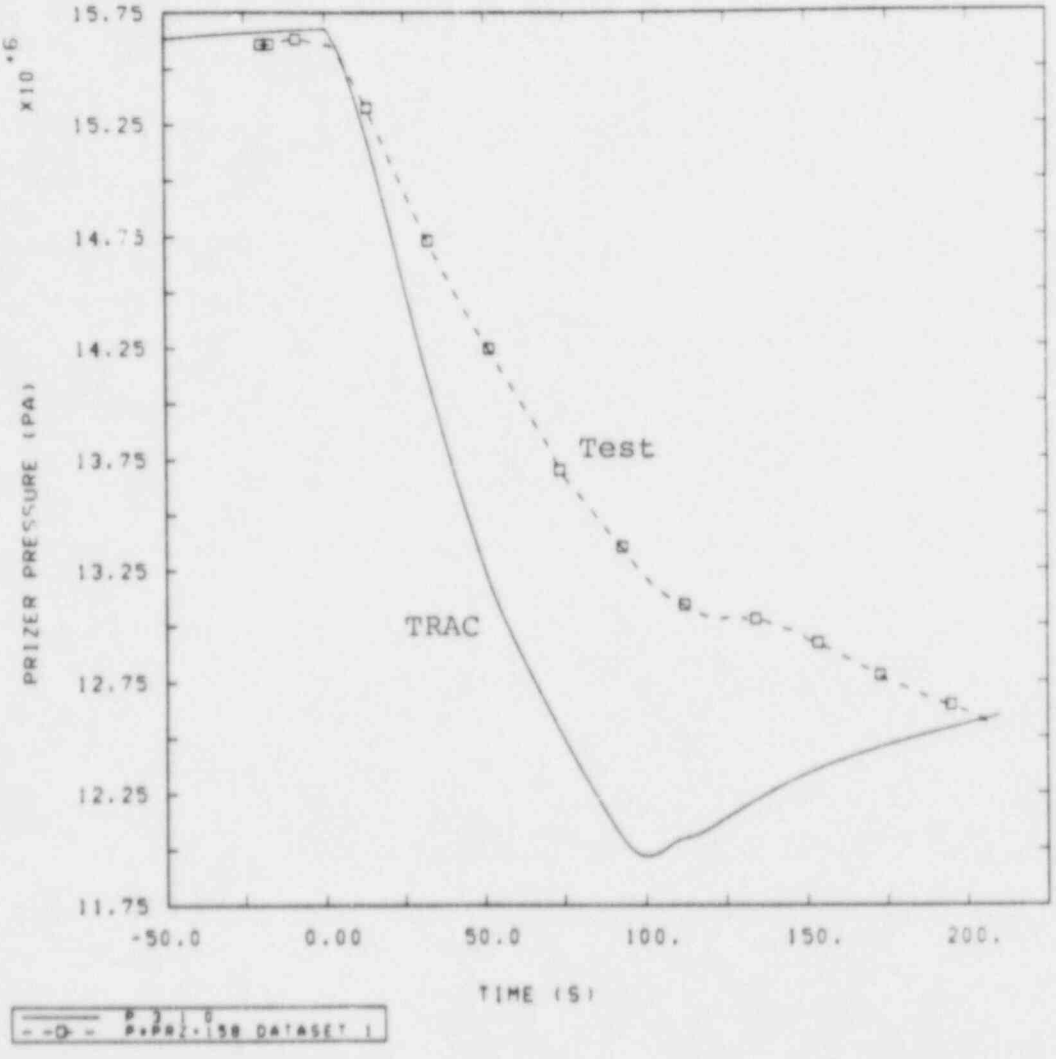


Figure 10.1.2 Pressurizer Pressure, S-SF-5 BL Discharge Coefficient Parametric Transient

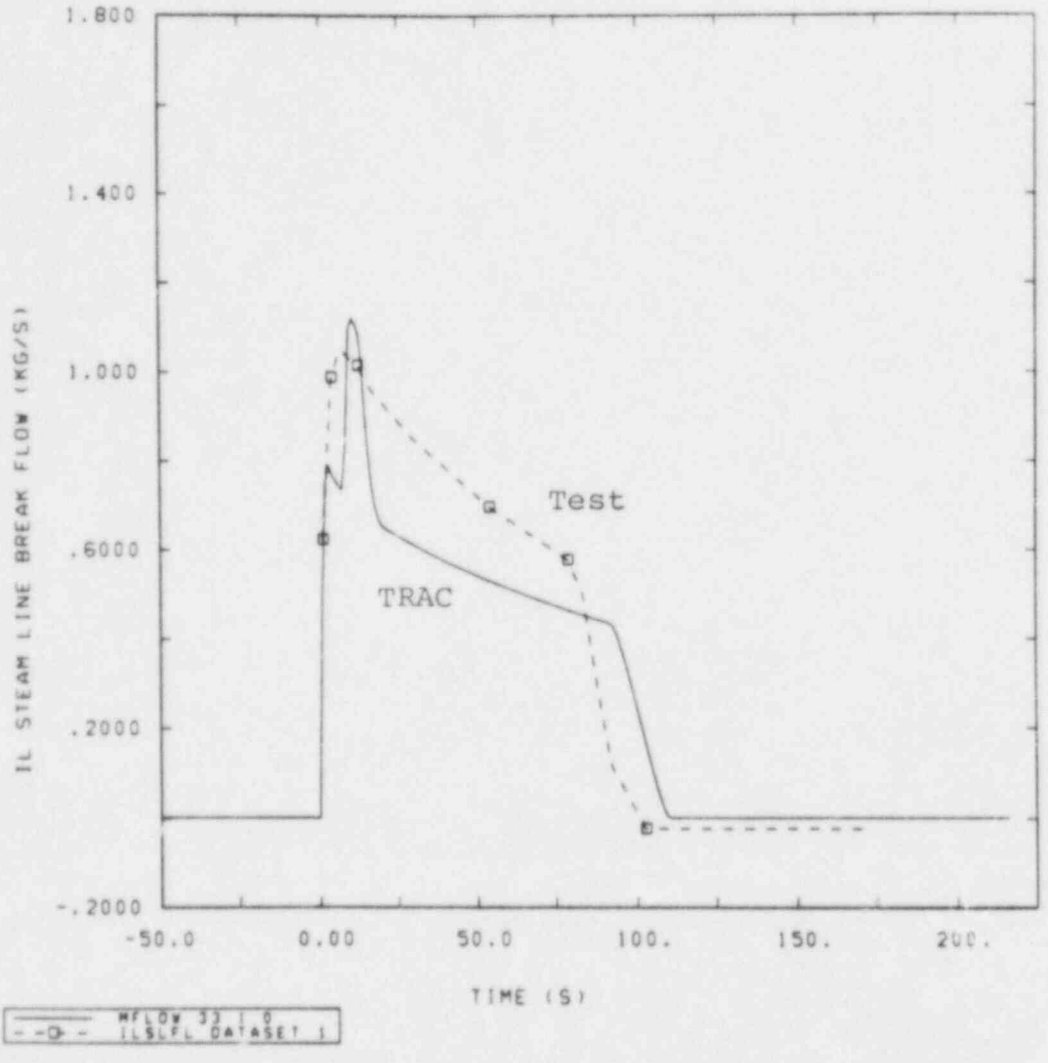


Figure 10.2.1 IL Steam-Line Break Flow Rate, S-SF-5 IL Discharge Coefficient Parametric Transient

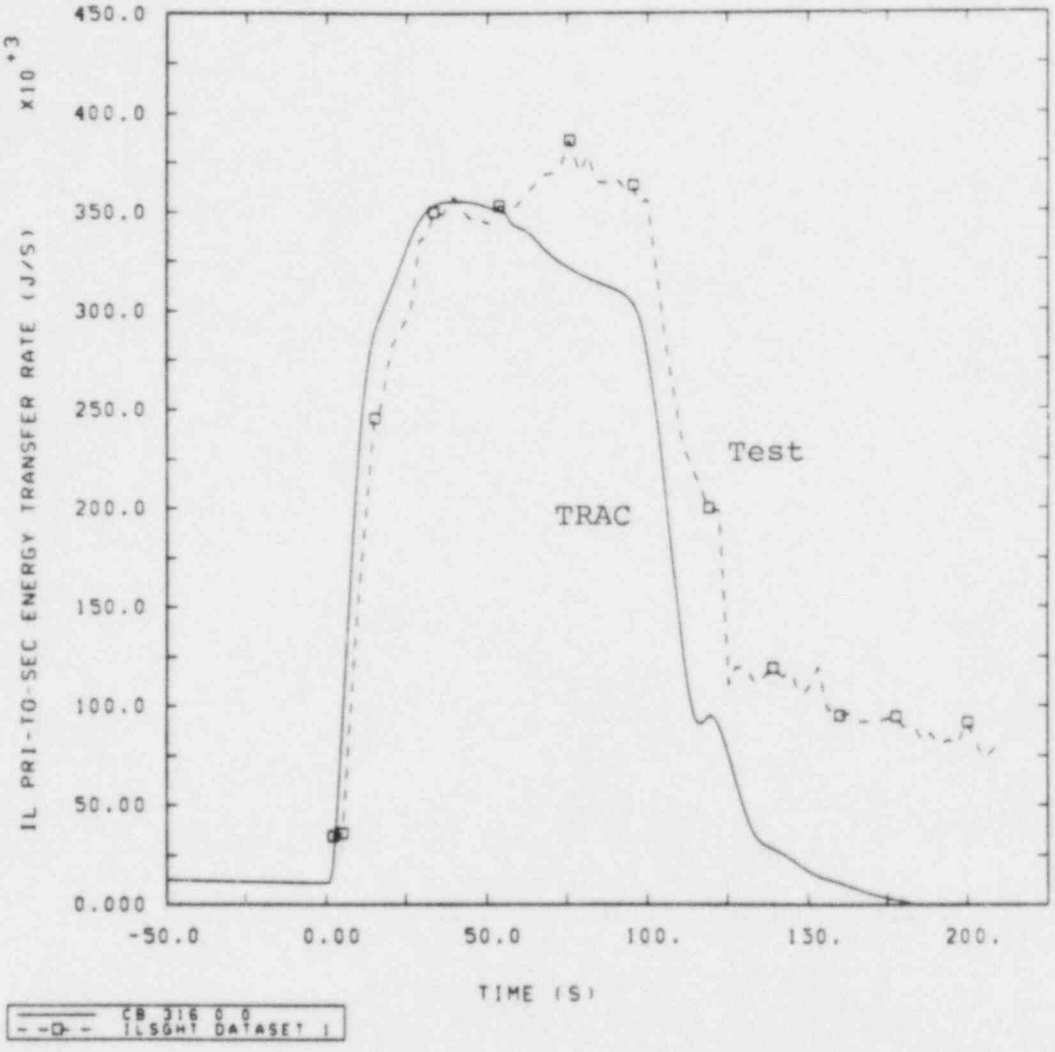


Figure 10.2.2 IL Primary-to-Secondary Heat Transfer, S-SF-5 IL Discharge Coefficient Parametric Transient

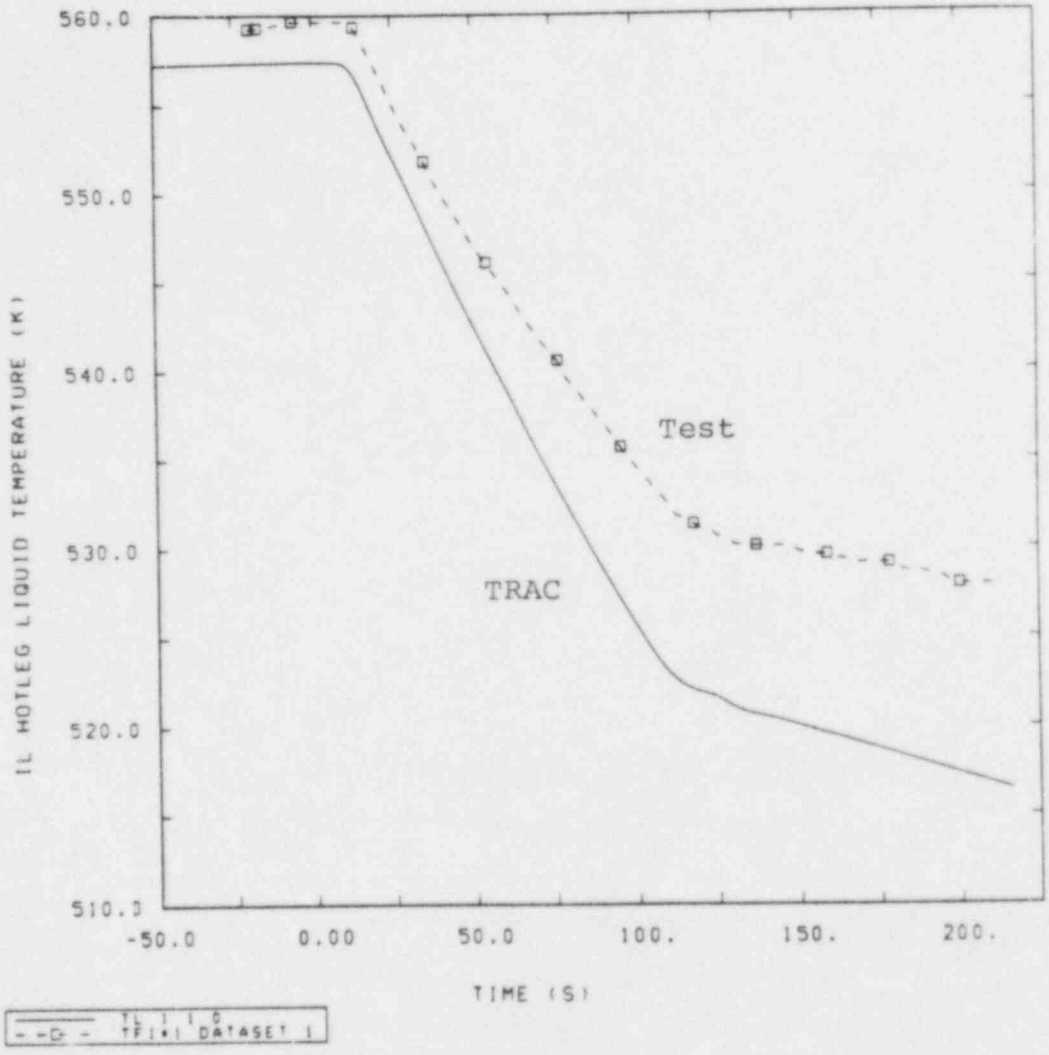


Figure 10.2.3 IL Hot-Leg Liquid Temperature, S-SF-5 IL Discharge Coefficient Parametric Transient

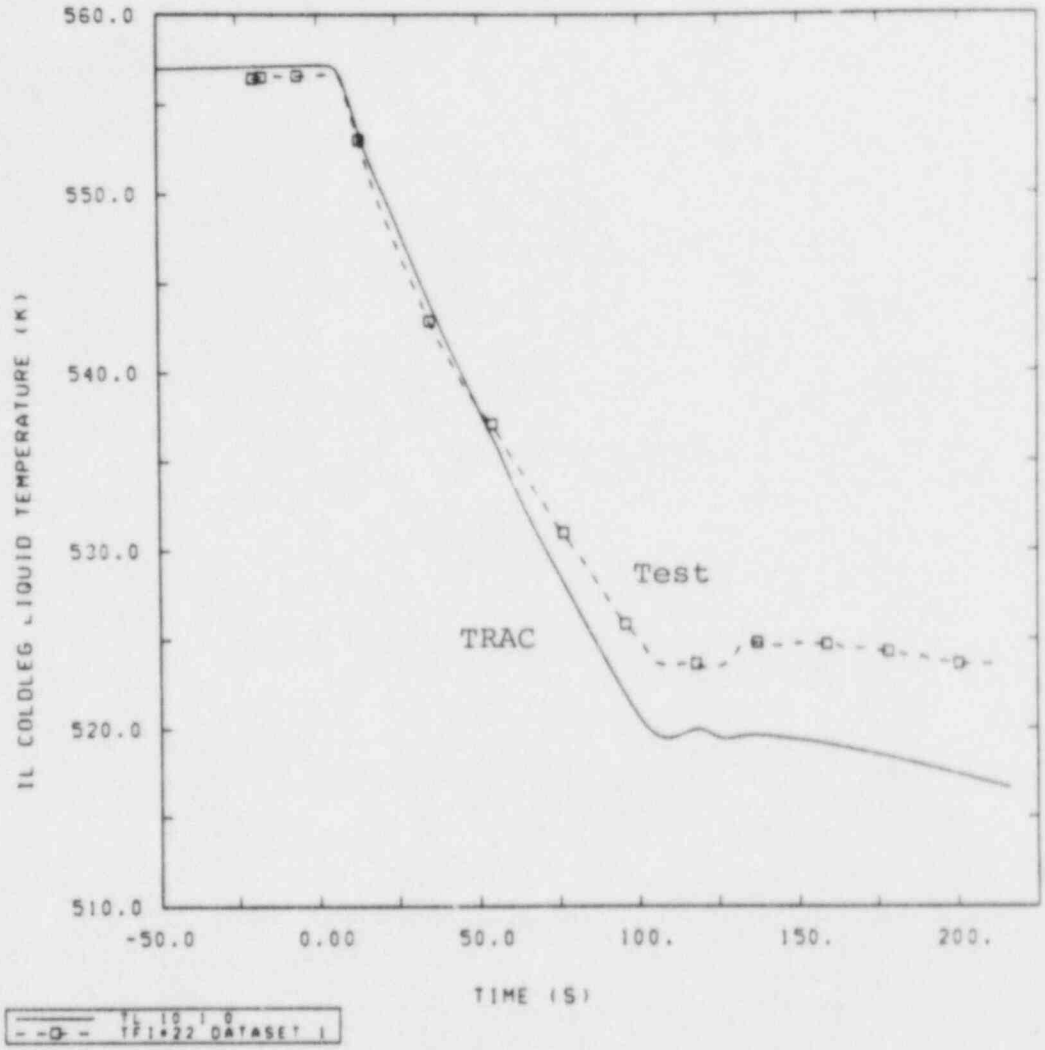


Figure 10.2.4 IL Cold-Leg Liquid Temperature, S-SF-5 IL Discharge Coefficient Parametric Transient

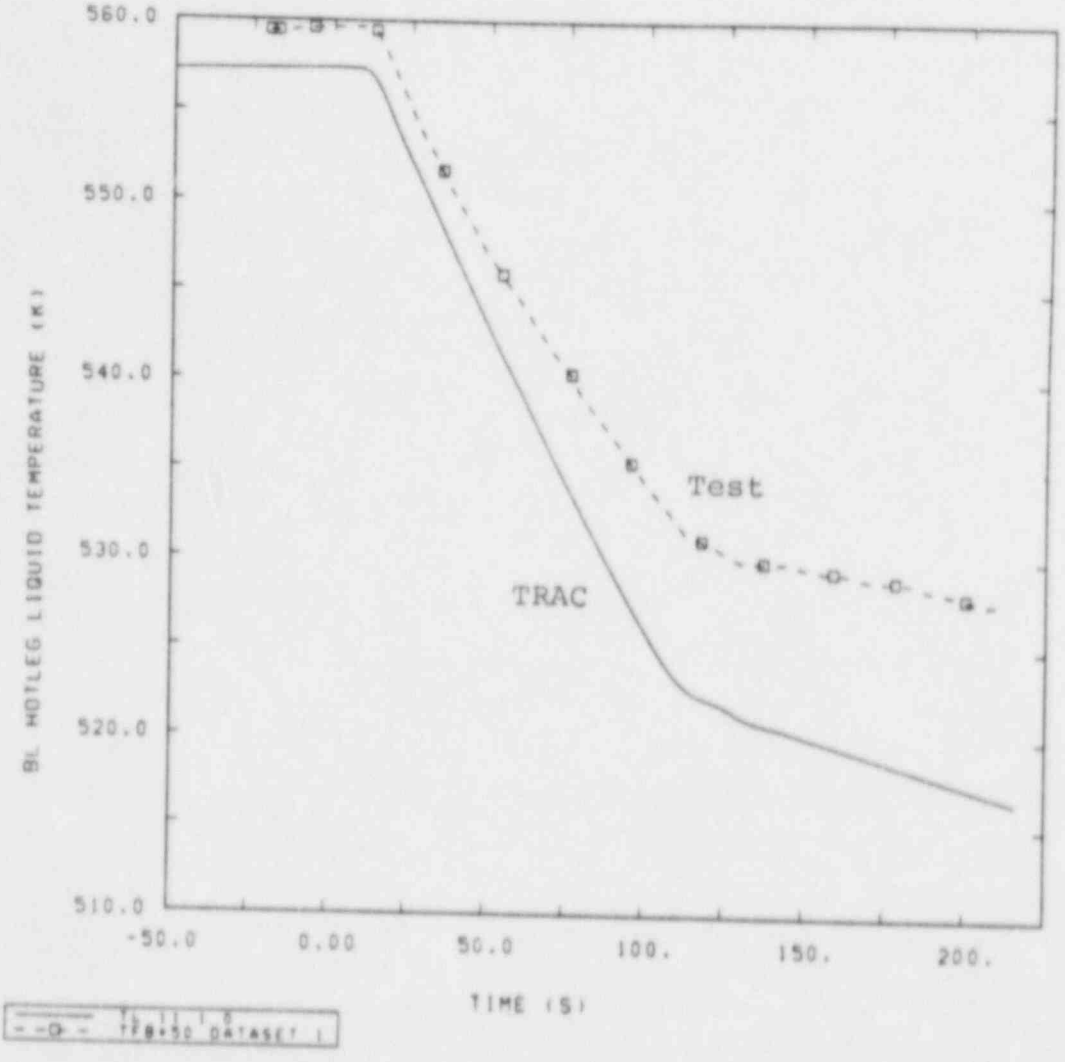


Figure 10.2.5 BL Hot-Leg Liquid Temperature, S-SF-5 IL Discharge Coefficient Parametric Transient

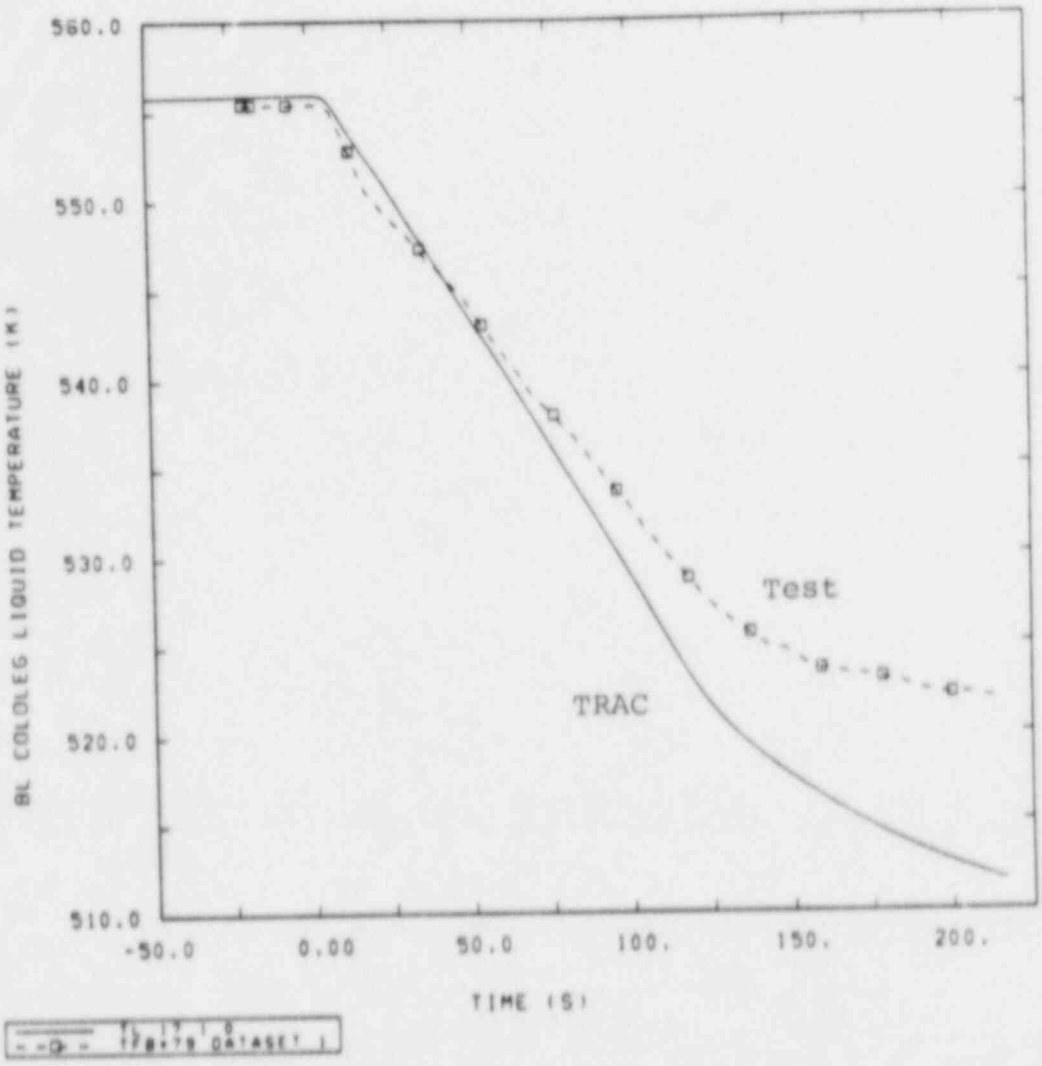


Figure 10.2.6 BL Cold-Leg Liquid Temperature, S-SF-5 IL Discharge Coefficient Parametric Transient

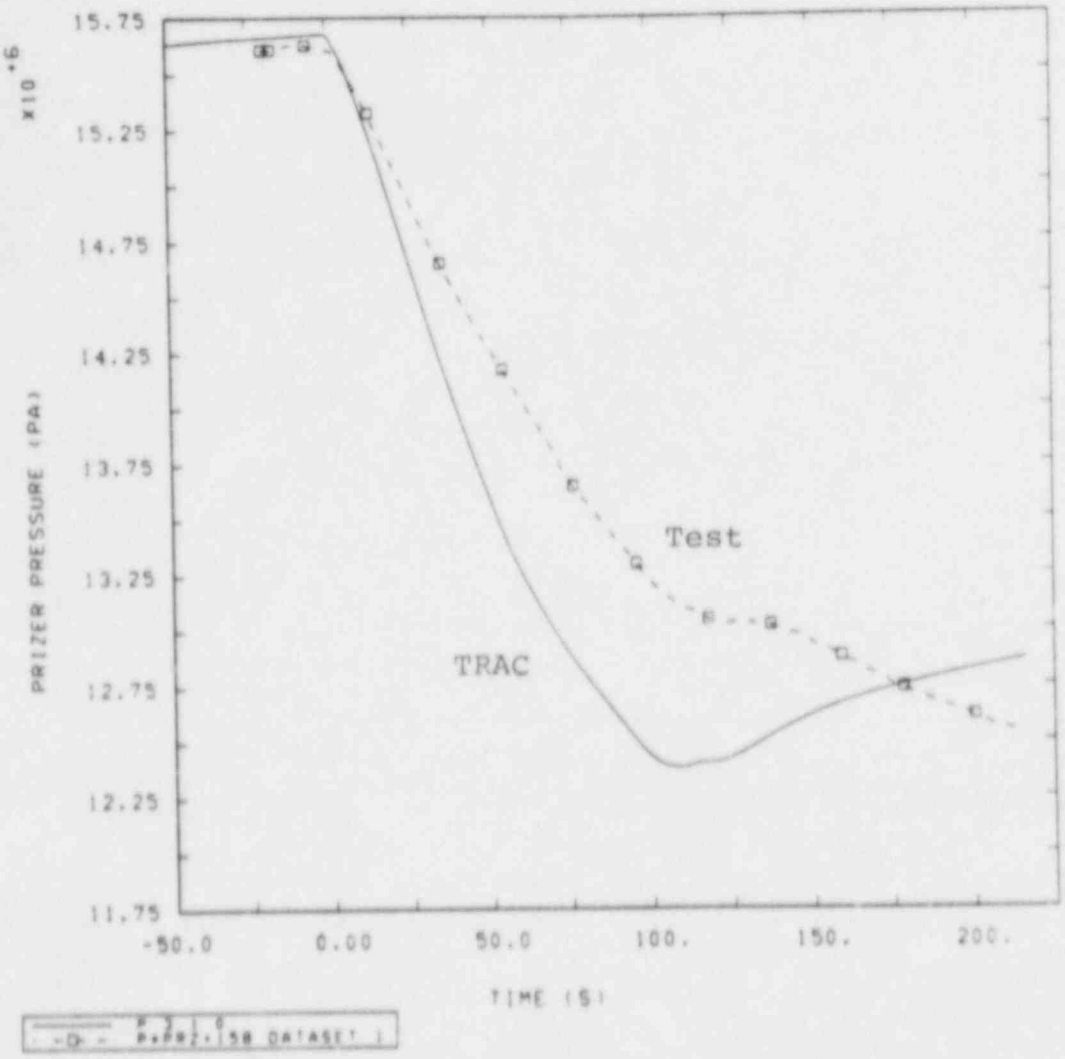


Figure 10.2.7 Pressurizer Pressure, S-SF-5 IL Discharge Coefficient Parametric Transient

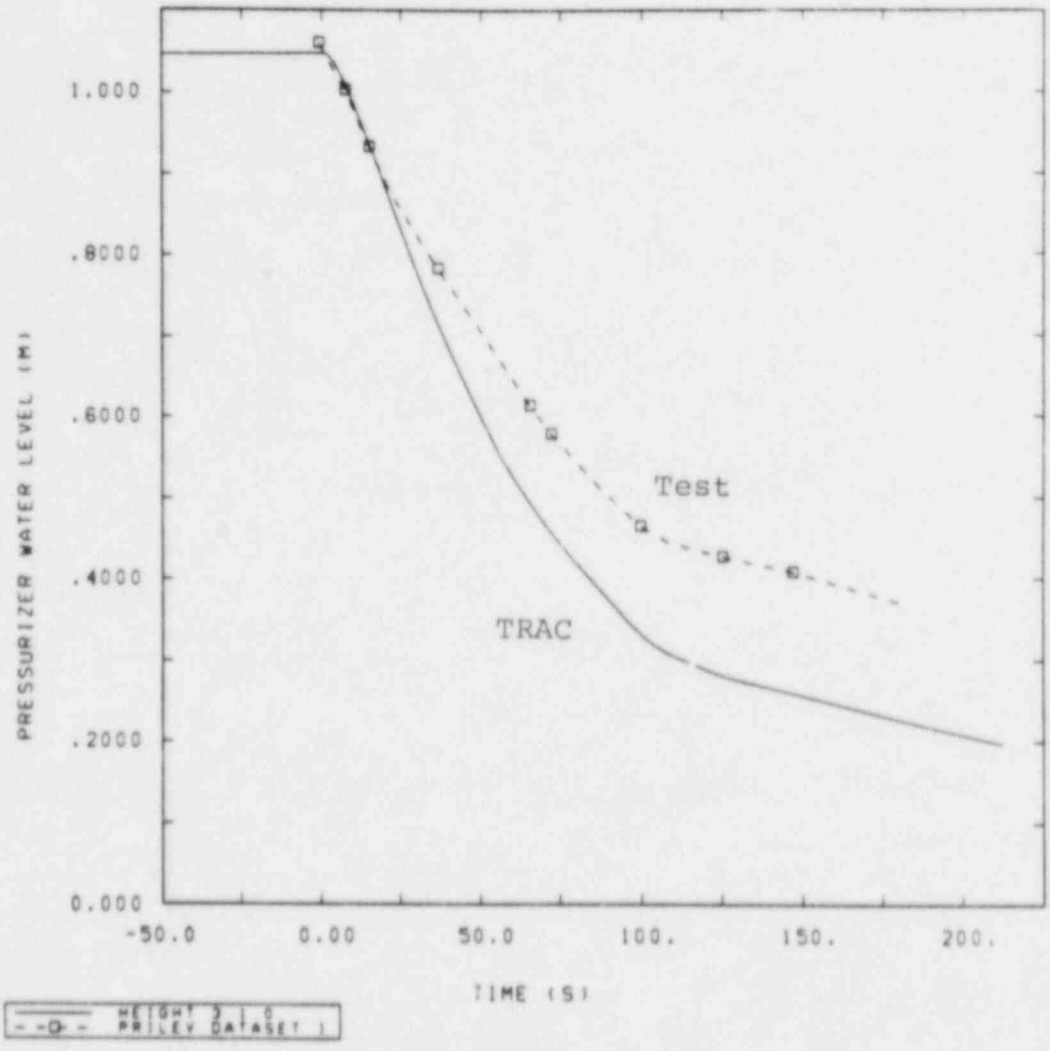


Figure 10.3.1 Pressurizer Water Level, S-SF-5 Leakage Parametric Transient

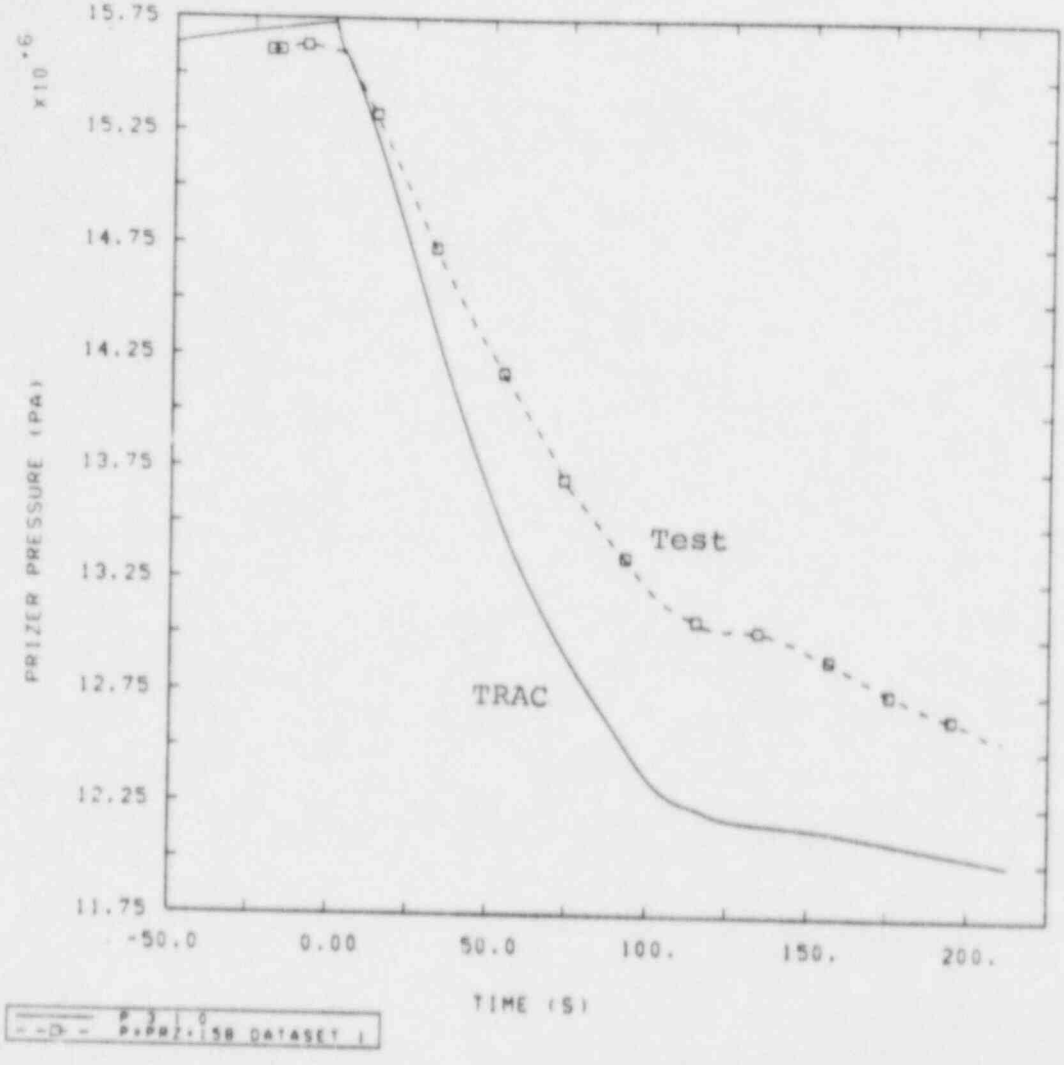


Figure 10.3.2 Pressurizer Pressure, S-SF-5 Leakage Parametric Transient

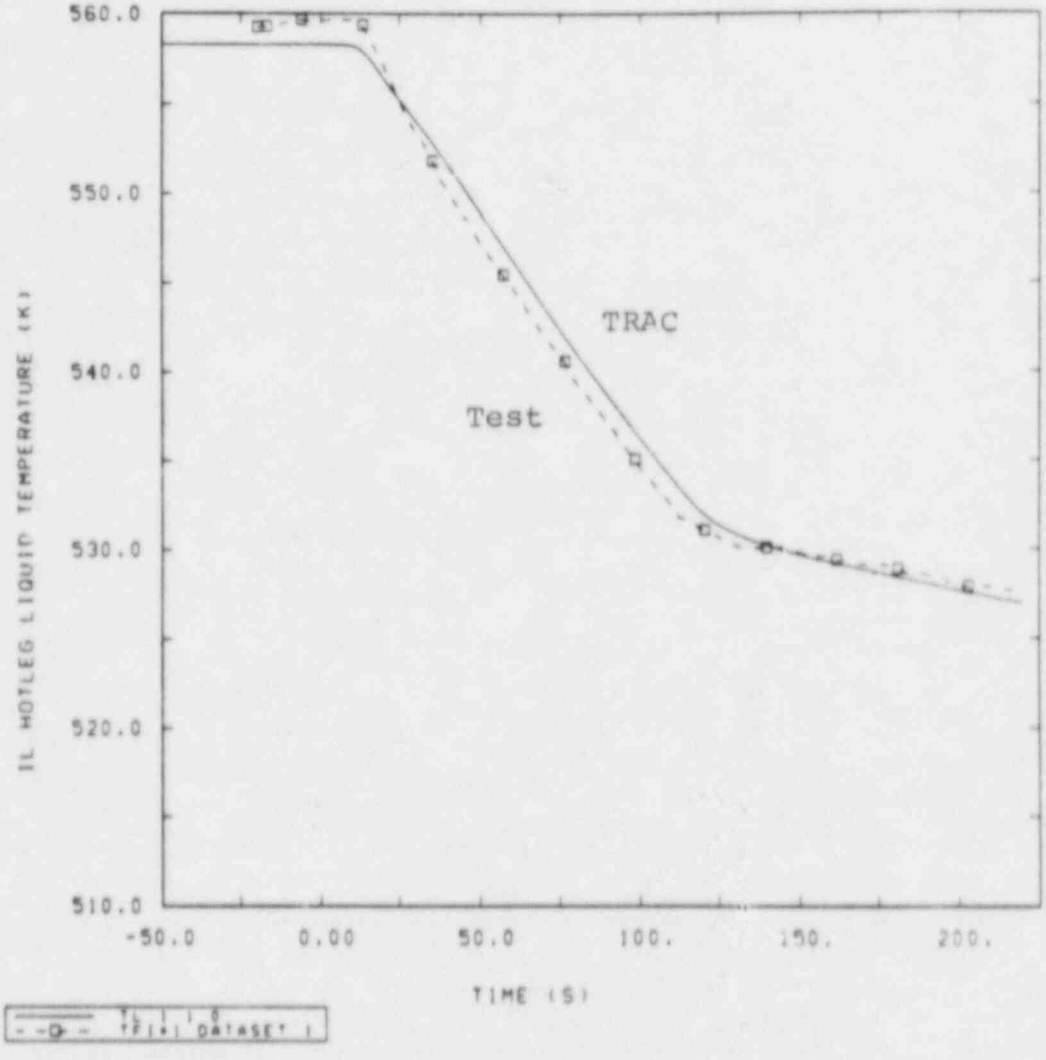


Figure 10.4.1 IL Hot-Leg Liquid Temperature, S-SF-5 Vessel Structure Parametric Transient

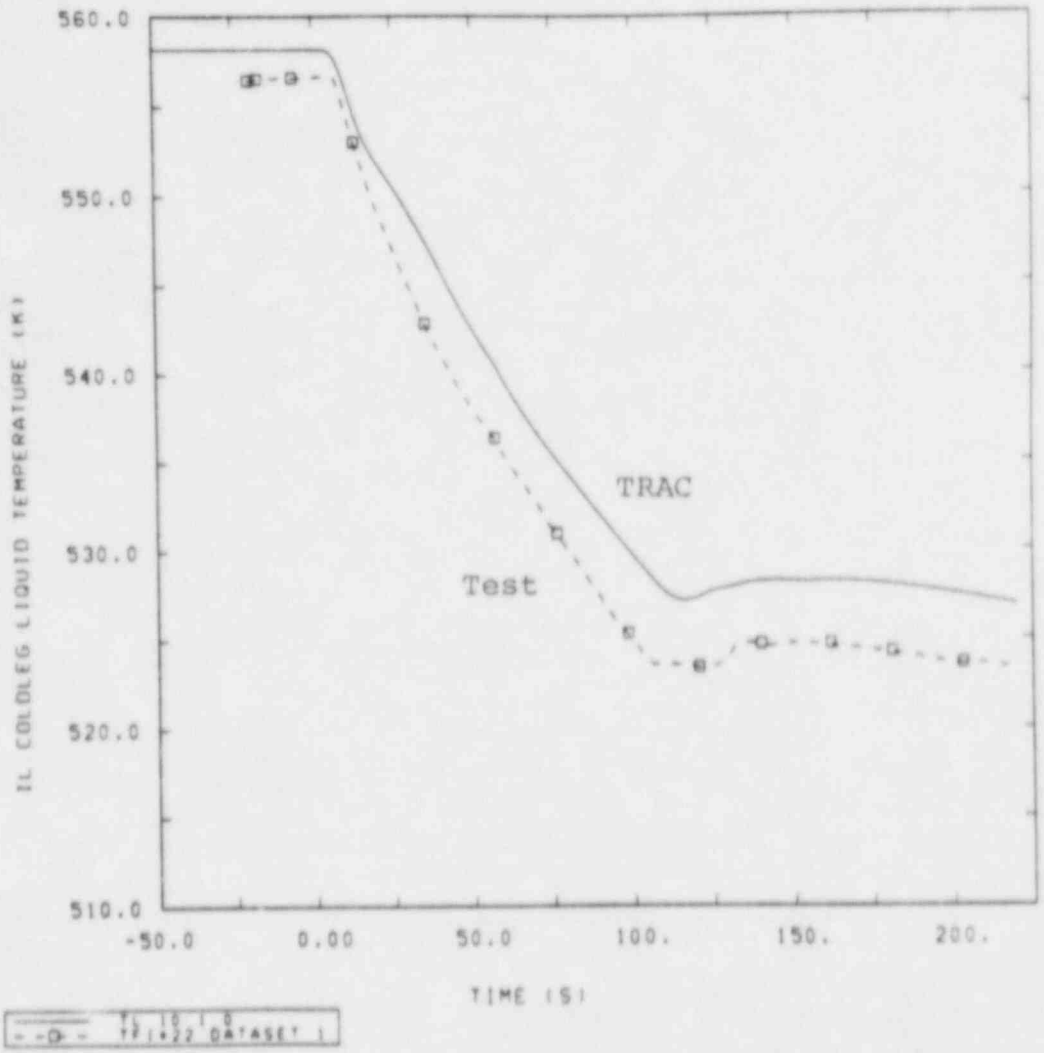


Figure 10.4.2 IL Cold-Leg Liquid Temperature, S-SF-5 Vessel Structure Parametric Transient

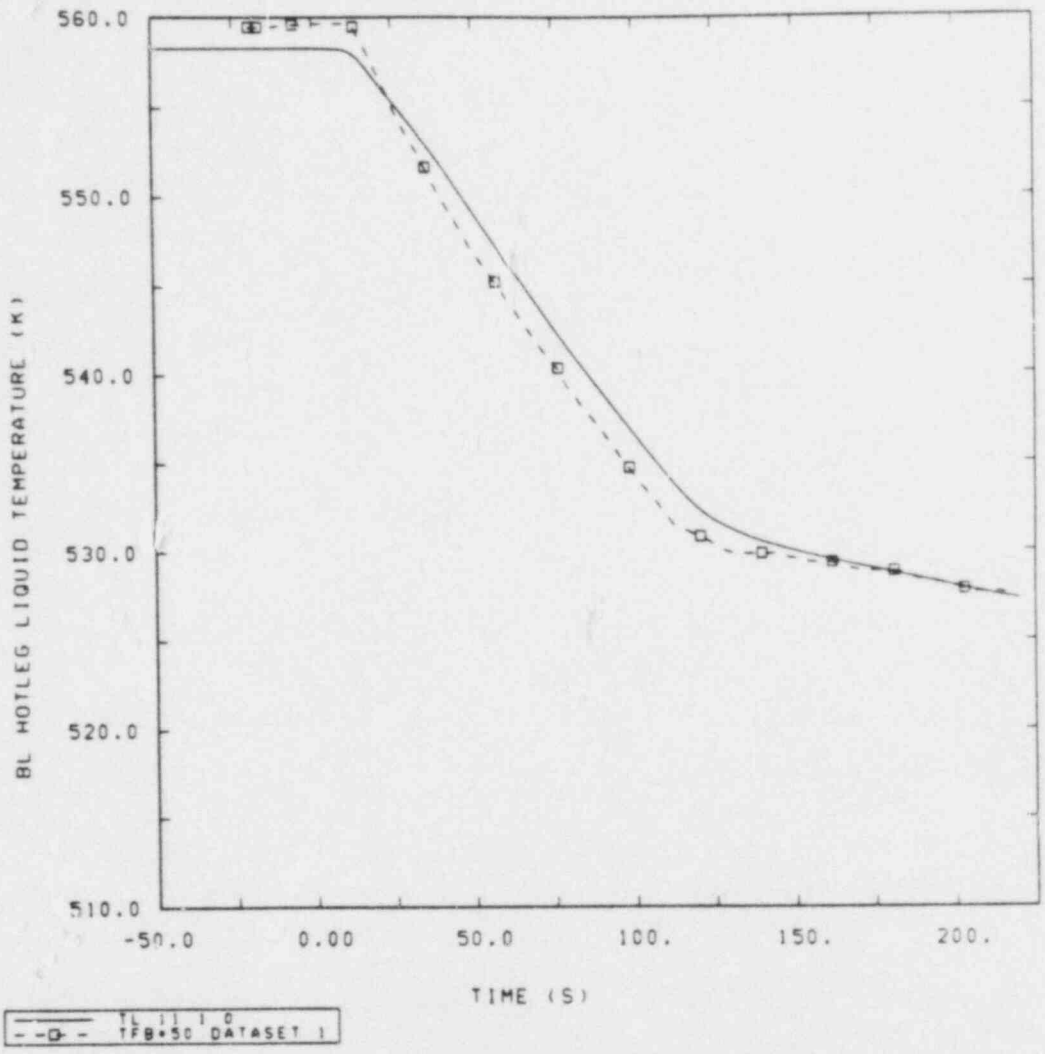


Figure 10.4.3 BL Hot-Leg Liquid Temperature, S-SF-5 Vessel Structure Parametric Transient

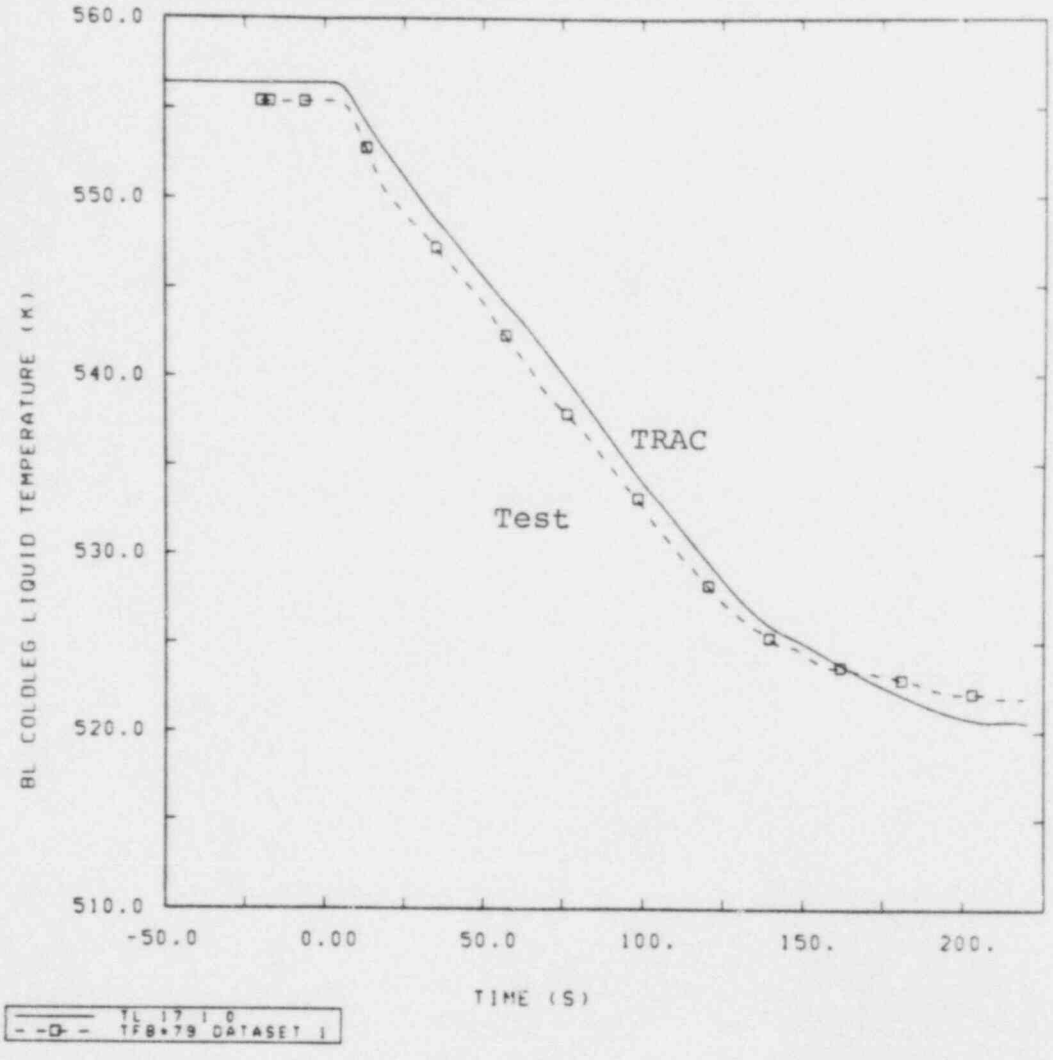


Figure 10.4.4 BL Cold-Leg Liquid Temperature, S-SF-5 Vessel Structure Parametric Transient

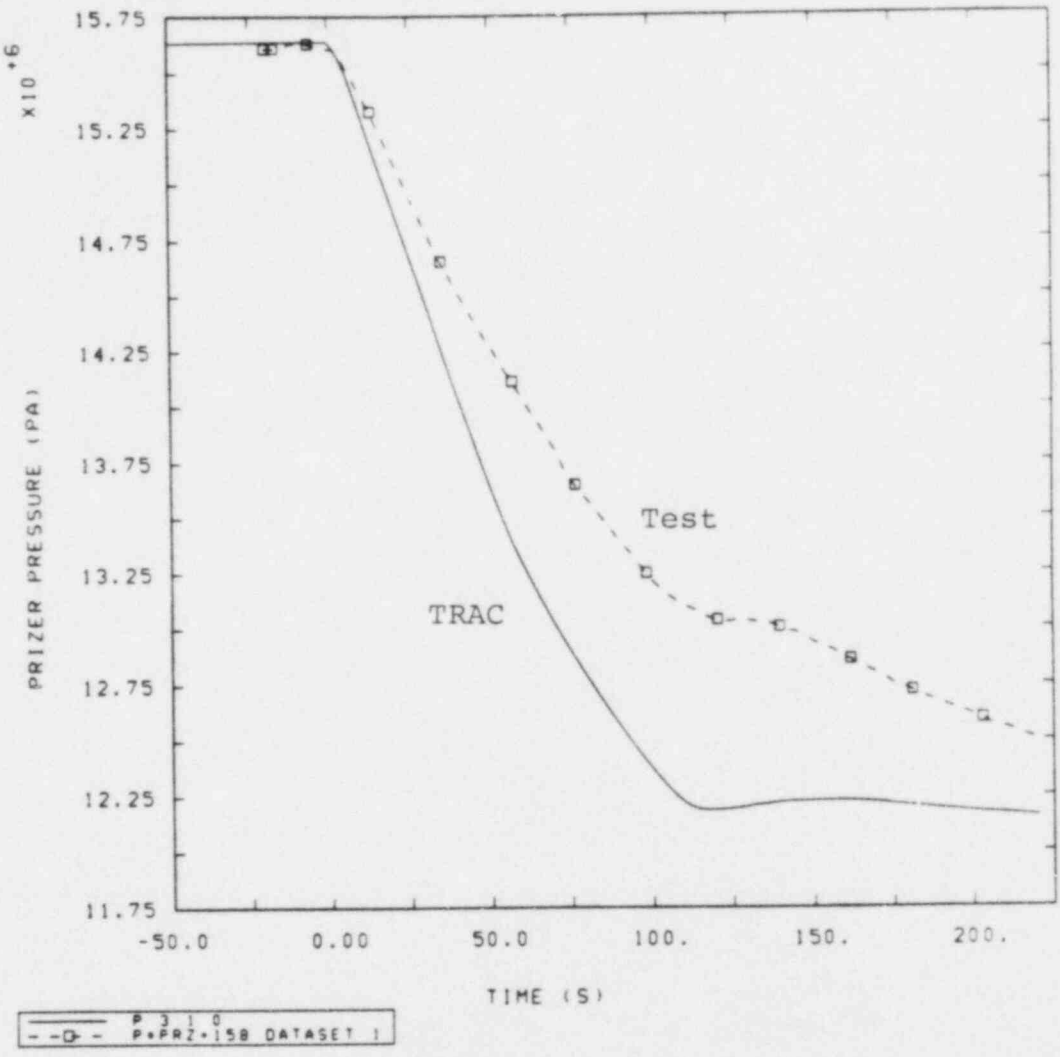


Figure 10.4.5 Pressurizer Pressure, S-SF-5 Vessel Structure Parametric Transient

## 11.0 S-SF-5 CONCLUSIONS

The steady-state calculation results (such as temperatures and flow rates) agree reasonably well with the measured results. However, it is difficult in some instances to make valid comparisons of test results with calculated results. For example, the reported total core power was 107 kW, of which 77 kW was estimated by the experimentors to be lost to the environment. Thus, there was a net core power of 30 kW. Calculating the core power using the measured loop mass flow rates and temperatures indicates a core power of 130 kW. This discrepancy occurs due to measurement uncertainty and because the heat losses do not occur at the same locations as the makeup heat sources. We did not account for this effect because we modeled the system adiabatically (due to a lack of sufficient information describing the system insulation and makeup power supplies). Because of the relatively low power of this test, these difficulties become significant and make it difficult to assess TRAC's steady-state capability.

As with the S-SF-3 transient calculation, the timing of key events was not correctly predicted in the S-SF-5 calculation. The primary-side pressure was calculated to decrease at a rate somewhat greater than the measured pressure, resulting in an early low-pressure signal. The prediction of the pressure was really not that bad when one considers the sensitivity of the pressure to the factors influencing it, such as the primary-side leakage during the test which is really an unknown quantity. Also influencing the pressure was the primary-side fluid temperatures; the calculated temperatures dropped faster than the temperatures in the test.

On the secondary side, the calculated break flow rate for the BL steam line was about 40% too high while the break flow rate for the IL steam line agreed reasonably well with the data. The BL steam-line break orifice geometry is the same as for the IL break orifice except the area of the orifices differed by a factor of three. Therefore, because steam at about the same temperature was flowing through both orifices, one would expect the break flow rates to also differ by a factor of about three. This was the case for the calculation but not for the test. In the test, the IL break flow rate was a factor of four greater than the BL break flow rate.

Another anomaly related to the break flows concerns the primary-to-secondary heat transfer rate. The BL heat transfer rate was slightly lower than the measured heat transfer rate when a two-phase multiplier was applied to the BL steam-line break to achieve the measured break flow rate. However, even though the calculated IL break flow rate was about the same as that measured, the calculated heat transfer rate was greater than that measured.

The primary-side pressure was calculated to decrease too rapidly primarily because the liquid temperatures were dropping too fast. However, even when the break flows of the intact and broken loops were adjusted to yield the approximately correct primary-side fluid temperature response, the pressure was still observed to decrease too fast. This indicates that perhaps the phase change rate in the pressurizer is incorrect for this calculation.

## 12.0 RUN-TIME STATISTICS

The steady-state run-time statistics are given in Table 12.0.1 for the S-SF-3 and S-SF-5 base case calculations along with the statistics for the S-SF-3 calculation using the 1-D input model. (The calculations were run on the CYBER 76 at SNLA). This table shows that the CPU/STEP/CELL value (or "grind time") for the 1-D S-SF-3 calculation is about 33% larger than the value for the S-SF-3 base case calculation. However, the CPU/PROBLEM TIME value is about a factor of 7 times smaller. (Recall that the 1-D model was somewhat simpler and contained fewer cells than the 3-D model.) This is due to the larger average time-step size that occurs in the 1-D model calculation. This factor of 7 decrease demonstrates the cost savings realized by using an all 1-D model, thereby eliminating the Courant time-step limitation. The statistics for the S-SF-3 and S-SF-5 base case steady-state calculations are almost identical because the same input models were used for both calculations; the only difference was in the initial conditions.

Table 12.0.2 gives the run-time statistics for the corresponding transient calculations. This table shows that the all 1-D model calculation ran only about 3.3 times faster than the base case calculation during the transient (the steady-state calculation ran 7 times faster). The reason for the smaller increase in running speed is that the coolant pumps were tripped off early in the calculation; therefore, the Courant limit in the 3-D VESSEL increased such that the time-step size of the base case calculation approached that of the 1-D calculation. The CPU/PROBLEM TIME value remained relatively high in the S-SF-5 calculation because the pumps remained operating throughout this transient.

Table 12.0.1. Steady-State Run-Time Statistics

| | S-SF-3 | S-SF-3 (1-D) | S-SF-5 |
|---|---|---|---|
| CPU (s) | 3400.0 | 551.0 | 3010.0 |
| STEPS | 4822 | 658 | 4397 |
| PROBLEM TIME (s) | 240.0 | 250.0 | 250.0 |
| CPU/PROBLEM TIME | 14.2 | 2.2 | 12.0 |
| PROBLEM TIME/STEP (ms) | 49.8 | 379.9 | 56.9 |
| CPU/STEP/CELL (ms) | 3.0 | 4.1 | 3.0 |

Table 12.0.2. Transient Run-Time Statistics

| | S-SF-3 | S-SF-3 (1-D) | S-SF-5 |
|---|---|---|---|
| CPU (s) | 1653.0 | 525.0 | 2749.0 |
| STEPS | 2115 | 734 | 3622 |
| PROBLEM TIME (s) | 388.0 | 398.0 | 204.0 |
| CPU/PROBLEM TIME | 4.3 | 1.3 | 13.5 |
| PROBLEM TIME/STEP (ms) | 183.5 | 542.2 | 56.3 |
| CPU/STEP/CELL (ms) | 3.4 | 3.5 | 3.3 |

## 13.0 OVERALL COMMENTS

One difficulty in using an integral test facility to assess the capabilities of a thermal-hydraulics code is that it is not always possible to determine why a particular phenomenon was not accurately simulated. The simulation of the entire transient depends on the correct prediction of several different mechanisms and the interaction of these mechanisms with each other. For example, the magnitudes of the HPI flow rate and the primary-side leakage rate affect the pressure but are themselves a function of pressure.

An additional complication with Semiscale tests is that there is sometimes a question of whether or not the geometry is what it is thought to be (particularly since there is no detailed facility description for Mod-2A) or if a representative input model can be built to reflect the peculiar geometry of parts of the Semiscale facility. Parametric calculations, as discussed in this report, help to determine the sensitivity of the results to such uncertainties but can not always provide a clear explanation of why certain things happen as they do.

Inconsistencies in the experimental data, as discussed throughout the report, also complicate the assessment. In addition to the inconsistencies, the uncertainties associated with the environmental heat losses and the primary-side leakage significantly affect the assessment because the SF tests are very sensitive to these factors.

With regards to the break flow, there is a good deal of uncertainty. In the S-SF-5 transient, TRAC provided a good prediction of the data for the intact loop but only a fair prediction for the broken loop. In the S-SF-3 transient, the prediction of the subcooled break flow was very poor. As reported in reference 7, the RELAP5 choked-flow models had provided good predictions of break flow for other tests containing similar geometry breaks. However, as mentioned earlier, analysts using the RELAP5 code found it necessary to use discharge coefficients untypical of the assumed break geometry in order to reproduce the data. Further investigation using other choked-flow models also resulted in failure to reproduce the data for the S-SF-3 transient. They also found it necessary to use different discharge coefficients for the IL and BL breaks in S-SF-5, even though both breaks had similar geometries. What all of this can be interpreted to mean is that the Semiscale SF series of tests are not reliable tests for assessment of a choked-flow model.

For the SF series, prediction of the steam generator secondary-side response is of major importance. In particular, the correct prediction of the fluid distribution on the secondary side is crucial. Indirect evidence indicates that the distribution was not calculated correctly by TRAC. This may be a result of an inadequate interfacial drag calculation or a poor geometric representation of the complex secondary side. There simply was not enough data available to determine the source of the difficulty with any certainty. A vapor fraction profile throughout the secondary side, particularly in the boiler, would be invaluable in this regard. (A major conclusion of our assessment calculations for the B&W steam generator loss-of-feedwater tests [15] was that the transient could not be accurately simulated unless a good prediction of the secondary-side fluid distribution during the steady state was achieved.)

There is also indirect evidence that the rate of phase change in the pressurizer during the S-SF-5 transient is incorrect. Again, this is very difficult to determine with any certainty because of all the interacting phenomena occurring in this integral test.

To summarize, the fundamental phenomena involved in the tests were predicted qualitatively but not quantitatively; the magnitude of the quantitative error and its exact cause could not be determined with certainty because of the limited data available.

## 14.0 REFERENCES


[1] TRAC-PF1/MOD1: An Advanced Best-Estimate Computer Program for Pressurized Water Reactor Thermal-Hydraulic Analysis (Draft), Safety Code Development Group, Energy Division, Los Alamos National Laboratory, Dec. 1983.

[2] D. J. Shimeck, Experiment Operating Specification for Semiscale Mod-2A Steam and Feedwater Line Break Scoping Experiment Series, EGG-SEMI-5830, Idaho National Engineering Laboratory, March 1982.

[3] D. J. Shimeck, L. J. Martinez and G. R. Berglund, Quick Look Report for Semiscale Feedwater Line Break Experiments (Tests S-SF-1, S-SF-2, and S-SF-3), EGG-SEMI-5940, Idaho National Engineering Laboratory, July 1982.

[4] Thomas M. O'Connell, Experiment Data Report for Semiscale Mod-2A Feedwater Line Break Experiment (Test S-SF-1, S-SF-2, and S-SF-3), NUREG/CR-2912, EGG-2216, Idaho National Engineering Laboratory, September 1982.

[5] G. R. Berglund, D. J. Shimeck, Quick Look Report for Semiscale Mod-2A Main Steam Line Break Tests S-SF-4 and S-SF-5, EGG-SEMI-6079, Idaho National Engineering Laboratory, November 1982.

[6] Ronald A. Larson, Experimental Data Report for Semiscale Mod-2A Steam Line Break Experiments (Tests S-SF-4 and S-SF-5), NUREG/CR-2960, EGG-2224, Idaho National Engineering Laboratory, October 1982.

[7] J. E. Streit, Posttest Relap5 Simulations of the Semiscale Mod-2A Feedwater Line Break Tests S-SF-1,2, and 3C, EGG-SEMI-6062, Oct. 1982.

[8] R. A. Shaw, Posttest RELAP5 Simulations of the Semiscale S-SF-4 and 5 Steam Line Break Experiments, EGG-SEMI-6106, November 1982.

[9] G. W. Johnsen, Semiscale System Description, Handout at Joint LOFT/Semiscale Modeling Workshop, August 18 - 19, 1981, at Idaho Falls, ID.

[10] M. T. Leonard, RELAP5 Standard Model Description for the Semiscale Mod-2A System, EGG-SEMI-5692, Idaho National Engineering Laboratory, December 1981.

[11] J. Michael McGlaun and L. N. Kmetyk, RELAP5 Assessment: Semiscale Natural Circulation Tests S-NC-2 and S-NC-7, NUREG/CR-3258, SAND83-0833, Sandia National Laboratories, May 1983.

[12] A. C. Peterson, RELAP5 Assessment: Semiscale Small Break Tests S-UT-1, S-UT-2, S-UT-6, S-UT-7, and S-UT-8, NUREG/CR-3772, SAND84-0884, Sandia National Laboratories, November 1984.

[13] Lubomyra N. Kmetyk, TRAC-PF1/MOD1 Independent Assessment: Intermediate Break Tests LOBI B-R1M and Semiscale S-IB-3), NUREG/CR-3970P, SAND85-2264, (to be published).

[14] D. Dobranich and L. D. Buxton, TRAC-PF1/MOD1 Independent Assessment: B&W 19-Tube Once-Through Steam Generator Tests, NUREG/CR-3877P, SAND84-1229, July 1984.

[15] Letter from John E. Streit of INEL to Larry D. Buxton, Re: Request for Semiscale System Information, Oct. 3, 1984.

[16] A. C. Peterson, TRAC-PF1/MOD1 Independent Assessment: NEPTUNUS Pressurizer Test Y05, NUREG/CR-3919, SAND84-1534, December 1984.

# APPENDIX I - FACILITY DESCRIPTION

The standard Semiscale Mod-2A system, shown in Figure AI.1, consists of a vessel with its associated internals and an external downcomer, an intact loop, and a broken loop both with active steam generators and pumps, a break effluent measuring system, and a steam generator secondary system. Other subsystems include the emergency core cooling system, external heat loss makeup system, leakage makeup system, and a noncondensible gas injection system. The Semiscale system was scaled from a reference PWR system based on the core power ratio, 2/3411; component elevations, dynamic pressure heads, and liquid distribution were maintained as similar as practical, most notably in the design of a full-length core, full-length upper plenum and upper head, and full-height steam generators. The major primary coolant system elevations are given in Table AI.1.

The intact loop consists of a steam generator, primary coolant pump, and pressurizer connected by piping. The intact-loop piping itself is composed of individual pipe sections called spool pieces. These spool pieces and their relative locations in the intact loop are identified by spool numbers in Figure AI.2; the upper drawing unfolds the intact loop for easier viewing by preserving the orientation of the components in the vertical plane without regard to the actual horizontal orientation, which is shown in the lower drawing. The spool piece lengths and blue print numbers are given in Table AI.2. The intact loop piping, other than the vertical spool pieces leading to the steam generator inlet and outlet (spools 4 through 12) and spool 3, are constructed of 3-in. Sch 160 Type 316 stainless steel pipe; spool pieces 3 through 12 are constructed of 2-1/2-in. Sch 160 pipe. The intact loop pump is a volute-type, heavy duty, horizontal, centrifugal pump. A venturi is installed in the pump discharge to give the properly scaled locked rotor hydraulic resistance.

The broken loop is designed to simulate a single loop of a four-loop PWR and contains an active steam generator and pump. The spool pieces in the broken loop are constructed of 1-1/2-in. Sch 160 Type 316 stainless steel piping; these spool pieces and their relative locations in the broken loop are identified by spool numbers in Figure AI.3, and the corresponding spool piece lengths and blueprint numbers are given in Table AI.3. The broken loop pump is a high-speed, vertical, centrifugal pump with a bottom suction and side discharge, similar to PWR pumps. A flow restriction is incorporated into the pump discharge.

The intact and broken loop steam generators, shown in Figure AI.4 and summarized in Table AI.4, consist of a two-pass tube and shell design with primary fluid flowing through vertical inverted U-shaped tubes and secondary coolant passing through the shell side. With the secondary side operating at saturation conditions, a centrifugal separator at the top of the riser (or boiler) section increases the exit quality of the steam rising through the steam dome and out a discharge line, while liquid separated from the steam falls down a downcomer outside the boiler shroud, creating a recirculation flow path. The intact loop steam generator has two short, two medium, and two long tubes representative of the range of bend elevations in a PWR steam generator, while the broken loop steam generator contains just one short tube and one long tube. The same tube stock (2.22 cm OD, 0.124 cm wall) and tube spacing (3.175 cm triangular pitch) used for PWR U-tubes are used in this "Type II" steam generator. Since the heat transfer area is specified based on the ratio of PWR to Semiscale primary system volume, the number of tubes is thereby fixed by the specified tube diameter and lengths.

Fillers are installed on the shell side in both the boiler and downcomer regions to provide a more properly scaled secondary fluid volume. The addition of these filler pieces not only reduces the total secondary coolant volume, but also changes the flow geometry of the boiler and downcomer, as shown in the cross-sectional view in Figure AI.5. The boiler section filler pieces create a parallelogram-shaped flow channel along the length of the U-tubes, while the downcomer filler pieces reduce the downcomer annulus to a set of slotted flow channels. Baffle plates are located at several axial positions in the boiler section of the steam generator, creating a substantial flow restriction to the rising coolant. For the S-SF-3 and S-SF-5 tests, auxiliary feedwater enters the downcomer above the filler pieces at approximately the elevation of the top of the U-tubes; feedwater enters at the very bottom of the downcomer. The elevations of the steam generator nozzles, plena, and tubes are similar to those in a PWR; however, the steam dome is shorter than a PWR steam dome and the steam drying equipment is of a simpler and less efficient design. (As a result of these dissimilarities, the secondary fluid operating level at full power conditions is about 75% of the operating level in a PWR, with the lower level required to ensure stable steam generator operation.) Figures AI.5, AI.6, and AI.7 show details of the steam generator filler pieces, steam separator, and feedwater-entrance region, respectively.

The pressurizer, which is connected to the intact-loop hot leg, is shown in Figure AI.8. The pressurizer vessel is made of 10-in. Sch 160 Type 347 stainless steel pipe, is approximately 1.14 m high and has a total volume of 0.034 $m^3$. Heat is supplied by 24 0.05-kW vertically-oriented electric heater rods, which are inserted in 2.2 cm OD stainless steel tubes sealed at the bottom. A pressurizer spray system is not included in the Mod-2A system. The pressurizer operates in a manner similar to its counterpart in a large PWR in that the vessel is partially filled with water and maintained at a saturation temperature corresponding to the desired system pressure. The pressurizer surge line and tubing (1.27 cm OD, 0.165 cm wall, ~2.7 m length and ~1.53 m total elevation drop from bottom of pressurizer vessel to hot leg centerline) is sized for a flow restriction that provides representative PWR flow rates.

The Mod-2A vessel, shown in Figure AI.9, consists of a multi-section pressure vessel containing a lower plenum, heated core, upper plenum and upper head, and an external inlet annulus and downcomer. The pressure vessel is constructed primarily of 6-in. Sch XXS stainless steel pipe, with stainless steel Grayloc clamps used to connect the various vessel sections; the complete pressure vessel is approximately 10 m long.

The upper head region is contained within the top ~25% of the pressure vessel, and contains a filler to provide the proper upper head internal volume, an insulator designed to provide a steam gap between the filler ID and the insulator OD, and a simulated control rod guide tube. An upper core support plate simulator forms the boundary between the upper head and upper plenum regions; this upper core support plate provides support for the simulated guide tube and for the upper ends of the two simulated core support columns which extend down through the upper plenum region. Approximately 4% of the total primary coolant flow into the vessel bypasses the downcomer and core through an external upper head bypass line from the top of the downcomer inlet annulus to the upper head. The bypass coolant rejoins the

heated coolant in the vessel upper plenum via the simulated control rod guide tube and core support columns. The exit of the upper head bypass line standpipe and the inlets of the control rod guide tube and core support columns are at different elevations within the upper head.

The upper plenum region, shown in more detail in Figure AI.10, extends from the upper core support plate to the top of the heated core region, and is approximately 2.5 m long. The upper and lower sections of the upper plenum contain fillers and insulators similar to those in the upper head. Two hot leg nozzles extend from the vessel upper plenum approximately 21.6 cm above the cold-leg centerline to provide connections for the intact- and broken-loop hot-leg piping. The flow path above the core to the hot-leg nozzles is quite tortuous; in addition to a core flow measurement assembly, a simulated control rod guide tube and two simulated core support columns obstruct the flow path, and a short set of vertical tubes creates a horizontal flow restriction across the vessel at the hot leg elevation. This flow restrictor assembly simulates the flow restriction in a PWR caused by control rod guide tubes and core support columns. Above the hot legs, the upper plenum contains a significant amount of fluid which is not involved in the main flow path. The simulated control rod guide tube and core support columns extend from the upper head through the upper plenum and terminate open-ended in the upper core plate located in the heater ground hub which forms the boundary between the upper plenum and the top of the active heated core region. The guide tube is slotted in the upper plenum region.

The 3.66 m heated length of the core, shown in Figure AI.11, extends downward from the heater rod ground hub to the top of the mixer box (approximately 4.96 m below the cold leg centerline), which separates the core and the lower plenum regions. This figure includes a cross-sectional view of the Mod-2A vessel over the core region. The 25-rod electrically-heated core is enclosed in a square housing with no coolant bypass. The heater rods, 1.07 cm in diameter, are positioned and held in the core with 10 grid spacers (at elevations shown in Figure AI.11) which maintain the heater rods on a typical PWR pitch of 1.43 cm. The 16 peripheral rods are powered separately from the 9 central rods, permitting a radial profile (although normally no radial peaking is simulated); two of the 16 peripheral rods, however, are not powered. The Semiscale Mod-2A heater rod design consists of a helically-wound constantan filament, electrically insulated from the dual-sheath stainless steel clad by compacted boron nitride powder. Chromel-alumel thermocouples are swaged between cladding sheaths in six symmetrical polar locations and ten axial elevations distributed along the rod. The heater rods have a symmetric chopped-cosine axial power distribution (shown in Figure AI.12); the peak-to-average power ratio is 1.55.

The lower plenum, shown in Figure AI.13, consists of an annular region between the flow mixer box and the pressure vessel, which serves to distribute flow from the downcomer pipe around the vessel periphery, and a lower head chamber region below the mixer box which approximates the scaled volume of a PWR lower plenum. (The lower plenum is the only part of the vessel which is not height-scaled.) Coolant flow from the downcomer distribution annulus changes direction within the lower head, turning up into the core housing. A simulated lower core plate at the entrance of the core housing provides a significant reduction in coolant flow area. The outer walls of the downcomer distribution annulus and the lower head are lined with honeycomb

insulation to reduce heat transfer between the outer vessel wall and the fluid in the lower plenum. The heater rods pass through the length of the lower plenum and penetrate the vessel through the bottom head.

The downcomer inlet annulus assembly contains the cold-leg nozzles and is designed to provide an annular inlet geometry similar to that in a PWR. Both surfaces of the inlet annulus are covered with insulators that maintain a steam gap to isolate the fluid from the hot walls of the assembly. The lower end of the inlet annulus contains a transition section that funnels the flow into the downcomer pipe. The downcomer inlet annulus is connected to the vessel upper head with 1/2-in. tubing which simulates the bypass flow paths in a PWR; as already mentioned, about 4% of the total combined loop flows is normally routed through the bypass line into the upper head. Coolant enters the vessel through an external downcomer inlet annulus (shown in Figure AI.10). This annular entrance section reduces to an instrumented pipe over the major length of the lower vessel, until the bottom of the downcomer rejoins the vessel at the lower plenum through an annular distribution annulus, as shown in Figure AI.13. The downcomer pipe is fabricated from 3-in. Sch 160 pipe, and the inner wall of the downcomer pipe is lined with a honeycomb insulator to limit heat transfer between the pipe wall and the fluid. An instrumented spool piece provides the connection between the lower end of the downcomer pipe and the downcomer nozzle connecting to the downcomer distribution annulus.

The break orifice geometry for the feedwater-line break tests is shown in Figure AI.14. The geometry for the steam-line break tests is shown in Figure AI.15.

The high pressure injection systems, low pressure injection systems, and the loop accumulators are connected to the cold legs between the pump and the vessel in the intact loop and between the pump and the break in the broken loop. Positive displacement pumps supply the HPI and LPI flows, which are scaled to represent PWR ECC systems. The accumulators were not used for the SF tests.

Table AI.1 Semiscale Primary Coolant System Elevations

SEMISCALE PRIMARY COOLANT SYSTEM ELEVATIONS[a]

| LOCATION | ELEVATION (IN.) |
|---|---|
| VESSEL | |
| TOP OF UPPER HEAD | +166.6 |
| TOP OF GUIDE TUBE | +132.1 |
| BOTTOM OF UHI INJECTION TUBE | +127.1 |
| TOP OF CORE SUPPORT TUBES | +67.1 |
| TOP OF UPPER SUPPORT PLATE | +61.4 |
| BOTTOM OF UPPER SUPPORT PLATE | +53.4 |
| HOT LEG NOZZLE CENTERLINE | +8.5 |
| COLD LEG NOZZLE CENTERLINE | 0.0 |
| TOP OF HEATED CORE | -51.1 |
| BOTTOM OF HEATED CORE | -191.1 |
| TOP OF LOWER PLENUM | -215.0 |
| BOTTOM OF LOWER PLENUM | -227.6 |
| INTACT LOOP | |
| BOTTOM OF STEAM GENERATOR TUBE SHEET | +81.6 |
| SHORT TUBE TOP, SPILLOVER | +436.9 |
| MIDDLE TUBE TOP, SPILLOVER | +465.4 |
| LONG TUBE TOP, SPILLOVER | +491.9 |
| PUMP SUCTION CENTERLINE | -111.0 |
| BOTTOM OF PRESSURIZER INTERNAL VOLUME | +68.8 |
| TOP OF PRESSURIZER INTERNAL VOLUME | +117.3 |
| BROKEN LOOP | |
| BOTTOM OF STEAM GENERATOR TUBE SHEET | +81.6 |
| SHORT TUBE TOP, SPILLOVER | +436.9 |
| LONG TUBE TOP, SPILLOVER | +491.9 |
| PUMP SUCTION CENTERLINE | -110.3 |

[a] ELEVATIONS ARE RELATIVE TO COLD LEG CENTERLINE

Table AI.2 Intact-Loop Spool Pieces

Intact Loop Spool Pieces

| Spool Piece Number | Spool Piece Indent | Total Length (in) | Blueprint Number |
|---|---|---|---|
| H. L. Nozzle | | 8.65 | 407968 |
| 1 | 3-PC-1B | 23.06 | 414684 |
| 2 | 3-PC-18 | 15.61 | 407346 |
| 3 | 2½-PC-2 | 52.51 | 415155 |
| 4 | 2½-PC-6 | 26.31 | 414431 |
| 5 | 2½-PC-7 | 13.995 | 414425 |
| 6 | 2½-PC-8 | 14.00 | 414426 |
| 7 | 2½-PC-9 | 19.195 | 414427 |
| SG Inlet | | 6.32 | 414271 |
| SG Outlet | | 6.32 | 414271 |
| 8 | 2½-PC-10 | 27.195 | 414428 |
| 9 | 2½-PC-11 | 13.995 | 414425 |
| 10 | 2½-PC-12 | 14.00 | 414426 |
| 11 | 2½-PC-13 | 14.00 | 414429 |
| 12 | 2½-PC-14A | 19.41 | 414430 |
| 13 | 3-PC-20 | 85.25 | 409027 |
| 14 | 3-PC-20 | 20.638 | 409027 |
| 15 | 3-PC-20 | 62.00 | 409027 |
| 16 | 3-PC-20 | 23.06 | 414684 |
| 17 | 3-PC-9A | 19.319 | 404749 |
| 18 | 3-PC-10A | 20.53 | 408613 |
| IL Pump | | | |
| 19 | 3-PC-11A | 17.00 | 412858 |
| 20 | 3-PC-12 | 17.25 | 404759 |
| 21 | 3-PC-13 | 23.06 | 404794 |
| 22 | 3-PC-19A | 37.90 | 414684 |
| C. L. Nozzle | | 7.15 | 407986 |

Table AI.3 Broken-Loop Spool Pieces

Broken Loop Spool Pieces

| Spool Piece Number | Spool Piece Indent | Total Length (in) | Blueprint Number |
|---|---|---|---|
| H. L. Nozzle | (3 in. Sch. 160) | 16.07 | 407975 |
| 50 | 1½-ABL-1 | 24.01 | 407670 |
| 55 | 1½-ABL-14A | 59.517 | 414670 |
| 56 | 1½-ABL-30 | 11.83 | 414671 |
| 57 | 1½-ABL-31 | 13.872 | 414672 |
| 58 | 1½-ABL-32 | 13.75 | 414673 |
| 59 | 1½-ABL-33 | 19.826 | 414674 |
| SG Inlet | | 4.142 | 414272 |
| SG Outlet | | 4.142 | 414272 |
| 60 | 1½-ABL-34 | 15.316 | 414675 |
| 61 | 1½-ABL-35 | 13.75 | 414676 |
| 62 | 1½-ABL-36 | 13.872 | 414672 |
| 63 | 1½-ABL-37 | 13.75 | 414673 |
| 64 | 1½-ABL-6A | 109.17 | 414677 |
| 65 | 1½-ABL-7 | 33.834 | 407384 |
| 72 | 1½-ABL-9 | 61.82 | 407380 |
| 73 | 1½-ABL-11 | 27.56 | 407673 |
| BL Pump | | | |
| 74 | 1½-ABL-12 | 23.64 | 407674 |
| 76 | 1½-ABL-17 | 19.77 | 407875 |
| 79 | 1½-ABL-15 | 28.01 | 407675 |
| CL Nozzle | (3 in. Sch 160) | 15.314 | 407986 |

Table AI.4 Type II Steam Generator Data (Mod-2A)

| | Intact Loop | Broken Loop |
|---|---|---|
| Number Tubes | 6 | 2 |
| Tube Dimensions | (0.875 in. OD x 0.049 in. | Wall x 1.25 in. Pitch |
| Tube Height(1) | 2 @ 391 in.<br>2 @ 364.5 in.<br>2 @ 336 in. | 1 @ 391 in.<br>1 @ 336 in. |
| Primary Volume, Bundle | 1.27 $ft^3$ | 0.40 $ft^3$ |
| Primary Plenum Volume | 0.058 $ft^3$ each | 0.042 $ft^3$ each |
| Secondary Volume(2) | 4.27 $ft^3$ | 2.97 $ft^3$ |
| Downcomer Volume | 1.34 $ft^3$ | 1.13 $ft^3$ |
| Total Secondary Volume(3) | 11.0 $ft^3$ | 9.45 $ft^3$ |
| Secondary Heat Transfer Area | 83.3 $ft^2$ | 27.76 $ft^2$ |

(1) Above top of tube sheet
(2) Tube sheet to top of tubes
(3) Tube sheet to top of separators

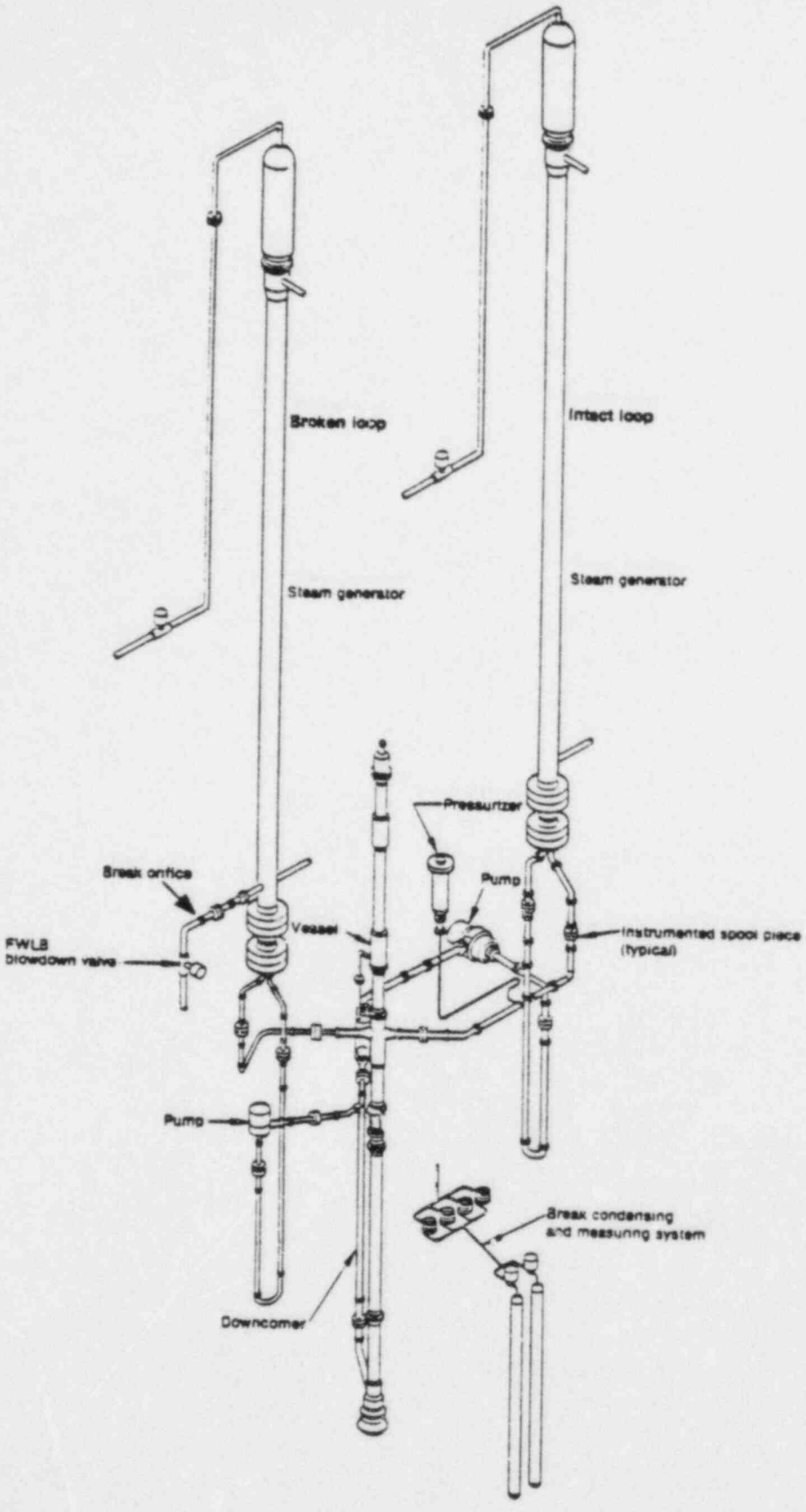


Figure AI.1 Semiscale Mod-2A Facility Diagram, SF Series

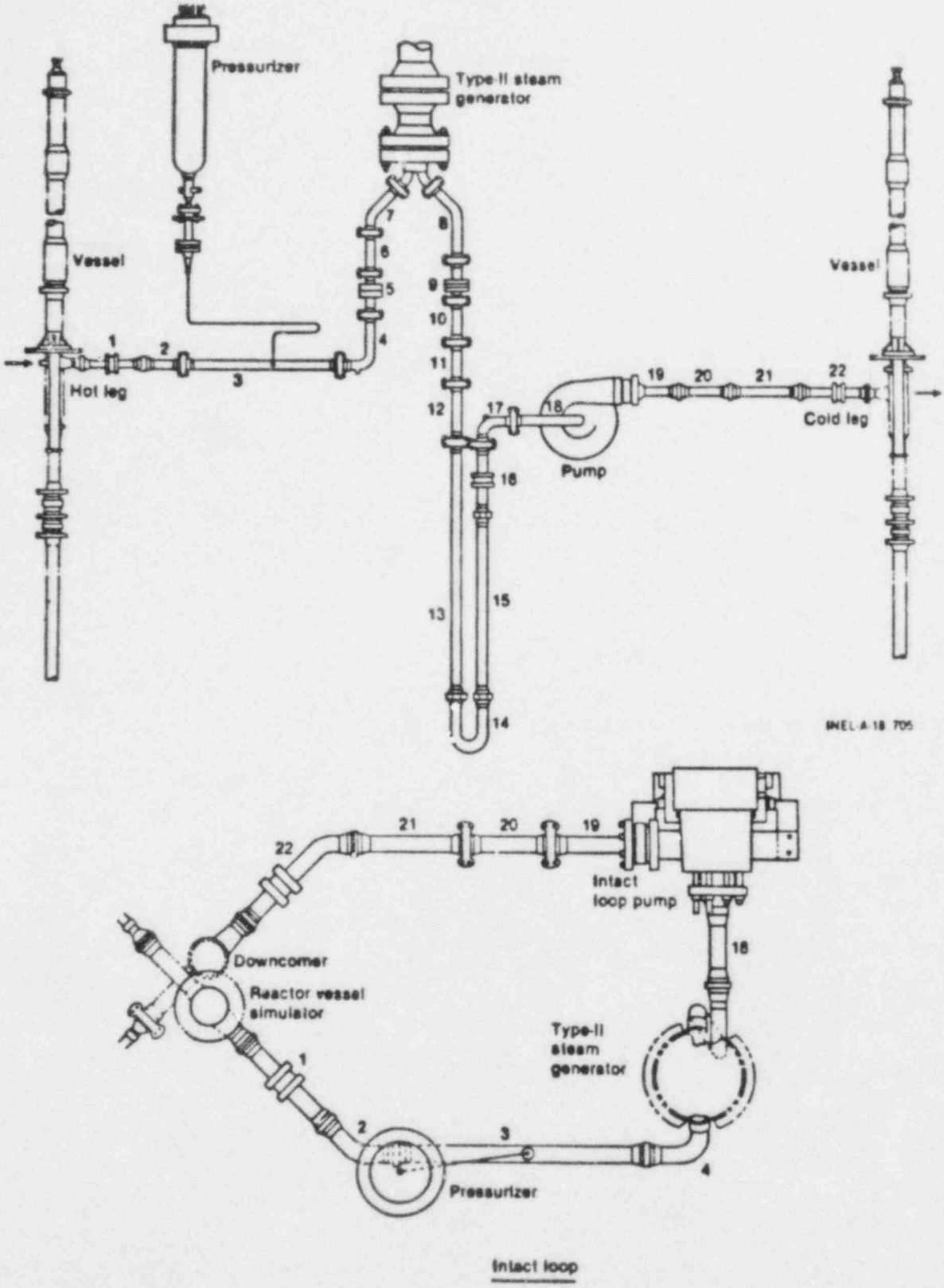


Figure AI.2 Intact-Loop Spool Pieces

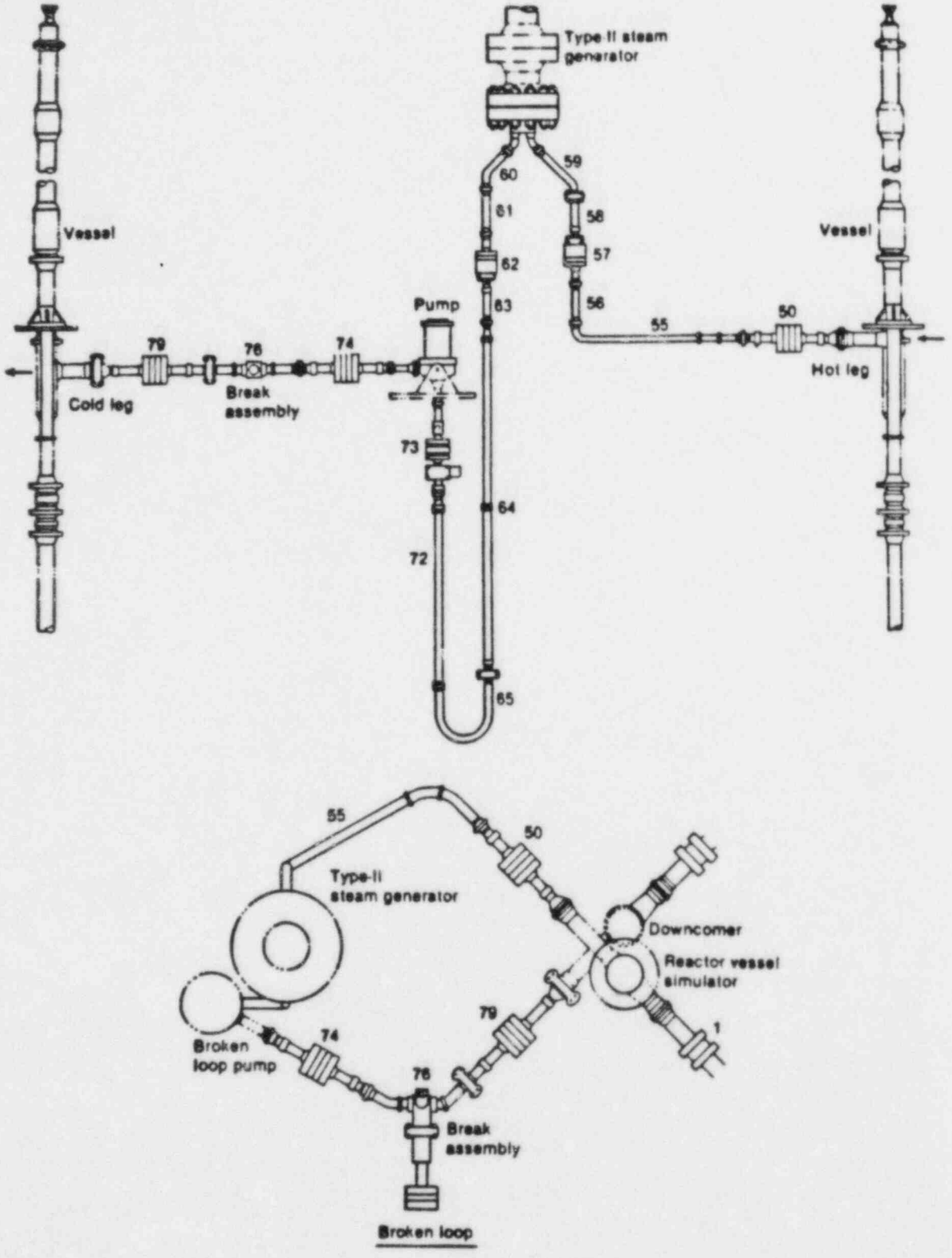


Figure AI.3 Broken-Loop Spool Pieces

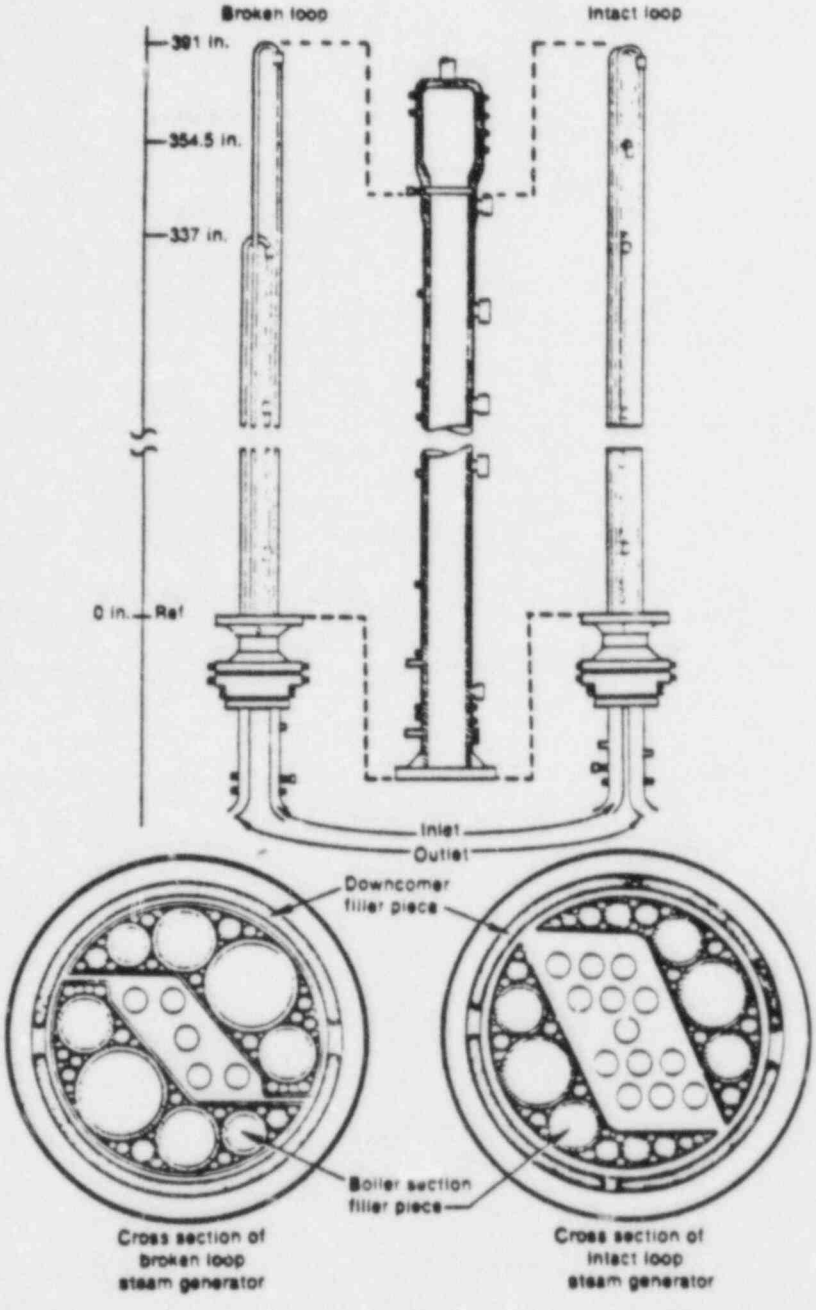


Figure A1.4 Steam Generator Assembly

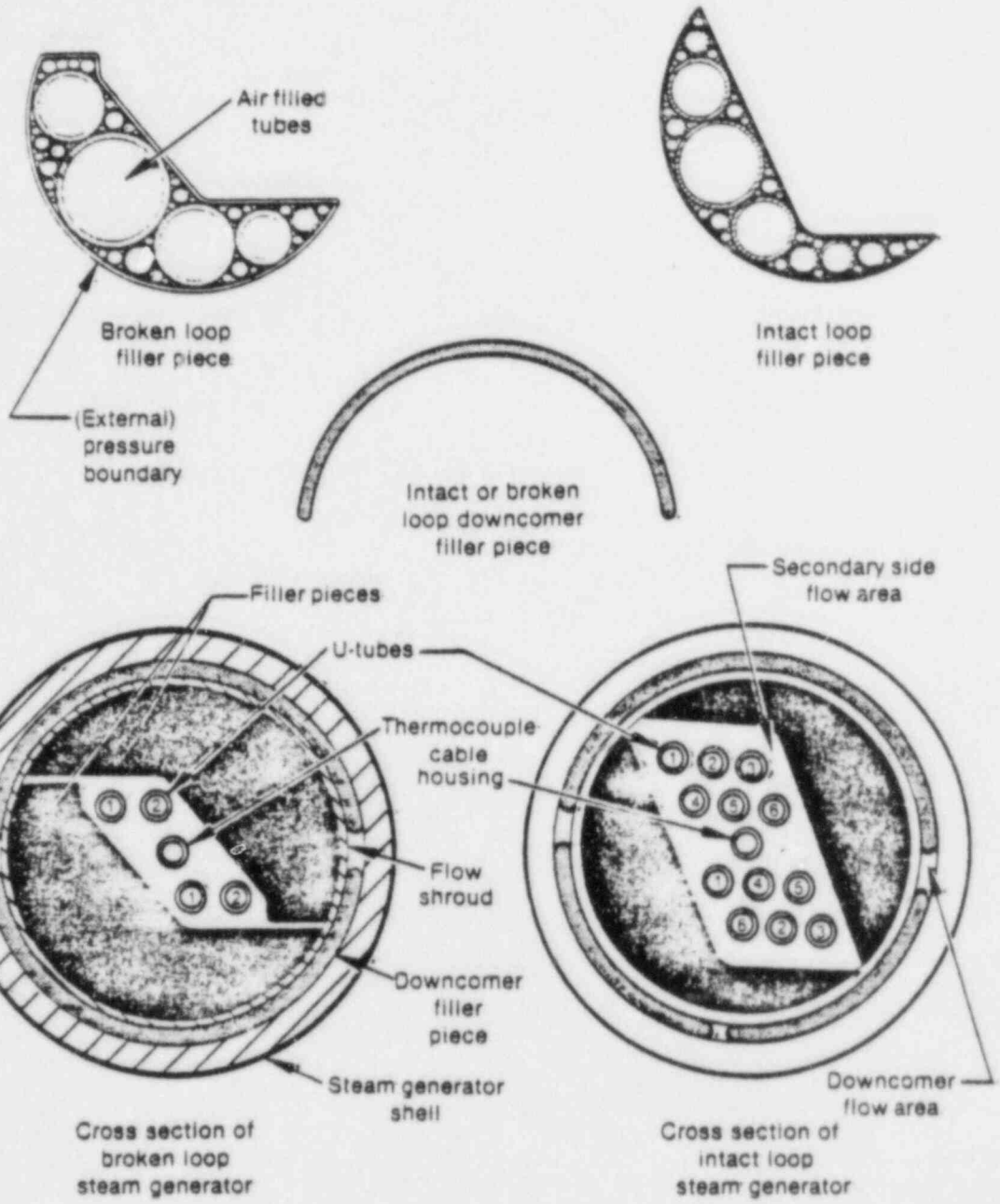


Figure AI.5 Steam Generator Cross-Sectional Views

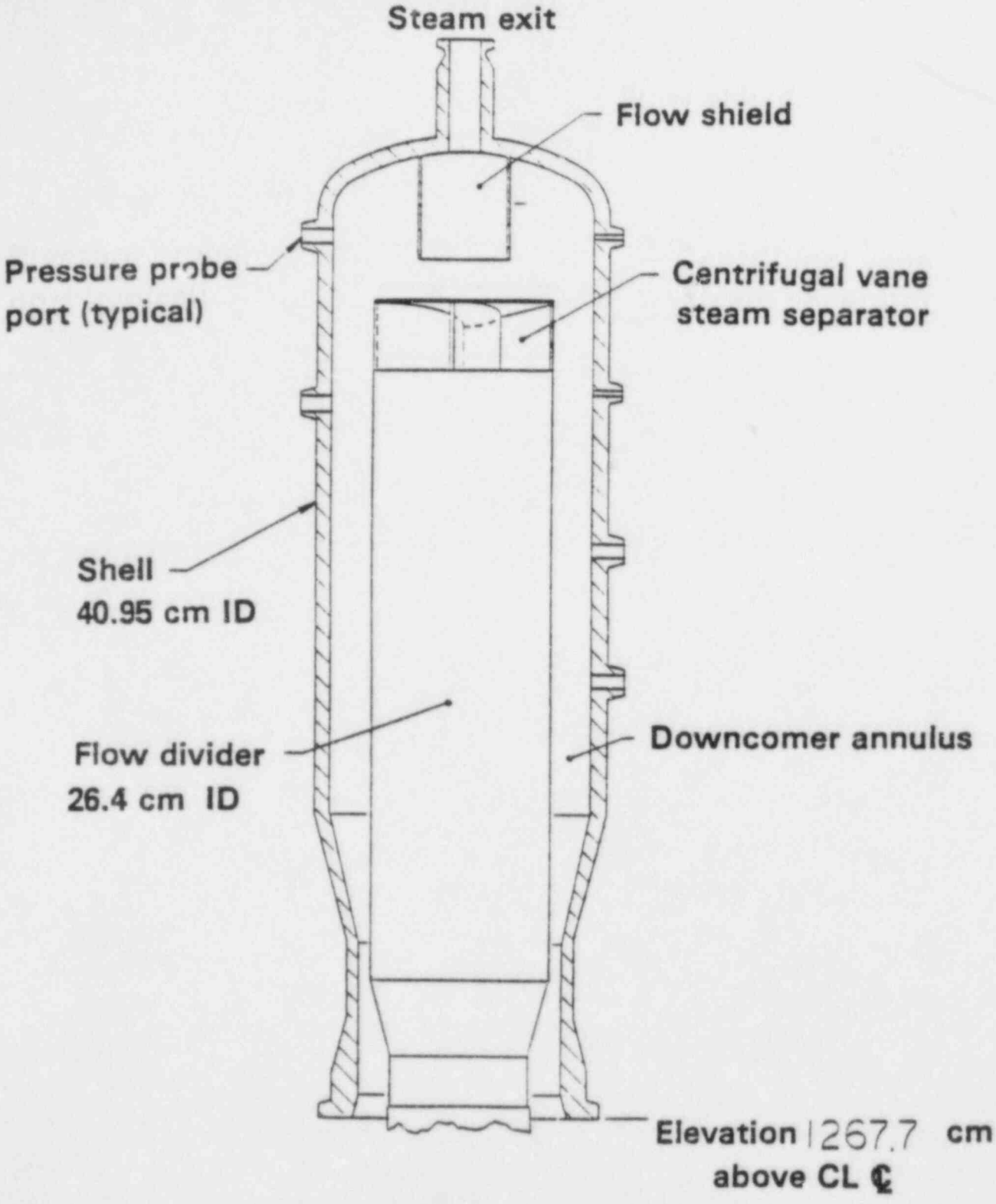


Figure AI.6 Steam Generator Steam Dome Detail

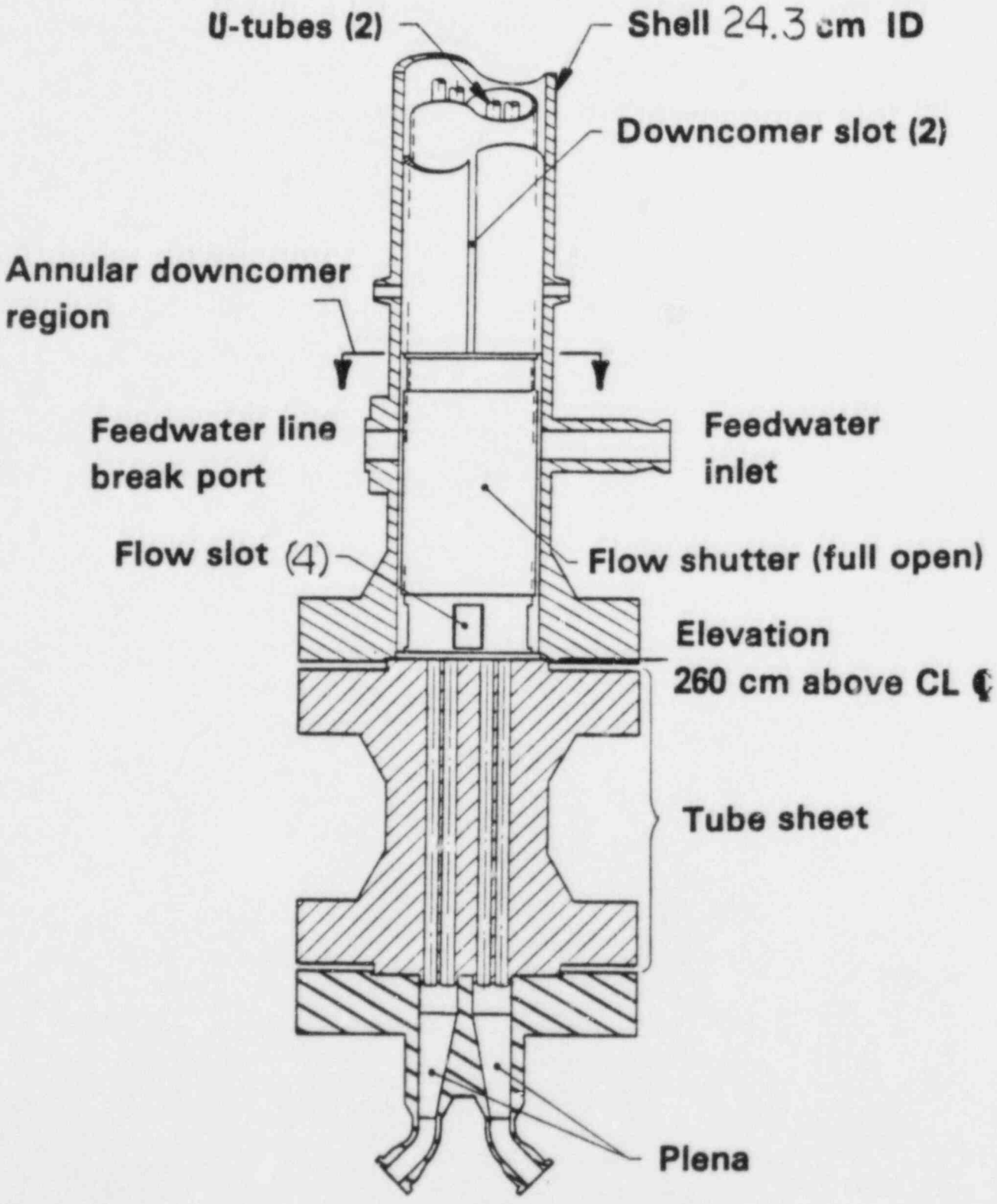


Figure AI.7 Steam Generator Feedwater-Entrance Region Detail

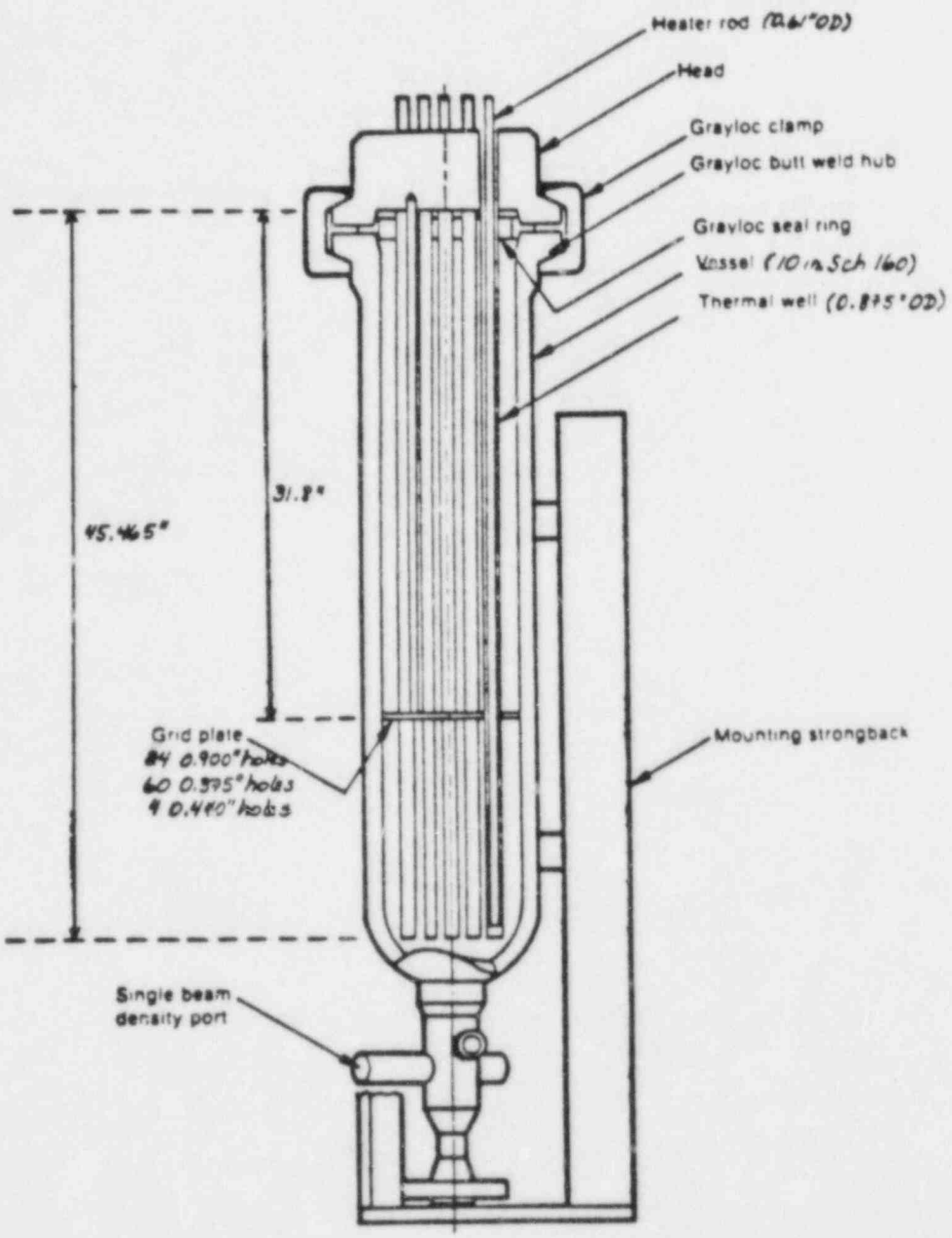


Figure AI.8 Pressurizer Diagram

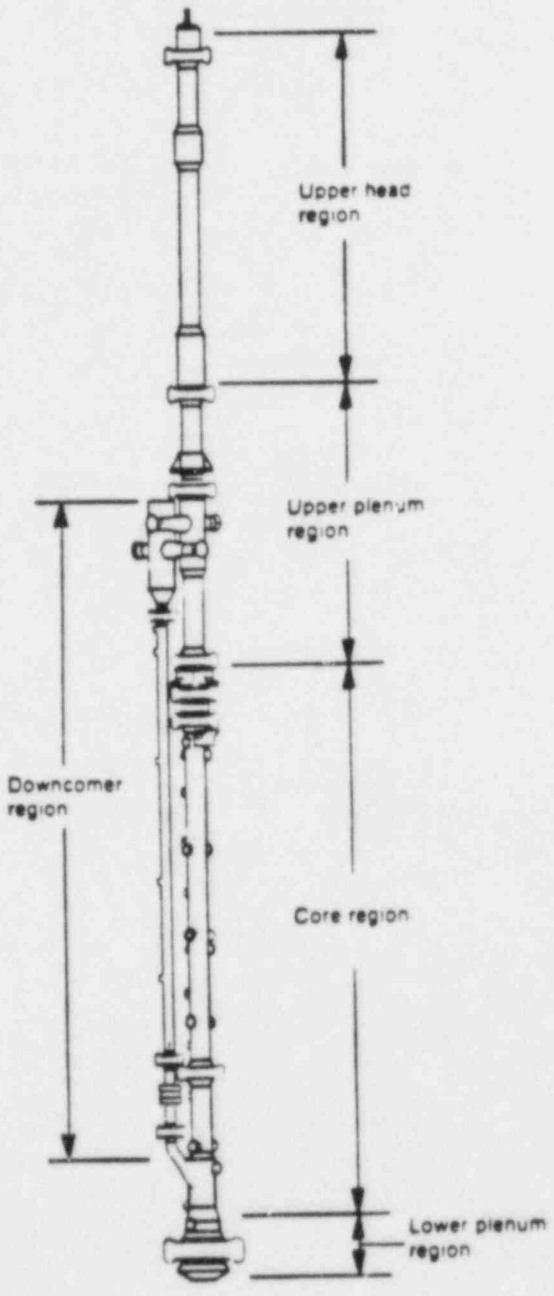


Figure AI.9 Semiscale Mod-2A Vessel Assembly

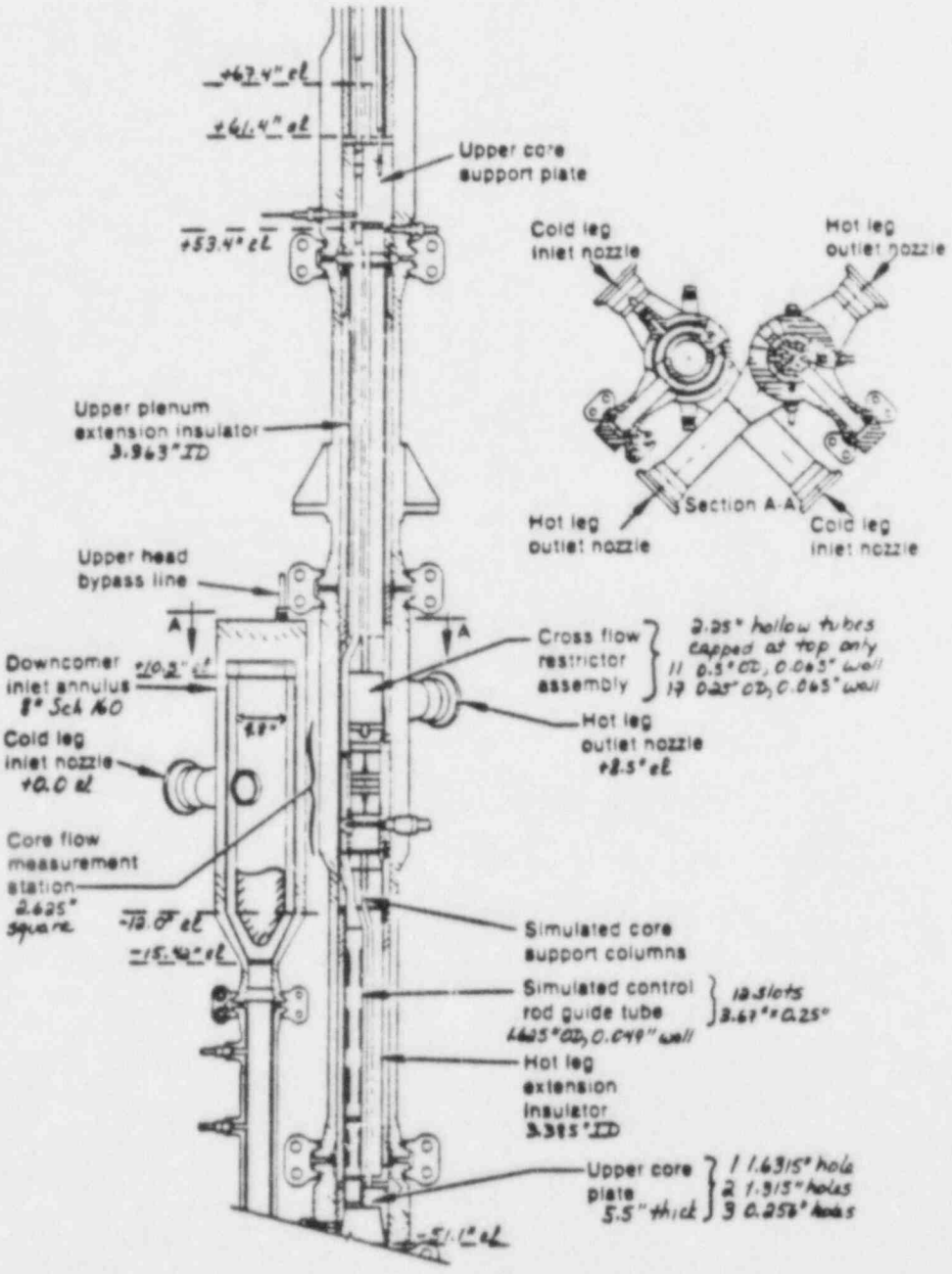


Figure AI.10 Vessel Downcomer Inlet and Upper Plenum Regions

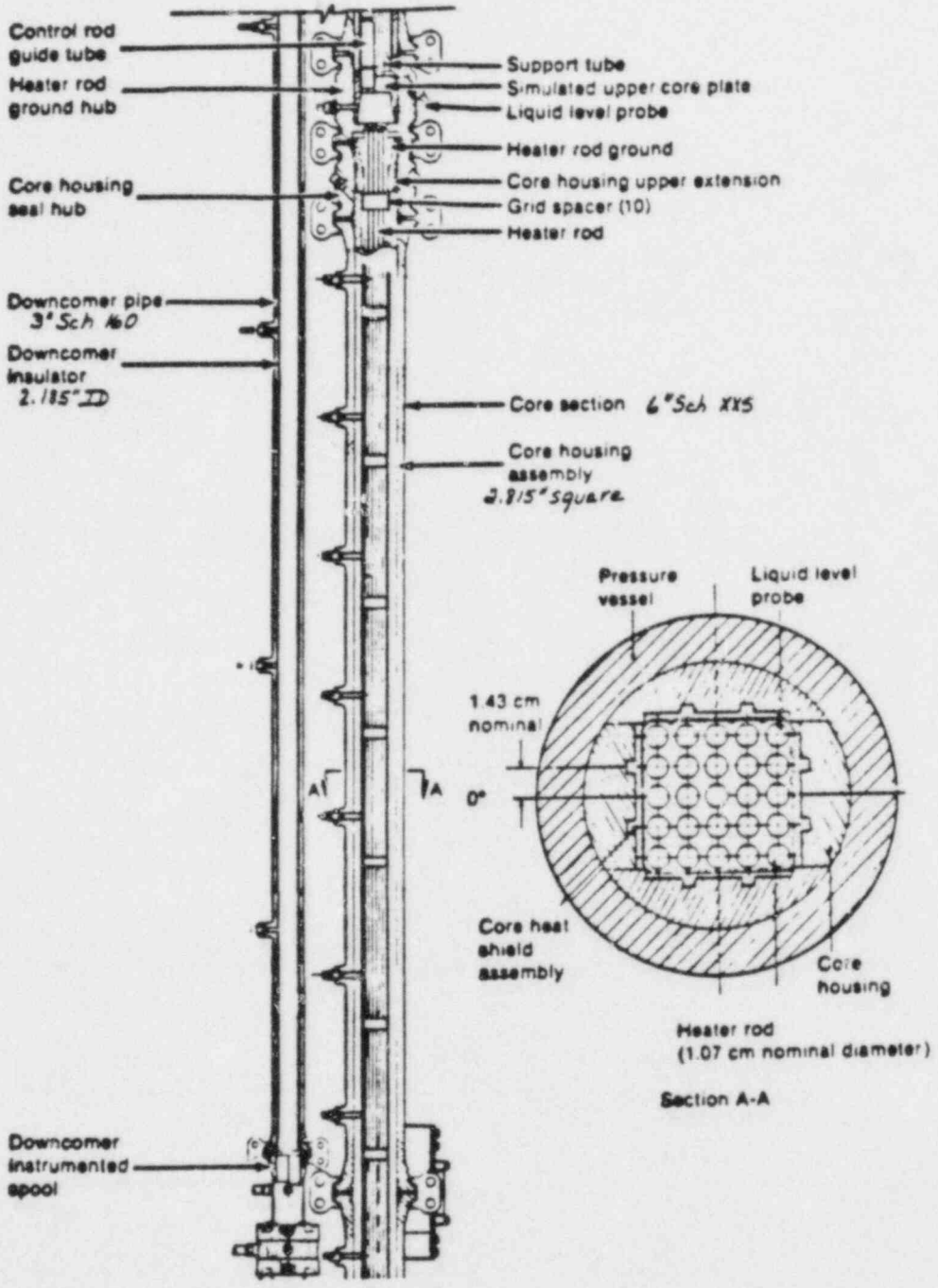


Figure AI.11 Vessel Core Region

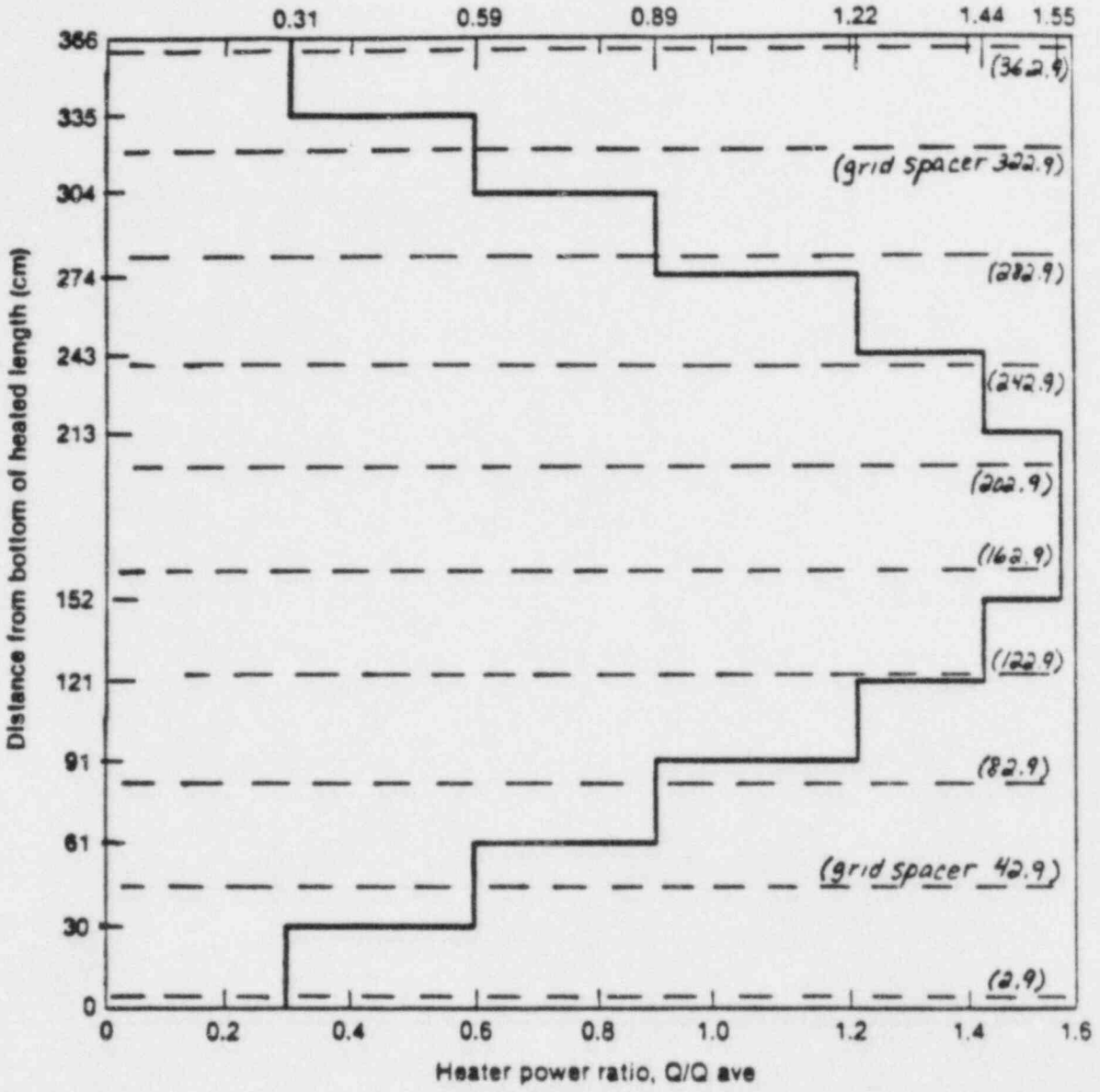


Figure AI.12 Core Axial Power Profile

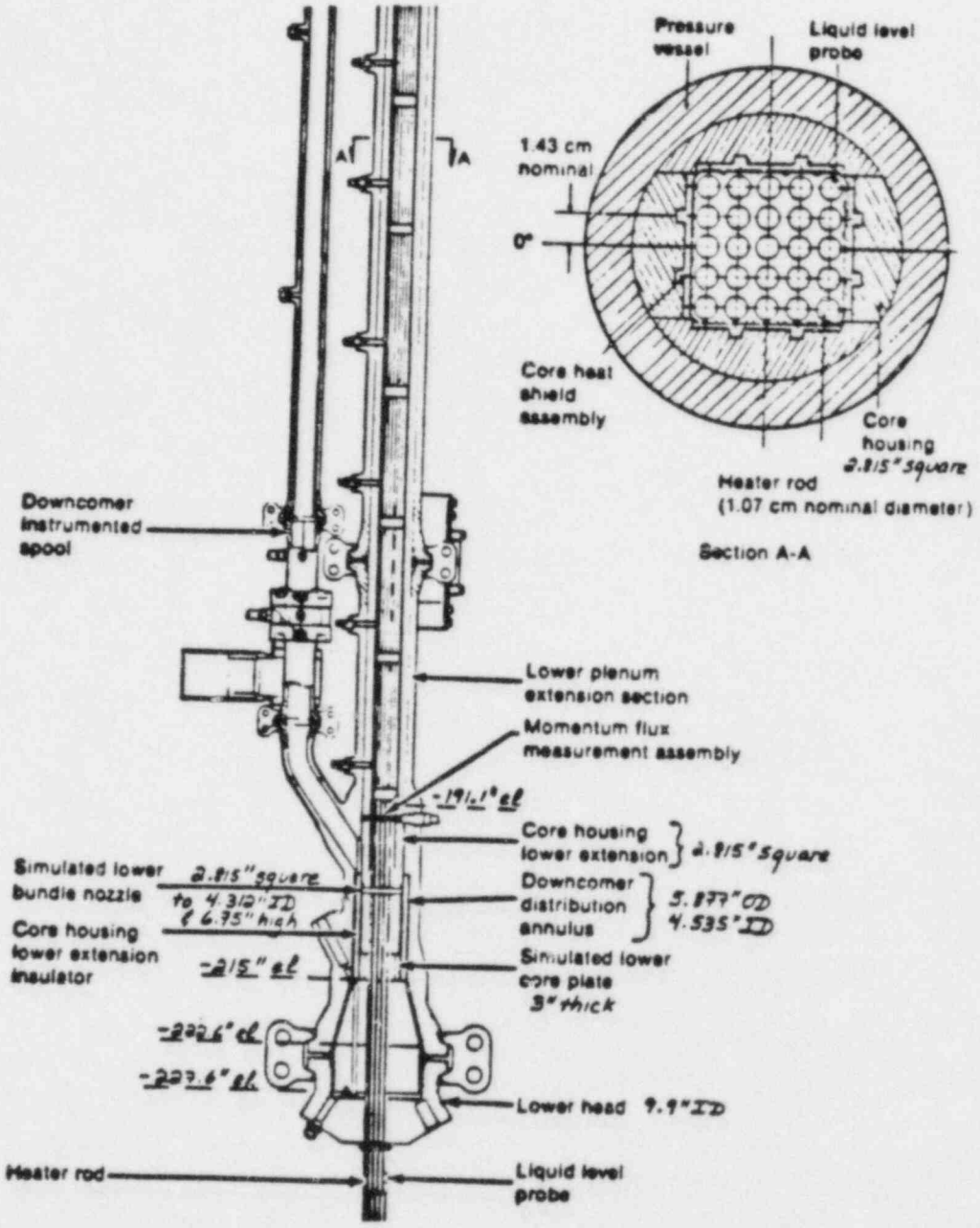


Figure AI.13 Vessel Lower Plenum and Lower Downcomer Regions

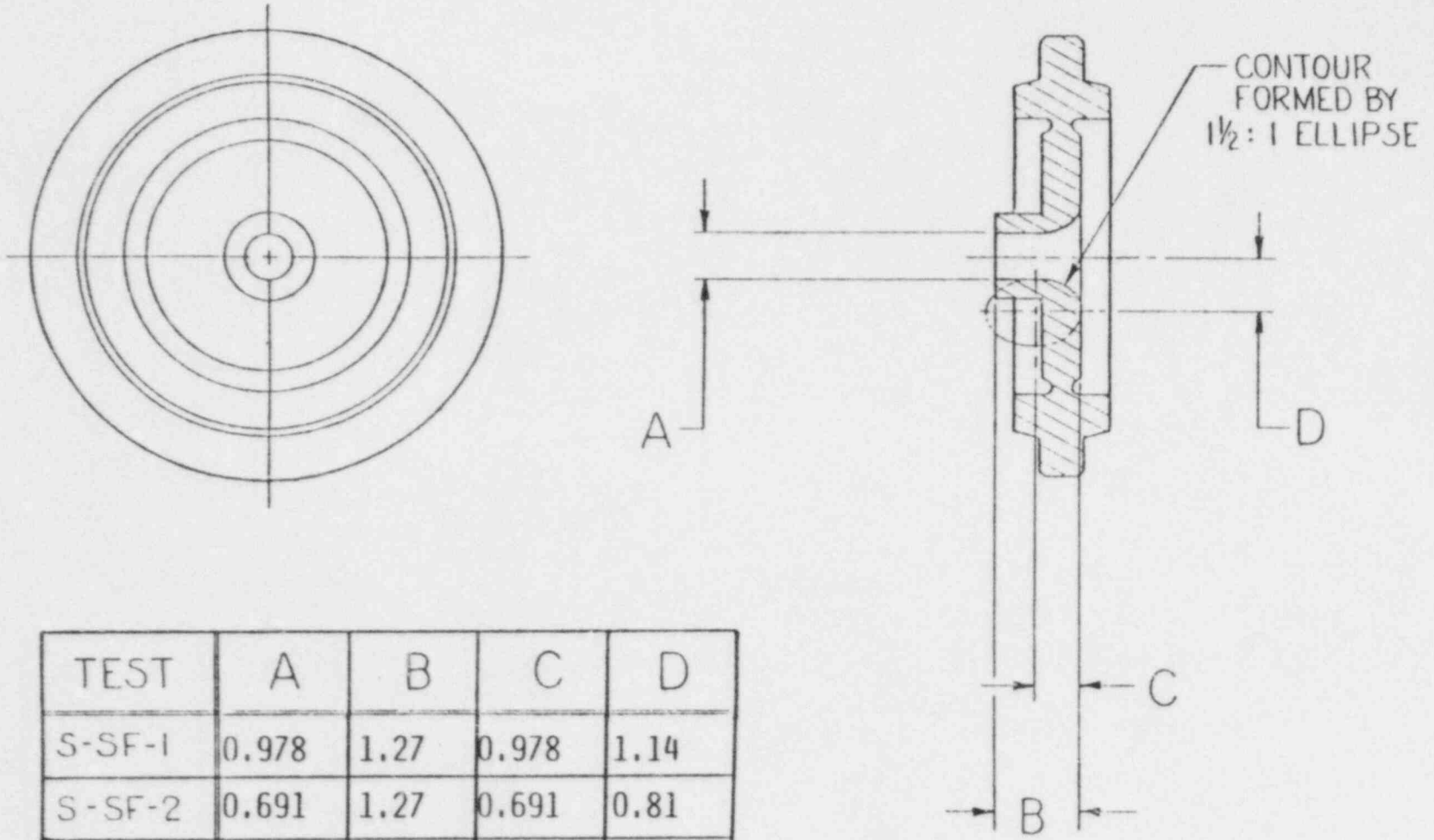


| TEST | A | B | C | D |
|---|---|---|---|---|
| S-SF-1 | 0.978 | 1.27 | 0.978 | 1.14 |
| S-SF-2 | 0.691 | 1.27 | 0.691 | 0.81 |
| S-SF-3 | 0.368 | 0.63 | 0.368 | 0.43 |

NOTE: DIMENSIONS IN CM.

Figure AI.14 Orifice Geometry for Feedwater-Line Break

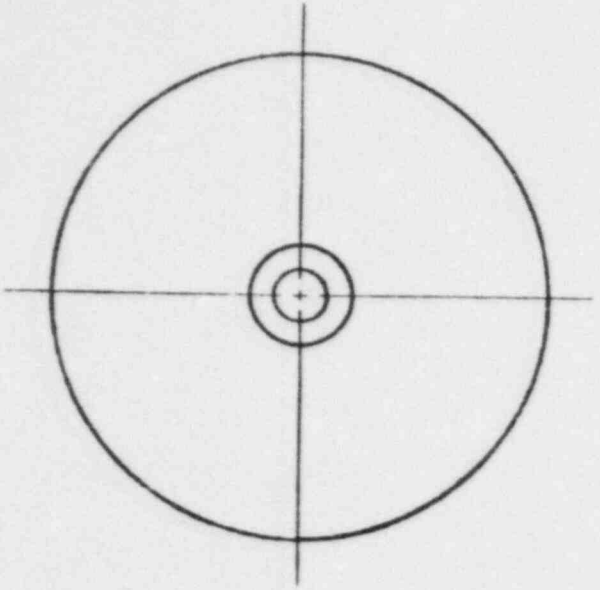

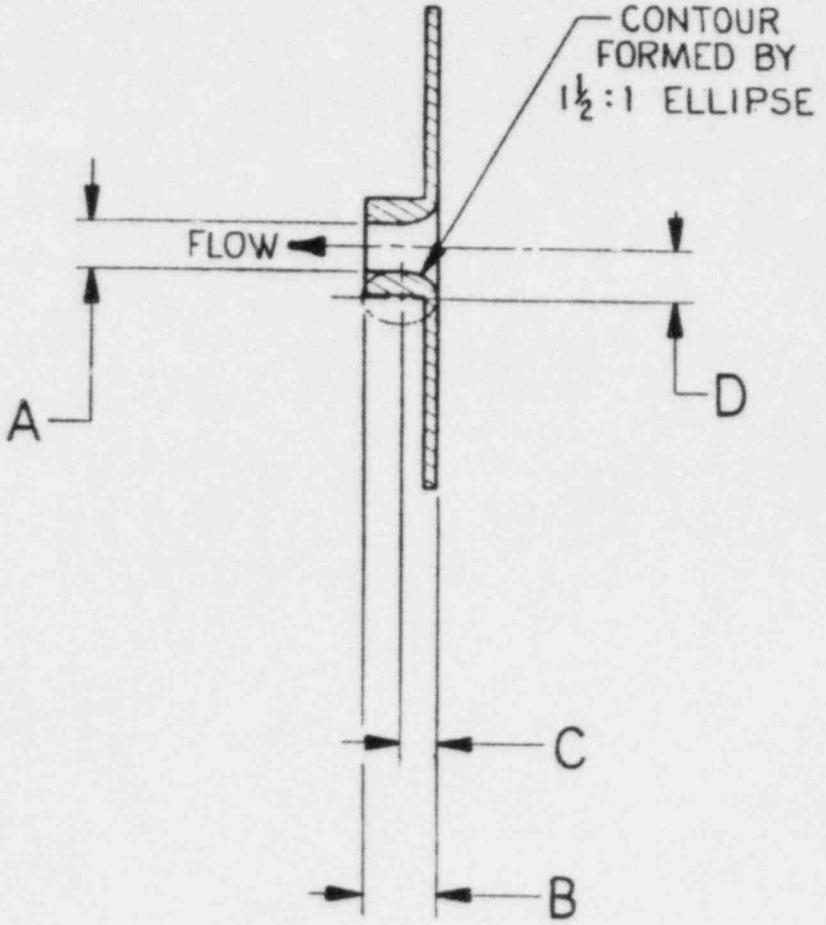


| TEST | LOCATION | A | B | C | D |
|---|---|---|---|---|---|
| S-SF-4 | BROKEN LOOP | .983 | 1.57 | .98 | 1.15 |
| | INTACT LOOP | 1.700 | 2.72 | 1.70 | 1.98 |
| S-SF-5 | BROKEN LOOP | .695 | 1.11 | .70 | .81 |
| | INTACT LOOP | 1.202 | 1.92 | 1.20 | 1.40 |

DIMENSIONS IN cm

Figure A1.15 Orifice Geometry for Steam-Line Break

## APPENDIX II - INPUT LISTINGS

Three input listings are included in the attached microfiche. The first listing is for the TRAC model of the Semiscale Mod-2A facility with S-SF-3 initial conditions and trip logic. The second listing is the TRAC model with S-SF-5 initial conditions and trip logic. The third listing is the TRAC model with all 1-D components and with S-SF-3 initial conditions and trip logic.

DISTRIBUTION:

U. S. Government Printing Office
Receiving Branch (Attn: NRC Stock)
8610 Cherry Lane
Laurel, MD 20707
300 copies for R4

U. S. Nuclear Regulatory Commission (5)
Reactor Systems Research Branch
Division of Accident Evaluation
Office of Nuclear Regulatory Research
7915 Eastern Avenue
Silver Spring, MD 20910
Attn: Louis M. Shotkin
Fuat Odar
D. Solberg
H. S. Tovmassian
N. Zuber

EG&G Idaho (6)
Idaho National Engineering Laboratory
P. O. Box 1625
Idaho Falls, ID 83415
Attn: T. R. Charlton
L. Feinauer
G. W. Johnsen
Edna Johnson
V. H. Ransom
R. J. Wagner

Brent Boyack
Thad D. Knight
Dennis R. Liles
Los Alamos National Laboratory (3)
K553 Q-9
Los Alamos, NM 87545

U. Rohatgi
Department of Nuclear Energy
Brookhaven National Laboratory
Associated Universities, Inc.
Upton, New York 11973

N. H. Shah
Babcock & Wilcox Co. (NPGD)
P. O. Box 1260
Lynchburg, VA 24505

Oddbjörn Sanderväg
Studsvik Energiteknik AB
S-611 82 Nyköping
SWEDEN

Jesse Fell (5)
Deputy Director, Water Reactor Programs
Atomic Energy Establishment
Winfrith
Dorchester, Dorset DT28DH
ENGLAND

6400 A. W. Snyder
6410 J. W. Hickman
6417 D. C. Carlson
6420 J. V. Walker
6421 T. R. Schmidt
6422 D. A. Powers
6423 P. S. Pickard
6425 W. J. Camp
6427 M. Berman
6440 D. A. Dahlgren
6442 W. A. von Riesemann
6444 L. D. Buxton (20)
6444 R. K. Byers
6444 R. K. Cole, Jr.
6444 P. N. Demmie
6444 D. Dobranich
6444 M. G. Elrick
6444 L. N. Kmetyk
6444 J. M. McGlaun
6444 J. Orman
6444 W. H. Schmidt
6444 R. M. Summers
6444 S. W. Webb
6449 K. D. Bergeron
3141 S. A. Landenberger (5)
3151 W. L. Garner
8024 P. W. Dean

NRC FORM 335 (2-84) NRCM 1102, 3201, 3202

U.S. NUCLEAR REGULATORY COMMISSION

**BIBLIOGRAPHIC DATA SHEET**

SEE INSTRUCTIONS ON THE REVERSE

1 REPORT NUMBER (Assigned by TIDC, add Vol. No., if any)

NUREG/CR-4189
SAND85-0576

2 TITLE AND SUBTITLE

TRAC-PF1/MOD1 Independent Assessment: Semiscale MOD-2A Feedwater-Line Break (S-SF-3) and Steam-Line Break (S-SF-5) Tests

3 LEAVE BLANK

4 DATE REPORT COMPLETED

MONTH: October — YEAR: 1985

5 AUTHOR(S)

Dean Dobranich

6 DATE REPORT ISSUED

MONTH: November — YEAR: 1985

7 PERFORMING ORGANIZATION NAME AND MAILING ADDRESS (Include Zip Code)

Thermal/Hydraulic Analysis Division
Sandia National Laboratories
P. O. Box 5800
Albuquerque, NM 87185

8 PROJECT/TASK/WORK UNIT NUMBER

9 FIN OR GRANT NUMBER

A-1374

10 SPONSORING ORGANIZATION NAME AND MAILING ADDRESS (Include Zip Code)

Reactor Systems Research Branch
Division of Accident Evaluation
Office of Nuclear Regulatory Research
U. S. Nuclear Regulatory Commission
Washington, DC 20555

11a TYPE OF REPORT

Technical

b PERIOD COVERED (Inclusive dates)

12 SUPPLEMENTARY NOTES

13 ABSTRACT (200 words or less)

The TRAC-PF1/MOD1 independent assessment project at Sandia is part of an overall effort funded by the NRC to determine the ability of various systems codes to predict the detailed thermal/hydraulic response of LWRs during accident and off-normal conditions. As part of this effort, calculations for Semiscale Mod-2A test S-SF-3, a feedwater-line break test, and S-SF-5, a steam-line break test, were performed with TRAC-PF1/MOD1.

Most aspects of both the S-SF-3 and S-SF-5 steady-state calculations were found to be in good agreement with data. However, the need for a better steam separator model was identified from the S-SF-3 calculation. Overall, the qualitative behavior of both transients was calculated reasonably well; however, there were some discrepancies in the prediction of the quantitative behavior. The results for the S-SF-3 transient calculation indicate that the primary-to-secondary heat transfer degradation began too early. This was possibly due to overprediction of entrainment in the steam generator boiler, leading to an incorrect calculation of the secondary-side fluid distribution during the steady state. However, there was insufficient data to verify this. Results for the S-SF-5 transient calculation indicate that the primary-side fluid temperature response to a steam-line break was in reasonable agreement with data but the pressure response did not coincide with the data. Uncertainties in the data are sufficient to prevent us from determining the exact cause of this discrepancy, but there is indirect evidence that the calculated rate of phase change in the pressurizer was incorrect.

14 DOCUMENT ANALYSIS - a KEYWORDS/DESCRIPTORS

b IDENTIFIERS/OPEN-ENDED TERMS

15 AVAILABILITY STATEMENT

Unlimited

16 SECURITY CLASSIFICATION

(This page) Uncl

(This report) Uncl

17 NUMBER OF PAGES

18 PRICE

3151 - H. L. Garner